Acknowledgements

Many thanks to Professor Steinar Nordal for his committed and enthusiastic guidance during the process of developing the present master thesis. Also, to the International Centre for Geohazards for the financial support during my two years of MSc in Geotechnics and Geohazards studies at the Norwegian University of Science and Technology.

Tusen takk!

Table of contents

Index of Figures

Index of Tables

Introduction

The design of shallow foundations involves settlement and bearing capacity calculations. The bearing capacity aspect has always been one of the most highly interesting areas in geotechnical engineering with researchers and practising engineers (Manoharan and Dasgupta, 1995).

The bearing capacity estimation has been based on the superposition method proposed by Terzaghi (1943) which sums the contribution of the soil strength parameters (cohesion, friction angle, overburden and soil weight) in the form of non-dimensional bearing capacity factors Nc, Nq and Nγ. These factors can be computed by analytical solutions and are assumed to be functions of the soil friction angle.

Zhu and Michalowski (2005) say that such superposition of the three components is not strictly correct, since the differential equations describing the stress state at failure are not linear, but the method was accepted by engineers for its simplicity. This conclusion is also given by Manoharan and Dasgupta (1995).

Numerical methods can be used to compute the bearing capacity of footings and also its behaviour prior to failure with the advantage of combining all the parameters into a single problem. This has been done before by several authors (Griffiths, 1982; de Borst and Vermeer, 1984; Manoharan and Dasgupta, 1995; Frydman and Burd, 1997; Yin *et al.*, 2001; Erickson and Drescher, 2002; Salgado *et al.*, 2004; Hjiaj *et al.*, 2005; Zhu and Michalowski, 2005; Lyamin *et al.*, 2007; Zhao and Wang, 2009; Loukidis and Salgado, 2009) using different numerical tools (Finite Element method - FEM and Finite Difference method - FDM), approaches and assumptions (associative and non-associative materials, strip and circular footings, plane strain and axisymmetrical conditions, among others).

Griffiths (1982) used Finite Elements (FE) to compute each of the bearing capacity factors for strip footings and examine the superposition principle of Terzaghi's equation. The last aspect was done by comparing the computed

results of bearing capacity obtained in a single calculation with the result obtained by simple addition of the three individual components. It was concluded that FEM can be used to predict the bearing capacity of surface footing with confidence and that the superposition assumption was always conservative. Most of the errors introduced by superposition were due entirely to non-linearities in $N\gamma$ because the linear stress distributions in the Nc and Nq terms superpose almost exactly.

Manoharan and Dasgupta (1995) extended Griffiths (1982) work to circular footings and found the superposition error to be less than 10% for all the cases analyzed by them. They incorporated the associated and non-associated flow rules to the footing behaviour as a result of the significant role of the flow rule in the deformation prior to failure and on the plastic flow pattern at failure.

The effect of associative and non-associative materials in the bearing capacity problem has also been studied using limit analysis by Drescher and Detournay (1993) who found that the limit load for non-associative material with a coaxial flow rule is lower than the limit load for the associative material. Also, Michalowski (1997) using the same limit analysis approach found significant differences in estimations of bearing capacity factors from accounting for or not accounting for the non-associativity of the plastic soil deformation. Using numerical solutions Yin *et al.* (2001), Zhao and Wang, (2009) and Loukidis and Salgado (2009); demonstrated that decreasing the dilatancy angle (increasing non-associativity) decreases the bearing capacity factors gradually.

In the most recent studies (Salgado *et al.*, 2004; Zhu and Michalowski, 2005; Lyamin *et al.*, 2007; Puzakov *et al.*, 2009), special interest has been focused in studying the bearing capacity factors for rectangular footings. The main purpose has been to derived shape factors by computation of three-dimensional bearing capacity. The results got have been compared with earlier empirical proposals based on associated flow rule and empirical data for small footings.

The present study takes a closer look to the numerical modeling of the bearing capacity problem in order to: a) define the influence of the relative footing dimension in the bearing capacity factors for associative and non-associative materials, b) define the shape factors when rectangular and square footings are analyzed, and, c) describe the special features (unstructured vs. structured

mesh effect, associative vs. non-associative materials, among others) that should be taken into account when computing ultimate loads.

The aim is to identify the influence of the parameters involved when two- and three-dimensional numerical modeling of the bearing capacity problem is performed. First, describing theoretically the bearing capacity problem. Then, by using FEM with the codes PLAXIS 2D, PLAXIS 3D Foundation and PLAXIS 3D-Tunnel, simulate the bearing capacity problem and compare the results obtained with what has been proposed before theoretically, empirically and numerically.

The specific objectives lead to:

1) Describe the different bearing capacity theories proposed in the literature and that are applied during the general geotechnical engineering practice.
2) Describe the previous proposals about the influence of the relative footing dimension in the bearing capacity problem by the analysis of the shape factors equations proposed in the literature and preceding works.
3) Model numerically the bearing capacity problem for different footing sizes and cases of analysis according to the bearing capacity factor under investigation Nq or $N\gamma$.
4) Establish special features that should be taken into account when numerical modeling of the bearing capacity problem is performed, for instance: unstructured vs. structured mesh effect, associative vs. non-associative materials, among others.

The general case under analysis in the present study has been limited to shallow-surface foundations with a rough soil-footing interface, under vertical loading showing general shear failure and following an effective stress analysis. A strip footing is idealised as plane strain, a circular footings as axi-symmetric and a rectangular footing as a three dimensional problem. Consequently, the strip and circular footings are analyzed in 2D and rectangular footings in 3D (taken into account two vertical planes of symmetry).

The theory and results presented from the literature study and the numerical simulations are focus in the direction proposed above. Furthermore, the shape

factors under analysis (s_q and s_γ) correspond to the ones that modified the overburden effect (Nq) and the soil weight effect ($N\gamma$) according to general bearing capacity equation used in Norway (Equation 34).

Each chapter in the following report responds to the specific objectives define for the study. In the first chapter, a theoretical background of the bearing capacity problem is defined. The second chapter shows the literature study about the relative footing dimension and the bearing capacity problem. In the third part, the results of the numerical simulations to study the influence of the relative footing dimension in the bearing capacity problem are presented. Finally, the chapter four establishes the special features to take account of when numerical modeling of the bearing capacity problem is done.

The importance of studies, like the one presented in the following pages, is the possibility of testing the agreement between: the empirical/semi-empirical terms for computing the bearing capacity of foundations and the numerical tools available for those analysis, in order to perform better and safer bearing capacity calculations and therefore, better design of foundations.

Chapter 1

Theoretical background of the bearing capacity problem

The design of foundations must satisfy two main requirements, namely, complete failure of the foundation must be avoided with an adequate margin of safety, and, the total and relative settlement of the foundation must be kept within limits that can be tolerated by the superstructure (Meyerhof, 1951).

The ultimate bearing capacity of a foundation is defined as the maximum load that the ground can sustain. Vesić (1973), by analyzing the simple case of a footing on a homogeneous soil, loaded by a central and vertical load, stated that the bearing capacity failure usually occurs as a shear failure of the soil supporting the footing. Three principal modes of shear failure under foundations are: general shear failure, local shear failure and punching shear failure.

Vesić (1973) describes that the general shear failure has a well-defined failure pattern which consists of a continuos slip surface from one edge of the footing to the ground surface (Figure 1a). The punching shear failure mode is characterized by a failure pattern that does not produce movements of the soil on the sides of the footing as the load increases, the vertical movement of the footing is accompanied by a compression of the soil on the sides of the footing (Figure 1b). Finally, the local shear failure is characterized by a failure pattern which is clearly defined only immediately below the foundation (Figure 1c).

Furthermore, Figure 1 shows typical load-displacements curves where the ultimate load can be read. The criterion for choosing the ultimate load defines this load as the point which the slope of the load-settlement curve first reaches zero or a steady, minimum value (Vesić, 1963). De Beer (1970) proposes that the ultimate load should be taken at the break point of the load-settlement curve in a log/log plot.

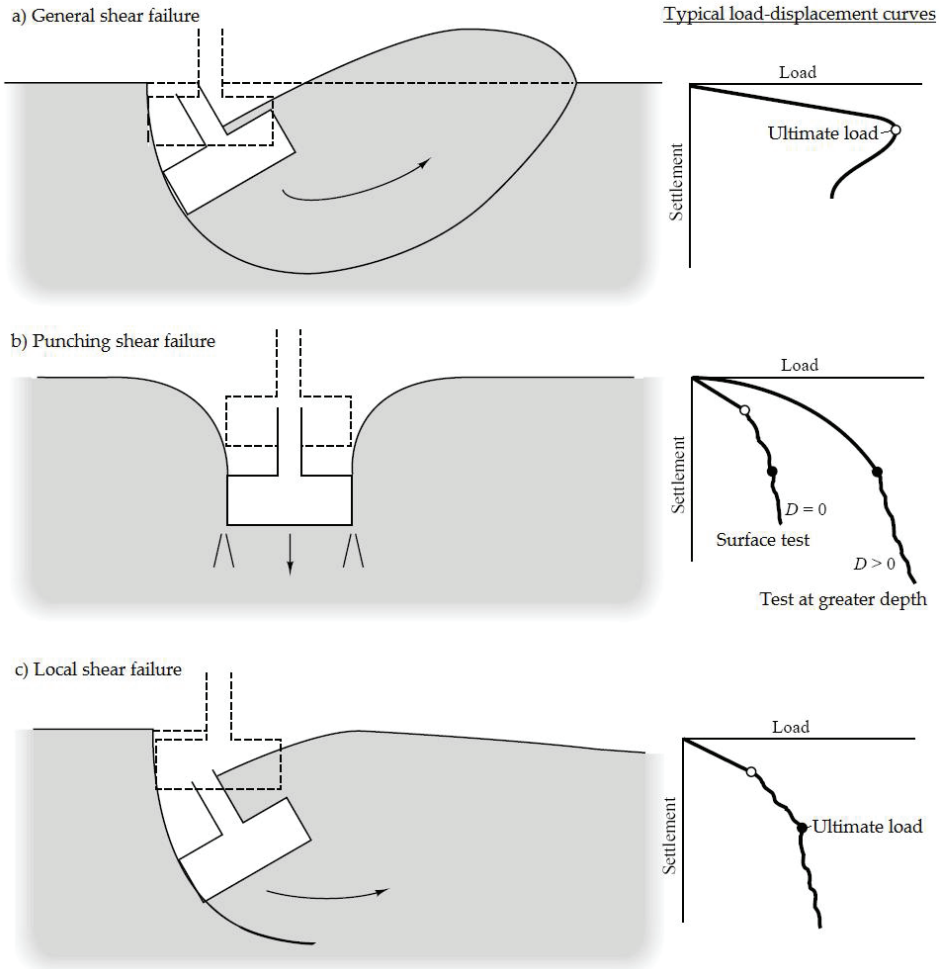

Figure 1: Modes of bearing capacity failure (Coduto, 2000).

Several bearing capacity theories for estimating the ultimate bearing capacity of shallow foundations have been proposed[1]. The most important works published about it are commented in the following lines. The general assumptions for the cases considered are that the foundation is subjected to centric vertical loading, the soil supporting the foundation extends to a great depth, and, the foundation is shallow and with a rough soil-footing interface.

[1] A foundation is considered shallow when the embedded length is less than five times the bearing surface dimension.

1.1. Plasticity bearing capacity theory: Prandtl (1921) and Reissner (1924)

The classical Theory of Plasticity solves the problem of bearing capacity for a shallow footing for a rigid-plastic solid that exhibits no deformation whatsoever prior to shear failure and a plastic flow at constant stress after failure (Vesić, 1963). Theoretically speaking, the prediction of the ultimate load is limited to relatively incompressible soil or to the general shear failure mode.

The problem is generally simplified as an elastic-plastic equilibrium of a rectangular foundation of width B and length L (Figure 2a) resting in a soil mass at a depth D. The soil mass is homogeneous and semi-infinite extended, with an effective unit weight γ and shear strength properties defined by a straight line Mohr-Coulomb envelope, with strength characteristics c and φ, and a stress-strain curve of a rigid-plastic body (Figure 2b). The unknown is the maximum load, $q_o = Q_o / B*L$, which the foundation can support.

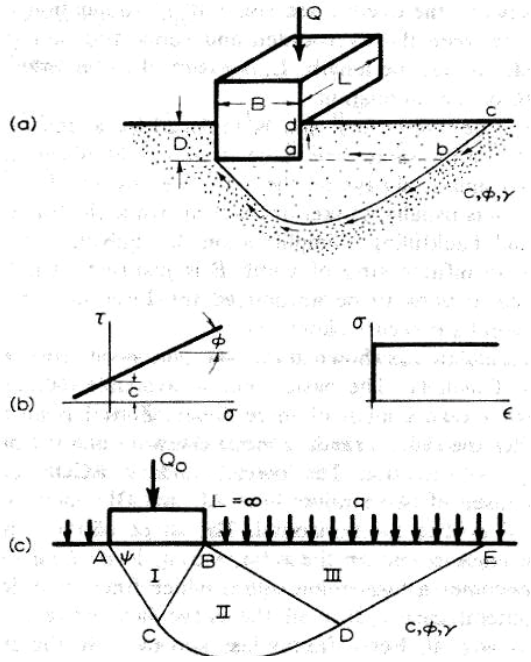

Figure 2: Problem of bearing capacity of shallow foundations (Vesić, 1963).

Vesić (1963) summarizes the simplifications that should be made to solve this problem:

(a) The shearing resistance of the overburden soil (along *bc*, Figure 2a) is neglected. Also, the friction between the overburden soil and the foundation (along *ad*, Figure 2a) as well between the overburden and supporting soil (along *ab*, Figure 2a) is neglected. These three simplifications are justified in the fact that the overburden soil is usually weaker or cracked because the foundation is placed by excavation and backfilling.

(b) The length, L, is assumed to be large in comparison with the width, B, of the foundation. That means the foundation is an infinite strip of width B for B/L < 0.2. For B/L > 0.2 and different shapes, a correction should be introduced in the solution.

Prandtl (1921) and Reissner (1924) solved the problem shown in Figure 2c by methods of Theory of Plasticity. They defined the failure pattern in three zones. Zone I is an active Rankine zone, which pushes the radial Prandtl zone II sideways and the passive Rankine zone III in an upward direction. The lower boundary, ACDE, of the displaced soil mass is composed of two straight lines: AC inclined at 45°+φ/2 to the horizontal; and DE inclined at 45°-φ/2 to the horizontal. The shape of the connecting curve, CD, depends on the angle φ and on the radio, γB/q. For γB/q → 0 (weightless soil) the curve becomes a logarithmic spiral which for φ = 0 (frictionless soil) degenerates into a circle. Therefore, Prandtl and Reissner found that, for a weightless soil (γ = 0):

$$q_{ult} = c * N_c + q * N_q \tag{1}$$

in which Nc and Nq are dimensionless bearing capacity factors (known as exact values), defined by:

$$N_q = tan^2(\tfrac{\pi}{4} + \tfrac{\varphi}{2}) * e^{\pi * tan\varphi} \tag{2}$$

$$N_c = (N_q - 1) * cotan\varphi \tag{3}$$

Figure 3 shows the variation of these factors with the friction angle φ.

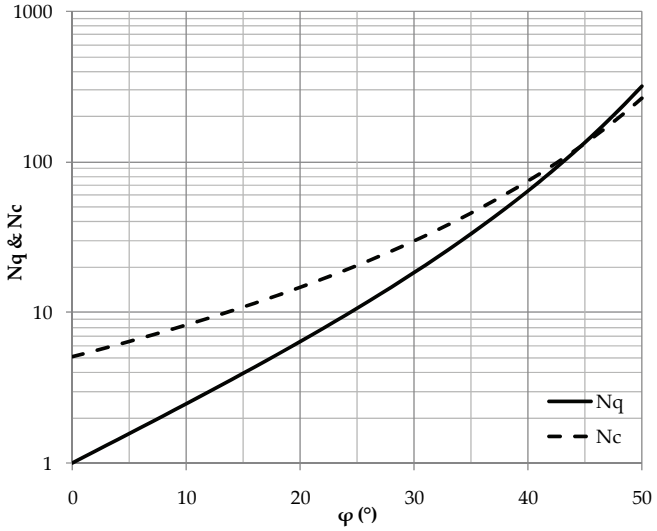

Figure 3: Variation of Nc and Nq with the friction angle φ.

The solution proposed by Prandtl (1921) and later applied by Reissner (1924) is based on the slip-line method (method of characteristics) in which basic differential equations of the slip-line network derived using the equilibrium of stresses and yield conditions are solved (Manoharan and Dasgupta, 1995).

1.2. Terzaghi's bearing capacity theory (1943)

The solution for the bearing capacity problem of a shallow (where the footing width B is greater than or equal to its foundation depth D), rigid, strip foundation, with a rough soil-footing interface, supported by a homogeneous soil layer extending to a great depth; proposed by Terzaghi in 1943, is based on the superposition method.

In the superposition method, the contribution of different loading and soil strength parameters (cohesion, friction angle, overburden and soil weight) expressed in the form of non-dimensional bearing capacity factors Nc, Nq and Nγ are summed. It is based on the limit equilibrium method where an

approximate failure surface of various simple shapes is assumed and a critical failure surface is found (Manoharan and Dasgupta, 1995).

The failure mechanism proposed by Terzaghi is shown in Figure 4. It consists of three major zones:

(a) Zone *adb*: which is an elastic zone below the bottom of the foundation, the inclination of sides *bd* and *ad* of the wedge with the horizontal is equal to the soil friction angle φ.

(b) Zone *ade*: which is the Prandtl's radial shear zone.

(c) Zone *aef*: which is the Rankine passive zone where the slip lines make angles of ±(45°-φ/2) with the horizontal.

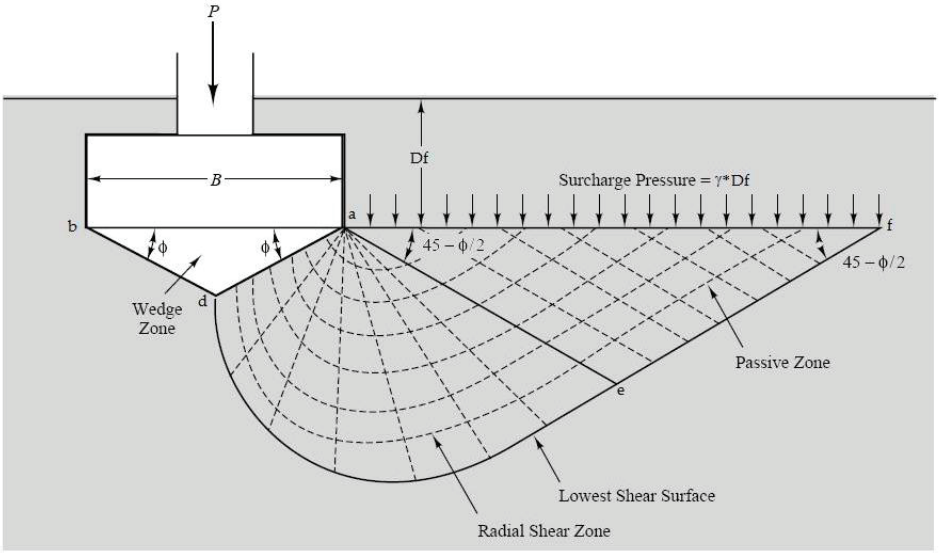

Figure 4: Geometry of failure surface for Terzaghi's bearing capacity formulas for a footing with a rough soil-footing interface (Coduto, 2000).

Therefore, the ultimate bearing capacity of the foundation can be obtained after considering the passive force required to cause failure that acts in faces *bd* and *ad* of the wedge zone *abd* (Figure 4). This passive force P_P is a function of the overburden pressure, p' = γ*D; cohesion, c; unit weight, γ; and angle of friction of the soil, φ; as shown in Equation 4.

$$P_p = P_{pq} + P_{pc} + P_{p\gamma} \tag{4}$$

where, P_{pq} is the passive force contribution obtained when $\varphi \neq 0$, $\gamma = 0$, $p' \neq 0$, $c = 0$; P_{pc} is the passive force contribution obtained when $\varphi \neq 0$, $\gamma = 0$, $p' = 0$, $c \neq 0$; and, $P_{p\gamma}$ is the minimum value of the passive force contribution obtained by trial and error when $\varphi \neq 0$, $\gamma \neq 0$, $p' = 0$, $c = 0$. The complete derivation of the equations can be found in Terzaghi (1943) or Das (2009).

The assumption of the passive force contribution is possible due to the effect of the rough soil-footing interface. According to Terzaghi (1943), if the load is transmitted onto the ground by means of a continuous footing with a rough soil-footing interface as shown in Figure 5b, the tendency of the soil located within the zone I to spread sideways is counteracted by the friction and adhesion between the soil and the base of the footing. For that reason, due to this resistance to lateral spreading, the soil located beneath the base of the footing remains permanently in a state of elastic equilibrium and the soil located within the central zone behaves as if it were a part of the sinking footing. On the other hand, in the case of a smooth footing, there is no resistance to lateral spreading and while the load sinks the footing into the ground, the soil located inside the zone I in Figure 5b spreads laterally.

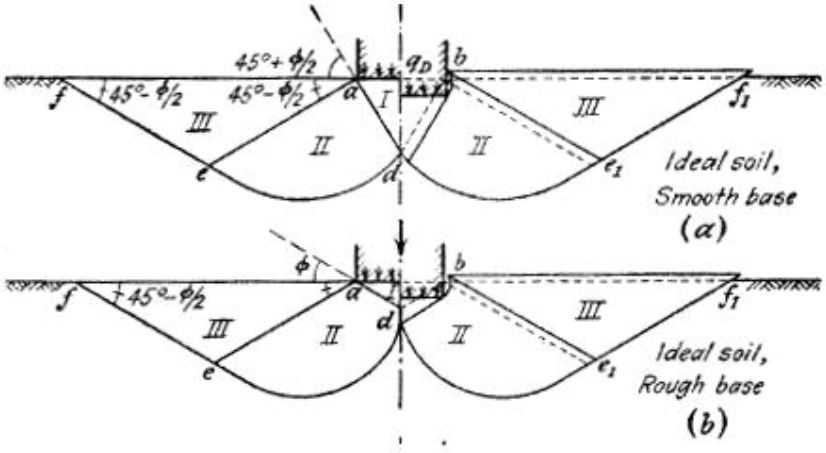

Figure 5: Boundaries of zone of plastic flow after failure of earth support of continuous footings (Terzaghi, 1943).

The ultimate load per unit area of the foundation (ultimate bearing capacity q_{ult}) for a soil with cohesion, friction and weight is given by Equation 5,

$$q_{ult} = p' * N_q + c * N_c + \frac{1}{2} * \gamma * B * N_\gamma \tag{5}$$

where, B is the width of the foundation; and, Nc, Nq and Nγ are the bearing capacity factors defined in Equation 3 (using the Nq value given in Equation 6); Equation 6 and Equation 7, respectively. Figure 6 shows the relation between φ and the bearing capacity factors.

$$N_q = \frac{e^{2*(\frac{3*\pi}{4} - \frac{\varphi}{2})*tan\varphi}}{2 * cos^2(45 + \frac{\varphi}{2})} \tag{6}$$

$$N_\gamma = \frac{1}{2} K_{p\gamma} tan^2\varphi - \frac{tan\varphi}{2} \tag{7}$$

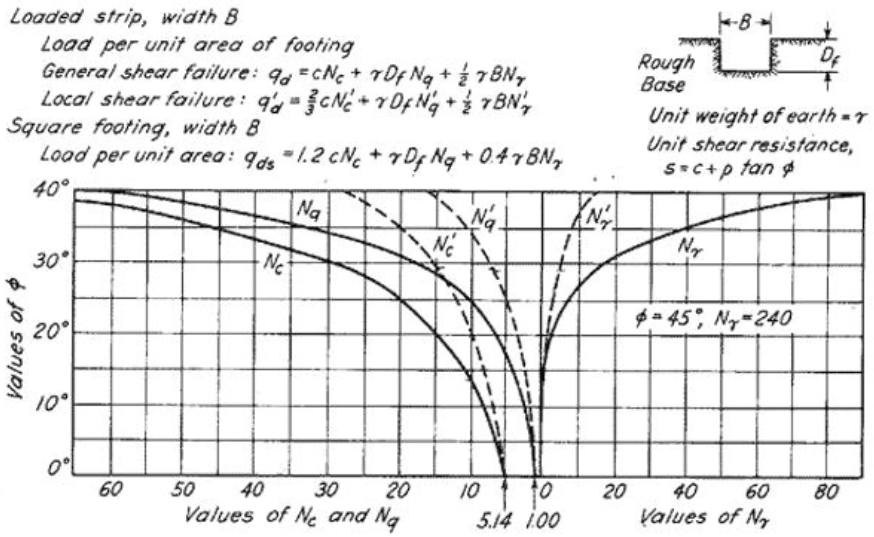

Figure 6: Relation between φ and Terzaghi's bearing capacity factors (Terzaghi, 1943).

It should be noted that Terzaghi proposed different formulas from Equation 5 for square and circular foundations justified in the absence of plane strain conditions for these cases. The equations are detailed in Equation 8 for square footings and Equation 9 for circular footings.

$$q_{ult} = 1.3cN_c + p'N_q + 0.4\gamma BN_\gamma \quad (8)$$

$$q_{ult} = 1.3cN_c + p'N_q + 0.3\gamma BN_\gamma \quad (9)$$

According to Das (2009), the equation and the failure surface in the soil proposed by Terzaghi appear to be essentially correct. However, the angles of the faces *bd* and *ad* with the horizontal in the wedge zone *abd* (Figure 4) are closer to 45+φ/2, changing with that the soil failure surface. Even though the centre of the arc of the log spiral *de* is located at the edge of the foundation for the derivations of Nc and Nq which not coincides for the derivation of Nγ, the use of two different failure surfaces for the derivation Equation 5 is still on the safe side.

1.3. Meyerhof's bearing capacity theory (1951)

The bearing capacity theory proposed by Meyerhof (1951) makes use of the limit equilibrium method to be applied to rough soil-footing interface, shallow and deep foundations. Figure 7 shows the failure surface at ultimate load under continuos foundation assumed for his theory, for the case of shallow foundation. The triangular wedge *abc* is elastic, the radial shear zone *bcd* has *cd* as an arc of a log spiral, and, the *bde* zone mixes the shear between the limits of radial and plane shear depending on the depth and the roughness of the foundation. An equivalent free surface is define by the plane *be*.

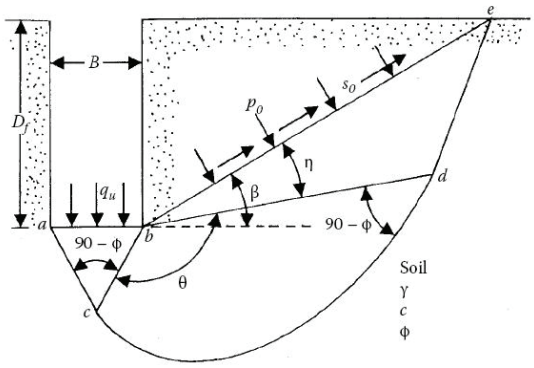

Figure 7: Plastic zones near rough shallow strip foundation according to Meyerhof's bearing capacity theory (Das, 2009).

Using the superposition method, the ultimate load is defined in the same way as was defined by Terzaghi (see Equation 5). However, the values for the bearing capacity factors Nc, Nq and Nγ are now depending on the depth and shape of the foundation as well as the friction angle of the soil and the roughness of the base. The values Nc and Nq are derived when $\varphi \neq 0$, $\gamma = 0$, $p' \neq 0$, $c \neq 0$; and the values for Nγ are derived by trial and error when $\varphi \neq 0$, $\gamma \neq 0$, $p' = 0$, $c = 0$. The corresponding values for these factors are shown in Equation 10 for Nc, Equation 11 for Nq and Equation 12 for Nγ. The complete derivation of the equations can be found in Terzaghi (1943) or Das (2009).

$$N_c = (\frac{(1 + sin\varphi) * e^{2\theta tan\varphi}}{1 - sin\varphi * sin(2\eta + \varphi)} - 1)cotan\varphi \tag{10}$$

$$N_q = \frac{(1 + sin\varphi) * e^{2\theta tan\varphi}}{1 - sin\varphi * sin(2\eta + \varphi)} \tag{11}$$

$$N_\gamma = \frac{4 * P_{p\gamma} * sin(45 + \frac{\varphi}{2})}{\gamma B^2} - \frac{1}{2}tan(45 + \frac{\varphi}{2}) \tag{12}$$

Figure 8 shows the variation of the bearing capacity factors Nc, Nq and Nγ according to the proposals given by Meyerhof (1951).

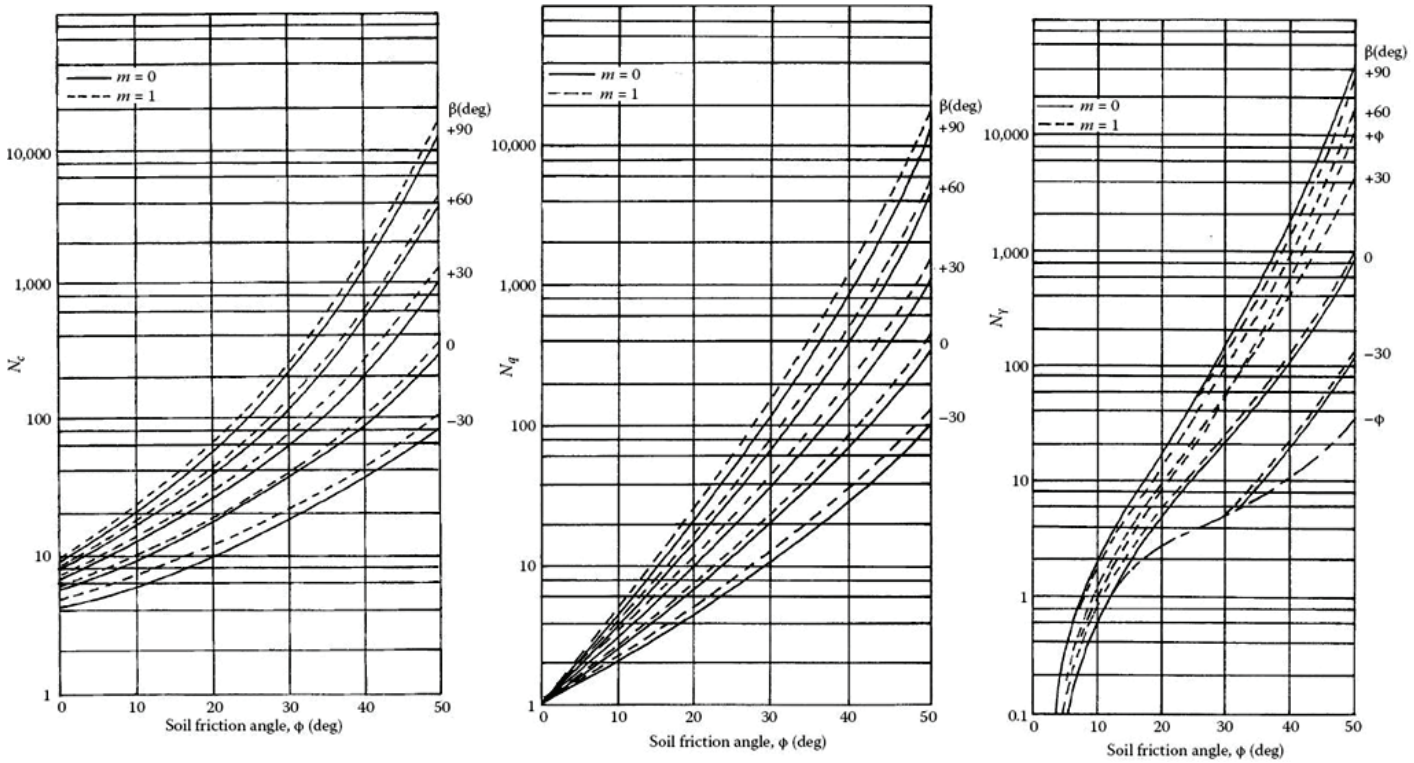

Figure 8: Meyerhof's bearing capacity factors (Meyerhof, 1951).

For a surface condition ($\beta = 0$, $\eta = 45\text{-}\varphi/2$, $\theta = \pi/2$), the expressions for Nc and Nq given above, are transformed to the ones shown below in Equation 13 and Equation 14. Both equations coincide with the ones given by Prandtl (1921) and Reissner (1924) in Equation 2 and Equation 3. Then, in 1963, Meyerhof gave a simplified expression for $N\gamma$ that is shown in Equation 15.

$$N_q = \frac{1 + sin\varphi}{1 - sin\varphi} * e^{\pi * tan\varphi} \tag{13}$$

$$N_c = (N_q - 1) * cotan\varphi \tag{14}$$

$$N_\gamma = (N_q - 1) * tan(1.4\varphi) \tag{15}$$

Figure 9 shows the bearing capacity factors expressed in equations (13), (14) and (15) for strip foundations and the partly theoretical and partly semi-empirical factors for circular or square footings. Meyerhof (1963) suggested that theoretical bearing capacity factors for rectangular foundations with a side ratio of B/L can be estimated by interpolating between the factors for strips (B/L = 0) and circles (B/L = 1) in direct proportion to the radio B/L. Alternatively, the bearing capacity factors for rectangles can be obtained multiplying the factors in Equation 5 for strip foundations by the corresponding empirical shape factors shown below in Equation 16 and Equation 17.

$$s_c = 1 + 0.2tan^2(\frac{\pi}{2} + \frac{\varphi}{2}) * B/L \tag{16}$$

$$s_q = s_\gamma = 1 \, when \, \varphi = 0^o$$

$$s_q = s_\gamma = 1 + 0.1 * tan^2(\frac{\pi}{2} + \frac{\varphi}{2}) * B/L \, when \, \varphi = 10^o \tag{17}$$

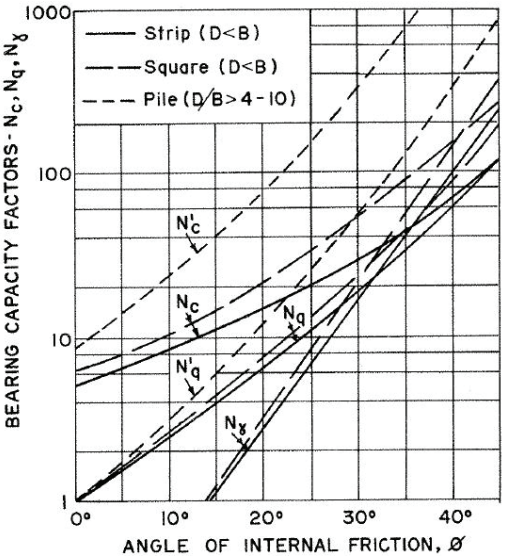

Figure 9: Bearing capacity factors for spread and pile foundation (Meyerhof, 1963).

Meyerhof (1963) affirms that for values of the angle of internal friction higher than 30°, the experimental factor Nγ for circular or square foundations is smaller than that for strip foundations, whereas the opposite result is expected from bearing capacity theory. This is due to the influence of the intermediate principal stress which under strip foundations increases the experimental bearing capacity for large friction angles above the theoretical value. For that reason, the same author suggest to use a triaxial compression test to determine the shear strength parameters for circular or square footings and a plane strain compression tests to determine the parameters for strip foundations.

1.4. Other proposals for the bearing capacity factors

In the geotechnical engineering practice and its applications for calculation of the ultimate bearing capacity of shallow continuos rough foundations, three aspects are generally accepted:

(a) The method of superposition by Terzaghi (1943) where the bearing capacity is represented as the sum of three terms due to cohesion, overburden and weight of soil (Equation 5).

(b) The failure surface shown in Figure 10 which is a modification, according to experimental results, of the one proposed by Terzaghi (1943).

(c) The equations for the bearing capacity factors, Nq (overburden term) and Nc (cohesion term), derived by Prandtl (1921) and Reissner (1924), which also coincide with the solutions given by Meyerhof (1951).

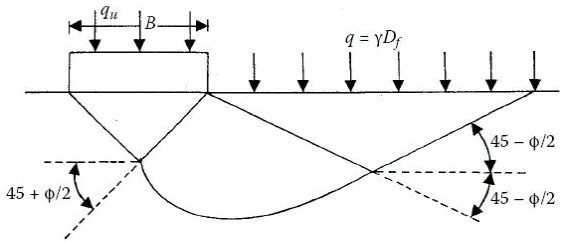

Figure 10: Modified failure surface in soil supporting a shallow foundation at ultimate load (Das, 2009).

The value that takes into account the effect of the weight of soil, Nγ, is the one that gives more uncertainties. In the literature, many authors proposed different approximation for estimating the Nγ value. Das (2009) says that the primary reason several theories for Nγ were developed, and their lack of correlation with experimental value, lies in the difficulty of selecting a representative value of the soil friction angle for computing the bearing capacity. The soil friction angle depends on factors like the intermediate principal stress condition, the friction angle anisotropy and the curvature of the Mohr-Coulomb failure envelope.

Another important reason for the various expressions for Nγ found in the literature is the different assumptions in the method of characteristics regarding the geometry of the part of the collapse mechanism located immediately below the footing base (active or rigid wedge) (Loukidis and Salgado, 2009).

Some of these proposals are discussed in the following paragraphs. They are based on the three aspects generally accepted in practice for calculation of the ultimate bearing capacity commented before and some additional-specific modifications.

1.4.1. Brinch-Hansen's bearing capacity formula (1961 and 1970)

In 1961, Brinch-Hansen proposed a modification to the bearing capacity formula proposed by Terzaghi (1943). This modification consists of including shape factors *s*, depth factors *d* and inclination factors *i*, as is shown in Equation 18.

$$q_u = c * N_c * s_c * d_c * i_c + p' * N_q * s_q * d_q * i_q + \frac{\gamma * B}{2} * N_\gamma * s_\gamma * d_\gamma * i_\gamma \quad (18)$$

where the Nq and Nc factors are calculated with Equation 2 and Equation 3; and the Nγ factor is calculated with Equation 19 based on the calculations done by Lundgren-Mortensen for vertical load on heavy earth Figure 11. The curves for all the three factors are shown in Figure 12.

$$N_\gamma = 1.5 * (N_q - 1) * tan\varphi \quad (19)$$

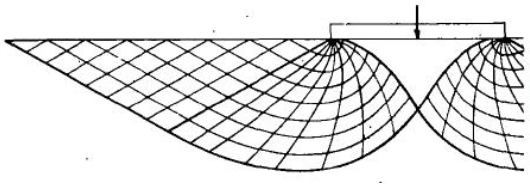

Figure 11: Lundgren-Mortensen rupture figure for calculation of Nγ. Vertical load on heavy earth (no surface load) (Brinch-Hansen, 1970).

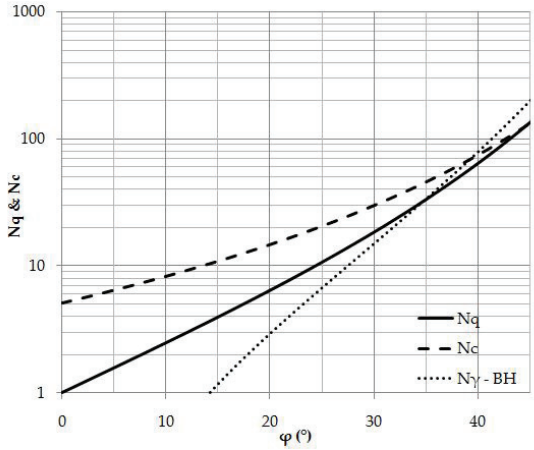

Figure 12: Bearing capacity factors Nq, Nc and Nγ as functions of φ (Adapted from Brinch-Hansen, 1970).

In 1970, Brinch-Hansen extended the formula for bearing capacity including base inclination factors *b* and ground inclination factors *g*, to be applied as the ones shown in Equation 18. From his publication, the formulas for the shape factors are of special interest due to the topic of analysis of the current study. In addition, the case of analysis of the present report is a shallow foundation under vertical loading applied on a horizontal base and horizontal ground. Therefore, following Brinch-Hansen formulations, the Equation 18 will be as in Equation 20 with the shape factors defined as Equation 21, 22 and 23.

$$q_u = c * N_c * s_c + p' * N_q * s_q + \frac{\gamma * B}{2} * N_\gamma * s_\gamma \tag{20}$$

$$s_c = 1 + N_q/N_c * B/L \tag{21}$$

$$s_q = 1 + sin\varphi * B/L = 1 + tan\varphi * B/L \tag{22}$$

$$s_\gamma = 1 - 0.4 * B/L \tag{23}$$

The formulas recommended by Brinch-Hansen (1970) for the shape factors are based on the experimental work done by De Beer (1970) for s_q and s_γ. More about this is commented in Chapter 2. The formulas for the shape factors presented before were also recommended by Vesić (1973), with a modification in the relationship for calculation of the Nγ bearing capacity factor. His solution is presented in Equation 24.

$$N_\gamma = 2 * (N_q + 1) * tan\varphi \tag{24}$$

1.4.2. Michalowski's bearing capacity proposals (1997 and 2005)

Michalowski (1997) made an estimation of the bearing capacity coefficient Nγ for a strip footing using the kinematical approach of limit analysis (upper bound limit analysis theorem). In this approach, the coefficients Nc and Nq were assumed as the existing proposals of Prandtl (1921) and Reissner (1924) and the coefficient Nγ was found making the c = 0 and q = 0. This causes that the geometry of the mechanism for which Nγ reaches its minimum is no longer consistent with the adopted coefficients Nc and Nq. However, the upper-bound approach was applied taking each term minimum in Equation 5.

The rigid-block mechanism used by Michalowski (1997) to estimate the best upper bound to the true limit load of the bearing capacity calculations is shown in Figure 13. The Equation 25 is the expression for the Nγ proposed by him.

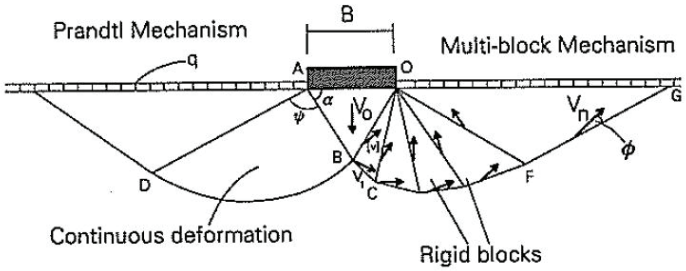

Figure 13: Prandtl mechanism with continual deformation and the rigid-block collapse pattern (Michalowski, 1997).

$$N_\gamma = e^{0.66+5.11tan\varphi} * tan\varphi \tag{25}$$

In 2005, Zhu and Michalowski proposed shape factors for limit loads on square and rectangular footings based on the elastoplastic model of the soil and Finite Element (FE) analysis. Their corresponding results are going to be commented in Chapter 2.

1.4.3. Loukidis and Salgado's bearing capacity proposals (2009)

Loukidis and Salgado (2009) used FEM to determine the vertical bearing capacity of strip and circular footings resting on a sand layer. The analyses were performed using an elastic-perfectly plastic Mohr-Coulomb constitutive model and the effect of the dilatancy angle on the footing bearing capacity was investigated using an associated ($\varphi = \psi$) and a non-associated flow rule ($\psi < \varphi$). The focus of the study was the values of the bearing capacity factors Nq and Nγ and the shape factors for circular footings, which results are discussed in Chapter 2.

The collapse mechanisms obtained for strip footing in the cases of associative and non-associative soil are shown in Figure 14. These collapse mechanisms are also compared against the mechanism yielded by Martin's ABC program (Martin, 2003) which makes use of the method of characteristics to solve the bearing capacity problem. It should be pointed out that the collapse mechanism for the $\varphi = \psi$ case is larger than the one for $\psi < \varphi$; also, the deformation in the non-associated cases is highly localized in thin shear bands, while in the associated flow cases, the plastic strains are more diffused inside the mechanism. According to Loukidis and Salgado (2009), the intense shear banding when $\psi < \varphi$ is a direct consequence of the apparent softening and energy release exhibited by a material with a non-associative flow rule.

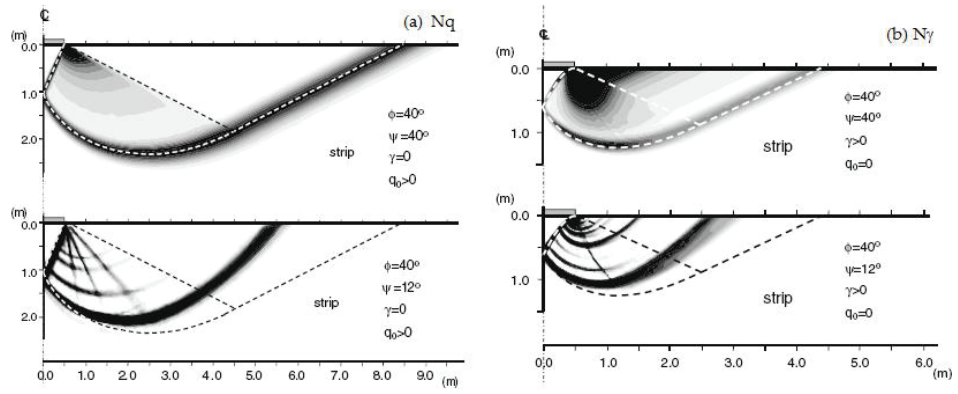

Figure 14: Collapse mechanism as maximum shear strain increments compared against the mechanism yielded by Martin's ABC program (dashed lines) for strip footings on: (a) $\gamma = 0$ and $p' \neq 0$ and (b) $\gamma \neq 0$ and $p' = 0$ (Loukidis and Salgado, 2009).

The results for the bearing capacity factors Nq and Nγ proposed by Loukidis and Salgado (2009) are shown in Equation 26 and Equation 27 which include the value defined in Equation 28. These equations incorporate the dilatancy angle in order to take account of the associative and non–associative flow rule.

$$N_q = \frac{1 + sin\varphi}{1 - sin\varphi} * e^{F(\varphi,\psi)*\pi*tan\varphi} \tag{26}$$

$$N_\gamma = (N_q - 1) * tan(1.34\varphi) \tag{27}$$

$$F(\varphi,\psi) = 1 - tan\varphi * (tan(0.8 * (\varphi - \psi)))^{2.5} \tag{28}$$

The last set of equations modify the bearing capacity factors as functions of both φ and ψ, considering realistic pairs of φ and ψ values suitable for sands (or frictional materials). New equations are also proposed by the same authors applied to shape factors s_q and s_γ for circular footings based on FE analysis results. These results are commented in Chapter 2.

1.4.4. Other proposals for bearing capacity factors

Some other approaches has been discussed in the literature for the bearing capacity factor Nγ. Lundgren and Mortensen (1953) developed numerical methods (using the theory of plasticity) for the exact determination of rupture lines as well as the bearing capacity factor Nγ for particular cases. Chen (1975) used the upper bound limit analysis theorem suggested by Drucker and Prager (1952) to give a solution for Nγ. The following relationship for Nγ was also recommended by Biarez *et al.* (1961):

$$N_\gamma = 1.8 * (N_q - 1) * tan\varphi \tag{29}$$

The slip line method was used by Booker (1969) to obtain numerical values of Nγ. The expression in Equation 30 was suggested by Poulos *et al.* (2001) as an approximation of these numerical results.

$$N_\gamma = 0.1045 * e^{9.6\varphi} \; with \; \varphi \; in \; radians \tag{30}$$

A numerical analysis solution for Nγ was approximated by Hjiaj *et al.* (2005) and it is shown in Equation 31.

$$N_\gamma = e^{\frac{1}{6}*(\pi+3\pi^2 tan\varphi)} * (tan\varphi)^{\frac{2\pi}{5}} \tag{31}$$

Martin (2005) used the method of characteristics to obtain the variations of Nγ. Salgado (2008) approximated these variations with Equation 32.

$$N_\gamma = (N_q - 1) * tan(1.32\varphi) \tag{32}$$

Figure 15 summarizes the different proposals for the Nγ bearing capacity factor mentioned before. It can be seen that the proposals made by Biarez *et al.* (1961) and Michalowski (1997) give values higher than the other ones because they are upper bound solutions. The curves for Meyerhof's and Brinch-Hansen's are virtually co-incident for φ < 30° and diverge only marginally as φ approaches 60°. However, the different proposals follow the same tendency with some more dispersion between the equations for lower friction angles.

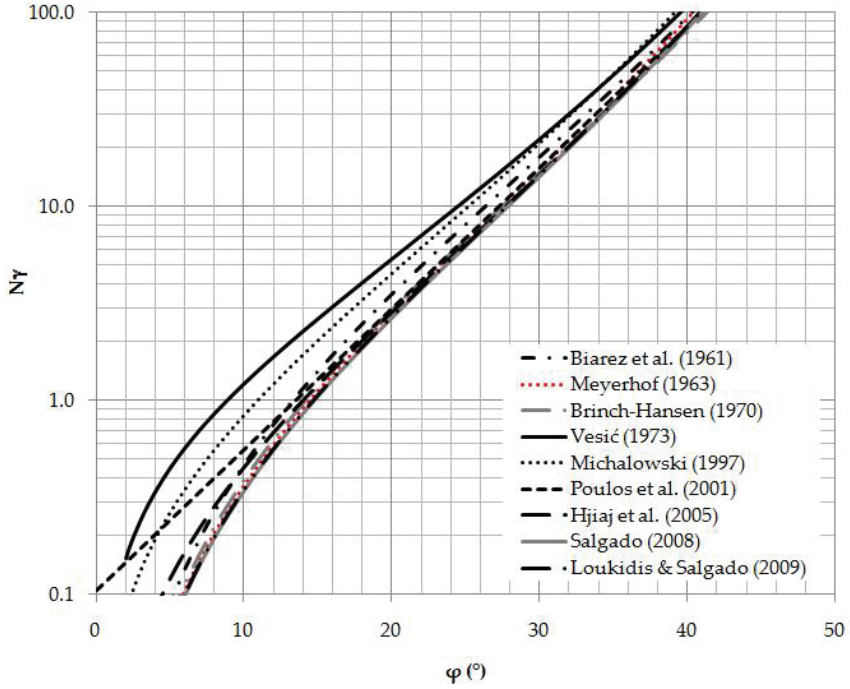

Figure 15: Comparison of the bearing capacity Nγ as function of φ.

1.5. General bearing capacity equation

The bearing capacity equation proposed by Terzaghi (Equation 5) refers to continuous (strip) foundations. In order to take account of the effect of rectangular foundations (that is, B/L > 0 where B = width and L = length) and the effect of the depth of the foundation on the increase in the ultimate bearing capacity, a general equation for vertical loading may be written as in Equation 33. It includes shape factors (s_c, s_q and s_γ) and depth factors (d_c, d_q and d_γ) that are available in literature. More about the shape factors is discussed in Chapter 2.

$$q_u = c * N_c * s_c * d_c + p' * N_q * s_q * d_q + \frac{\gamma * B}{2} * N_\gamma * s_\gamma * d_\gamma \quad (33)$$

1.6. Norwegian bearing capacity approach

The Norwegian assessment of the bearing capacity problem focuses on the stress condition in the soil under a foundation load. The foundation is placed on the surface or buried to moderate depths in a horizontal terrain defining the foundation level.

In the case of a weightless soil and centric load, the effective vertical stress at foundation level outside the foundation of the soil is p′ and may be caused by loads on the terrain surface or by the weight of the soil above the foundation level. As the foundation stress, σ'_v, is applied, it will first balance p′ at which time the stresses in the soil are practically equal to the initial stress before loading began. A further increase of σ'_v can be done only if the soil has sufficient shear stress capacity that can be mobilized through the stress fields (Emdal and Grande, 2006).

In an effective stress analysis (aφ-analysis) for centric vertical load and weightless soil, the major principal stress immediately under the foundation is vertical (σ'_v). It is an active Rankine stress field that tends to compress vertically and extend horizontally. Outside the foundation, the vertical stress p′ is the minor principal stress and act on a passive Rankine stress field. From

the active to the passive field, the principal stresses are rotated 90° and connected by a Prandtl stress field. Figure 16 shows the stress field combination for the case of bearing capacity discussed.

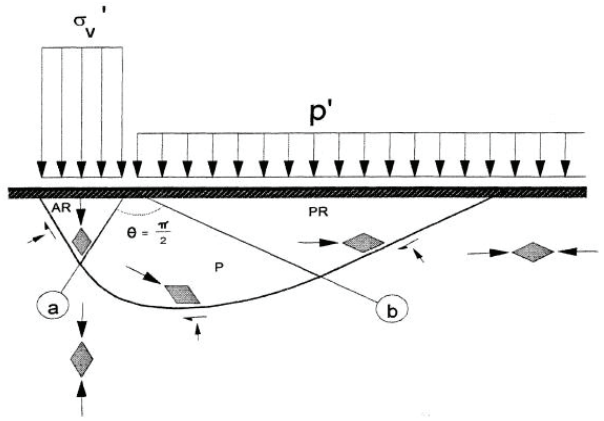

Figure 16: Stress field combination for bearing capacity under centric vertical load, in effective stress analysis (Emdal and Grande, 2006).

When the soil density effects are taking into account for the bearing capacity analysis, the stress level in all elements in the soil, the shear zone geometry and in general the bearing capacity are influence by the stress increase with depth as a result of $\gamma \neq 0$. Therefore, the stress fields cannot be superimposed. For that reason, approximated solutions have been developed by the method of characteristics.

In the method of characteristics, a solution for cohesionless soil (a = 0) has been obtained showing that the foundation pressure is nearly linearly increasing from the outer foundation border $\gamma'*N\gamma$ and inwards (for an infinitely wide foundation as shown in Figure 17a). When a finite width foundation is analyzed, this pressure model should be combined and it forms a triangular stress distribution of the foundation pressure (Figure 17b).

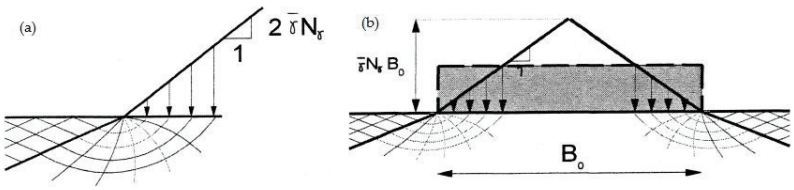

Figure 17: Bearing capacity solution taking soil density effects: (a) Based on the method of characteristics, (b) Combination of stress field by the method of characteristics (Emdal and Grande, 2006).

Therefore, the total foundation pressure (Equation 34) is obtained as the sum of the solution for weightless soil (first term in Equation 34) and the solution for the soil density effect (second term in Equation 34). It should be noted that the cohesion term is implicit in the formula in the form of the attraction a, where $a = c/tan\varphi$. Figure 18 shows the variation of the bearing capacity factors Nq and Nγ following the Norwegian analysis approach of the bearing capacity.

$$\sigma'_v + a = N_q * (p' + a) + \tfrac{1}{2} * \gamma' * N_\gamma * B \tag{34}$$

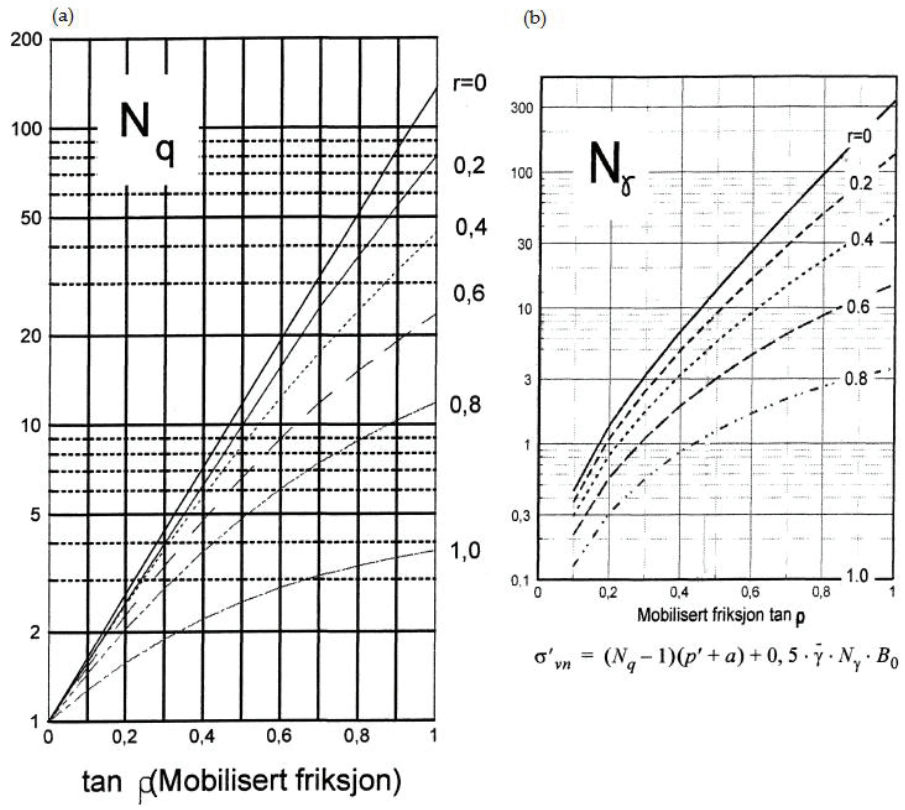

Figure 18: Bearing capacity factors (a) Nq and (b) Nγ, in effective stress analysis. As a result of the analysis for centric vertical load, the curves to use are the ones for r = 0 which means no shear stresses on the foundation interface (Emdal and Grande, 2006).

The analysis presented before assumed plane strain conditions, which means it applies for strip loading, and surface loading. In case of different geometries and deep seated foundation, some correction factors should be used for depth (D/B) and area-shape (B/L). More about the Norwegian recommendations for area-shape factors in an effective stress analysis are discussed in Chapter 2.

1.7. General practice in design of footings: drained bearing resistance

The drained ultimate bearing capacity of a spread foundations has traditionally been calculated from the Terzaghi formula (Equation 18). The overburden (surcharge) and cohesion factors (Nq and Nc) are calculated following the formulas given by Prandtl (1921) and Reissner (1924) (Equation 2 and Equation 3), which are in terms of the soil's friction angle.

Regarding the $N\gamma$ value, more discrepancies appear in deciding which value should be used. Traditionally in Europe, the Brinch-Hansen's Equation (Equation 19) is used. In America, designers typically employ Meyerhof equation (Equation 15). For offshore structures, engineers use Vesić's equation (Equation 24). In Eurocode 7, Chen's (1975) equation, which is similar to Equation 29 but changing the 1.8 value for 2.0, is proposed as an conservative alternative to Vesić's Equation but significantly more optimistic than Brinch-Hansen's, particularly at large angles of shearing resistance (Bond and Harris, 2008).

For taking account of the dimensionless factors for the bearing resistance, the inclination of the foundation base, the shape of foundation and the inclination of the load, the Eurocode 7 suggests that the calculation of the bearing resistance can be done using an analytical method that uses approximate equations derived from plasticity theory and experimental results. The formula proposed follows the Brinch-Hansen approach (Equation 18). More about these factors from Eurocode 7 are discussed in Chapter 2.

1.8. Effect of associative and non-associative flow rule in bearing capacity calculations

Theoretical approaches, like the method of characteristics or rigorous limit analysis, for computing the bearing capacity of shallow foundations assume a soil following an associated flow rule. This means that the methods apply to

soils with a dilatancy angle ψ equal to the friction angle φ, although in reality it is well known that ψ is significantly lower than φ for frictional soils (Loukidis and Salgado, 2009).

Taking the Coulomb's yield condition and the flow rule, the dilatancy is defined as the property causing that any plastic deformation of Coulomb material must be accompanied by an increase in volume if $\varphi \neq 0$ (Chen, 1975).

The basic theorems of limit analysis require this particular connection between yield condition and flow rule for mathematical convenience. It is a standard in rigorous limit analysis, since only for the normality rule the upper- and lower-bound theorems can be proven true (Michalowski, 1997). Therefore, the limit load for associative material is unique. However, when real soils are modelled as rigid perfectly plastic solids, do not obey the associative flow rule and the limit load is no longer unique. The only information available is that a non-associative material cannot be stronger that the associative one (Drescher and Detournay, 1993).

Michalowski (1997) studied the influence of the flow rule on bearing capacity coefficients. Using a technique devised by Drescher and Detournay (1993), he included the non-associativity of the soil deformation into a kinematical approach of limit analysis. The proposal was to modify the cohesion and the friction angle using a factor that includes the dilatancy angle, assuming the material to be coaxial and non-associative (coaxiality: principal directions of the stress tensor coincide with the principal directions of the strain-rate tensor). The new cohesion c* and friction angle φ* will be as indicated in Equation 35 and Equation 36.

$$c* = \frac{cos\varphi * cos\psi}{1 - sin\varphi * sin\psi} \tag{35}$$

$$tan\varphi* = \frac{cos\varphi * cos\psi}{1 - sin\varphi * sin\psi} * tan\varphi \tag{36}$$

Therefore, when $\psi < \varphi$, the bearing capacity can still be calculated with Terzaghi's formula (Equation 5) with c replaced by c* (when c* < c), and, with coefficients Nc, Nq and Nγ obtained using φ replaced by φ* (when φ* < φ). The resulting bearing capacity is reduced.

Figure 19 shows the effect of dilation angle on coefficient Nγ for rough footings derived by Michalowski (1997). It can be seen that the non-associativity has a negligible effect on Nγ for an internal friction angle below 25°, but the effect becomes more significant for larger φ.

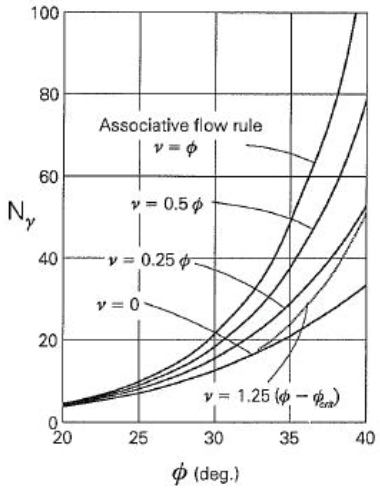

Figure 19: The effect of dilation angle on coefficient Nγ for rough footings derived by Michalowski (1997).

Significant differences in estimations of bearing capacity factors originate from accounting for or not the non-associativity of the plastic soil deformation. These differences become very substantial for large φ. For a given φ, coefficient Nγ drops significantly with a decrease in the dilation angle (Michalowski, 1997).

Some other researchers have used the FEM and FDM to calculate the bearing capacity of smooth or rough strip footings on non-associative elastoplastic soils (Zienkiewicz *et al.*, 1975; de Borst and Vermeer, 1984; Mizuno and Chen, 1990; Frydman and Burd, 1997; Yin *et al.*, 2001) concluding that the ultimate bearing capacity is affected by the dilation angle ψ. This effect influences the three bearing capacity factors Nc, Nq and Nγ, and it is more notorious for higher friction angles and lower dilatancy angles (increase in non-associativity). These results confirm the previous findings on Michalowski (1997).

More recent research done by Erickson and Drescher (2002), and, Zhao and Wang (2009) for circular footings confirm the behaviour that was also found for strip footings: the bearing capacity factors gradually decrease with the decrease of ψ (increase in non-associativity).

According to Loukidis and Salgado (2009), some typical characteristics can be identified when numerical simulations of bearing capacity problem including the non-associated flow rule have been performed:

a) The analysis with a non-associated flow rule produce a load-displacement curves that oscillate as the collapse load (peak load) is approached and after its attainment. This oscillations has been observed in previous studies when the Mohr-Coulomb is used as constitutive model and $\psi < \varphi$ (de Borst and Vermeer, 1984; Manoharan and Dasgupta, 1995; Yin and Wang, 2001; Erickson and Drescher, 2002). However, the oscillations do not undermine the validity of the numerical simulations; the only problem is the choice of the collapse load value.

b) The collapse mechanism is larger for the $\psi = \varphi$ than the one for $\psi < \varphi$, as was seen in Figure 14 and also discussed in previous studies (de Borst and Vermeer, 1984; Manoharan and Dasgupta, 1995; Potts and Zdravkovic, 1999; Yin and Wang, 2001; Erickson and Drescher, 2002). Furthermore, the deformation in the non-associated flow cases is highly localized in thin shear bands, while, in the associated flow cases, the plastic strains appear to be more diffused inside the mechanism.

Finally, Loukidis and Salgado (2009) conclude that the effect of flow rule non-associativity on bearing capacity is important. There are differences of 5% to 45% between the non-associated and associated flow rule cases. The larger values correspond to strip footings and high friction angles. Therefore, assuming $\psi = \varphi$ can produce no conservative results.

Chapter 2

The relative footing dimension in the bearing capacity problem: literature study

The bearing capacity equation proposed by Terzaghi (Equation 5) is for a continuous (strip) footing. In a strip foundation, the length, L, is assumed to be large in comparison with the width, B, of the foundation. The foundation is an infinite strip of width B for B/L < 0.2.

When the Equation 5 is used to calculate the bearing capacity of square or rectangular footings (or when B/L > 0.2); the components of Equation 5 should be modified by factors s_c, s_q and s_γ like in Equation 37, rewritten in Equation 38 using Equation 14. From now, the Equation 38 is the one that is used for future analysis.

$$q_{ult} = s_c * c * N_c + s_q * p' * N_q + s_\gamma * \tfrac{1}{2} * \gamma' * B * N_\gamma \tag{37}$$

$$q_{ult} = s_q * (p' + a) * N_q + s_\gamma * \tfrac{1}{2} * \gamma' * B * N_\gamma - a \tag{38}$$

These factors are called shape factors or shape modifiers. There is a considerable amount of literature regarding experimental and theoretical studies dedicated to the them (Golder, 1941; Meyerhof, 1963; Brinch-Hansen, 1970; De Beer, 1970; Bolton and Lau, 1993; Michalowski, 2001; Erickson and Drescher, 2002; Lyamin *et al.* 2007; Puzakov *et al.*, 2009).

Previous proposals of these factors are based on empirical and semi-empirical considerations, because three dimensional bearing capacity computations could not be performed with any degree of accuracy. In the following sections, more about the shape factors old and new proposals are discussed as a background for the numerical calculations performed in the present study.

2.1. Earlier proposals for shape factors based on non-numerical computations

Terzaghi (1943), Meyerhof (1963) and De Beer (1970) proposed different equations for the shape modifiers based on empirical and semi-empirical considerations leading to conflicting results. For example, for $\varphi = 15°$, Meyerhof's proposal indicates an increase in factor s_γ with a decrease in aspect ratio L/B, whereas De Beer's suggestion is quite the opposite and independent of φ. These opposite trends persist for all internal friction angles $\varphi > 0$ (Zhu and Michalowski, 2005).

In Chapter 1, it was presented that Terzaghi (1943) suggested the factors $s_c = 1.3$; $s_q = 1.0$ and $s_\gamma = 0.8$ for square and circular foundations justified in the absence of plane strain conditions for these cases. According to Zhu and Michalowski (2005), these factors were based on the test of Golder (1941) and some unpublished data, taking the factor $s_c = 1.3$ from Golder's test on clay with square and rectangular model footings (calculated as the ratio of the ultimate pressure under 3x3 inches model footings to the pressure under 18x3 inches footings) and the factor $s_\gamma = 0.8$ from Golder's largely scattered experimental results on sand with footings of 6 in. in width with aspect ratios from 1 to 5. However, Terzaghi (1943) took the most unfavourable test results as basis for the provisional equation and ignored the possible influence of the internal friction angle on the shape factors. After studying Golder's (1941) results and Terzaghi (1943) proposals, Zhu and Michalowski (2005) concluded that small-scale testing for influence of the soil weight on the bearing capacity is not likely to be representative of large prototypes.

Other approaches mentioned in Chapter 1 are the proposed by Meyerhof (1963) and De Beer (1970). About Meyerhof (1963), it was shown in Figure 9 the bearing capacity factors for strip foundations and for circular or square footings. The same author suggested that theoretical bearing capacity factors for rectangular foundations with a side ratio of B/L can be estimated by interpolating between the factors for strips (B/L = 0) and circles (B/L = 1) in direct proportion to the radio B/L. Alternatively, shape modifiers in Equation 16 and Equation 17 were proposed for rectangular footings.

On the other hand, De Beer (1970) performed experimental work based on the proposal of the bearing capacity formula of Brinch-Hansen (1961) for centrally vertical loaded footings (Equation 20). The aim of the tests was to determine the expression of the shape factors s_q and s_γ of sand. Then, Brinch-Hansen (1970) and by Vesić (1973) recommended the shape factors proposals of De Beer (1970) that were defined in Equations 21, 22 and 23.

The Meyerhof (1963) and De Beer (1970) proposals for the shape factors indicate large discrepancies, as under some circumstances, one suggests increasing the shape factor s_γ with the decrease in the footing aspect ratio, whereas the other recommends just the opposite, like is shown in Figure 20 (Zhu and Michalowski, 2005).

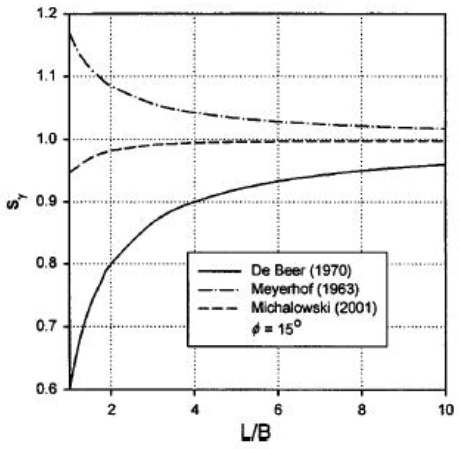

Figure 20: Inconsistencies in earlier proposals for shape factors (Zhu and Michalowski, 2005).

Michalowski (2001) used the upper-bound approach of limit analysis for constructing a three-dimensional failure mechanism for rectangular and square footings on frictional materials. The method of solution applied was based on the one used by Shield and Drucker (1953) for clays in undrained conditions. The geometry of the failure mechanism was approximated by four regions each with a plane-strain deformation.

It was unexpected by Michalowski (2001) to find that the least upper-bound estimates of loads on square footings occur for mechanisms with no symmetry with respect to diagonal planes, like the ones shown in Figure 21.

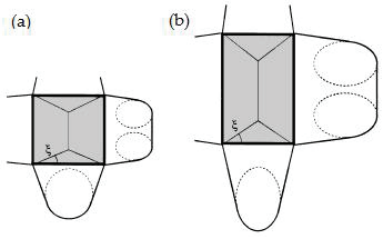

Figure 21: Failure patterns for (a) square and (b) rectangular footings (Michalowski, 2001).

The shape factors found by Michalowski (2001) are shown in Figure 22. These factors approach unity with an increase in the footing aspect ratio L/B, are typically larger than earlier empirical proposals in the literature and are very strongly dependent on the internal friction of the soil. For large internal friction angles, the shape factors are rapidly increasing when the footing aspect ratio L/N drops down to 1, whereas for small internal friction angles the increase is much smaller (Michalowski, 2001).

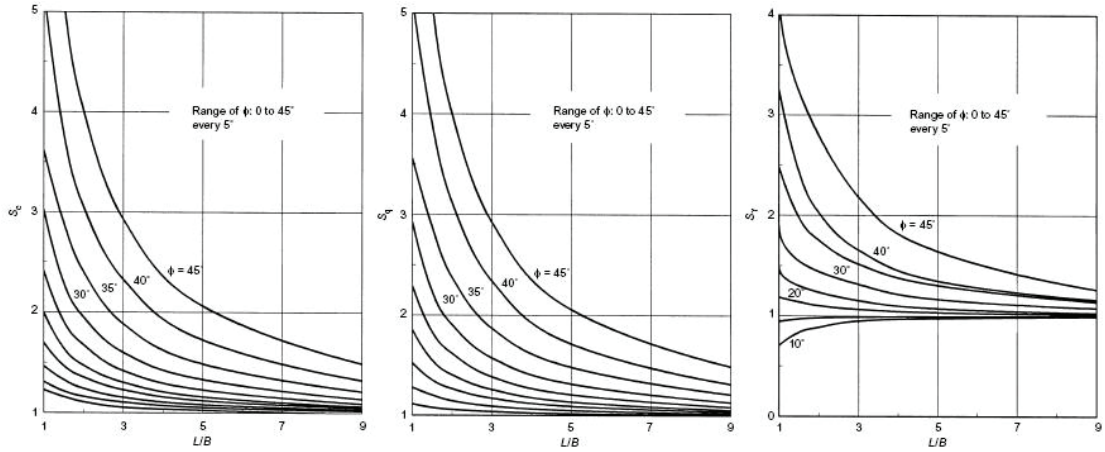

Figure 22: Shape factors (a) s_c, (b) s_q and (c) s_γ for rectangular footings (Michalowski, 2001).

Michalowski (2001) affirms that it is expected that an improvement in solutions for square and rectangular footings can be obtained by employing numerical techniques, such as FEM, which do not explicitly constrain the pattern of deformation.

2.2. Some new proposals for shape factors based on numerical computations

Zhu and Michalowski (2005) suggested new equations for the earlier proposals of the shape factors based on the elastoplastic model of the soil and FE analysis. The FE system ABAQUS was used to arrive at the limit loads (bearing capacity) of square and rectangular footings. One quarter of the footing (using symmetry) with 18 soil elements under it was modelled. It was pointed out by the authors that refinements of the mesh does produce slightly lower (better results). However, the shape factors are the ratios of the bearing capacity coefficients for the respective rectangular footing to those for the strip footing. Therefore, there are less sensitive to the mesh size than the bearing capacity factors. Figure 23 shows the FE mesh used in this study.

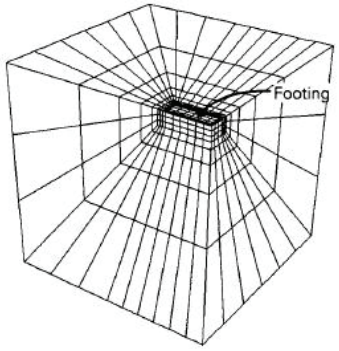

Figure 23: Finite Element mesh (Zhu and Michalowski, 2005).

The Mohr-Coulomb soil model was used and the computations were done for dilatancy angle ψ equal to the friction angle φ. The last assumption was justified by the authors in the fact that one of the objectives was to validate or

disprove the existing shape factors at that time, which are based on the normality rule (associative flow rule). The bearing capacity for rectangular footings was calculated for a range of footing aspect ratio from 1 to 5 and the internal friction angle spanning from 0° to 40°. Figure 24 illustrates the results got by Zhu and Michalowski (2005) for the shape factors s_c, s_q and s_γ.

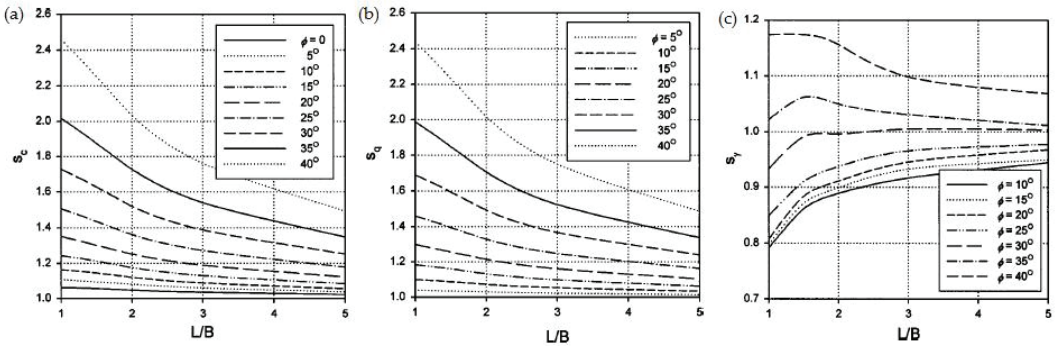

Figure 24: Shape factors (FEM) as function of aspect ratio L/B: (a) factor s_c, (b) factor s_q and (c) factor s_γ (Zhu and Michalowski, 2005).

The factors shown in Figure 24 can be approximated by the formulas presented below (Equation 39 for s_q, Equation 40 for s_c and Equation 41 for s_γ) that are depending on the friction angle and the relation B/L.

$$s_q = 1 + 1.9 * tan^2\varphi * \sqrt{B/L} \tag{39}$$

$$s_c = 1 + (1.8 * tan^2\varphi + 0.1) * \sqrt{B/L} \tag{40}$$

$$\begin{cases} s_\gamma = 1 + (0.6 * tan^2\varphi - 0.25) * B/L \, when \, \varphi \leq 30^0 \\ s_\gamma = 1 + (1.3 * tan^2\varphi - 0.5) * L/B^{1.5} * e^{-(L/B)} \, when \, \varphi > 30^0 \end{cases} \tag{41}$$

The shape factors for s_c and s_q got by Zhu and Michalowski (2005) with FEM are significantly larger than the ones found by Michalowski (2001) with a kinematical approach. Specially those with small aspect ratios L/B and large friction angles. It was concluded that the bearing capacity and the shape factors calculated by Michalowski (2001) are considerable overestimated when compared to those calculated using FEM. On the other hand, the results partially agree with Meyerhof (1963) and De Beer (1970) estimations for s_c and

s_q. The authors recommend that these last estimations are acceptable and on the conservative side for footing design.

For the s_γ shape factor, Zhu and Michalowski (2005), later corroborated by Puzakov *et al.* (2009), found that s_γ may increase or decrease with the change in the aspect ratio as a function of the internal friction angle (Figure 24c). However, a particular behaviour for large friction angles was observed: the factor s_γ increases with the decrease in the aspect ratio, whereas the trend is opposite for small friction angles. This can be explained by the influence of the dilatancy angle in the extent of the failure mechanism. The larger the dilatancy angle (more associative material), the larger the extent of the plastic deformation field (because more work against the soil is done at failure). For small dilatancy angles, the volume of displaced soil for a square footing (per unit area of the footing) is smaller than that for a plane-strain footing (strip footing), whereas for large dilatancy angles this relation is the opposite.

One important finding of Zhu and Michalowski (2005) is that contrary to was said by (Michalowski, 2001), the collapse mechanism under a square footing has diagonal symmetry and the deformation in the regions adjacent to the four sides of the footing is not plane. For that reason, it was concluded that enforcing plane-strain deformation in the segments of the collapse mechanism used by Michalowski (2001) appeared to overestimate the bearing capacity of square and rectangular footings. Therefore, Figure 25 is adopted as the failure mechanism for square footings for small and large internal friction angle.

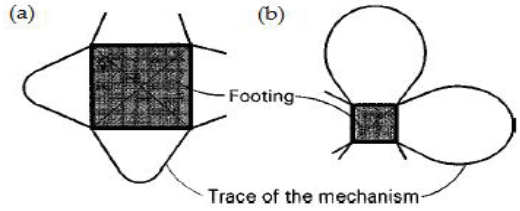

Figure 25: Failure mechanism for square footing: (a) small φ and (b) large φ (Zhu and Michalowski, 2005).

Other approaches to shape factors definition using FE have been done for clays by Salgado *et al.* (2004) and for sands by Lyamin *et al.* (2007). In these

studies, the bearing capacities of strip, circular, square and rectangular foundations in clay and frictional soils following an associated flow rule, are determined rigorously to propose definitive values of the shape and depth factors for foundations. The technique used was lower- and upper-bound limit analysis. Stress fields (in the case of lower bounds) and velocity fields (in the case of upper bounds) were optimised using non-linear optimisation techniques[2].

Concerning the shape factor, define as the ratio of the limit unit base resistance of a footing of any shape on the soil surface to that of a strip footing on the soil surface, the computations for both cases were performed for a rough soil-footing interface under centric vertical loads.

According to Salgado *et al.* (2004), the shape factors allow the conversion of values derived for strip footings to those appropriate for circular, square or rectangular footings. Footings of finite plane dimensions B and L have greater bearing capacity than strip footings with width B, this effect is due to the development of additional slip surfaces in front of and behind the footing.

The shape factor s_c proposed by Salgado *et al.* (2004) is defined in Equation 42. It does not depend on the friction angle; however, it varies with the depth to where the footing has been buried. Figure 26 illustrates this statement.

$$s_c = 1 + 0.12 * (B/L) + 0.17 * \sqrt{D/B} \tag{42}$$

[2] More about these techniques are discussed in Lyamin (1999); Lyamin and Sloan (2002a) and (2002b); and, Krabbenhøft *et al.* (2005).

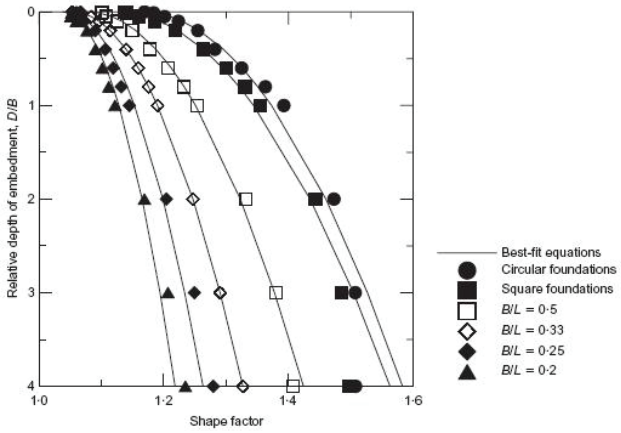

Figure 26: Shape factor s_c for foundations of various shapes as a function of relative depth (Salgado et al., 2004).

Using a very similar approach to Salgado *et al.* (2004), Lyamin *et al.* (2007) proposed the Equation 43 for the shape factor s_γ and Equation 44 for the shape factor s_q.

$$s_\gamma = 1 + (0.0336\varphi - 1) * (B/L) \tag{43}$$

$$s_q = 1 + (0.098\varphi - 1.64) * (D/B)^{0.7-0.01\varphi} * (B/L)^{1-0.16*(D/B)} \tag{44}$$

According to Lyamin *et al.* (2007), the results for the shape factor s_γ that resulted in Equation 43 present difficulties in finding physical generalizations. It can be greater or less than one, and increase or decrease with increasing B/L (Figure 27). For φ = 25° and φ = 30°, the shape factor s_γ is less than one and decreases with increasing B/L; whereas it is greater than one and increases with increasing B/L for φ = 35°- 45°. These results are 15-20% lower than the values of Erickson and Drescher (2002) obtained using FLAC for circular footings. Finally, the variation of s_γ is essentially linear for all φ considered, that coincides with the observations of Zhu and Michalowski (2005).

Figure 28 shows the variation of the shape factor s_q with B/L from where Equation 44 was derived. It depends on the friction angle and the depth to where the footing has been buried.

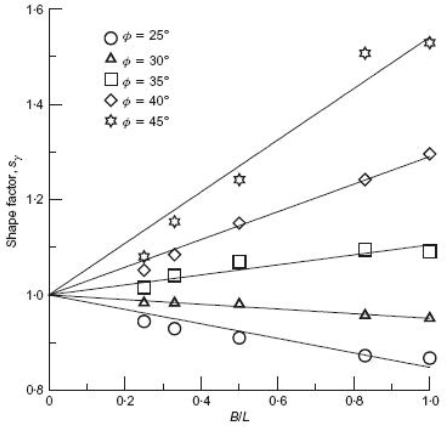

Figure 27: Variation of shape factor s_γ for surface footings with respect to B/L (Lyamin et al., 2007).

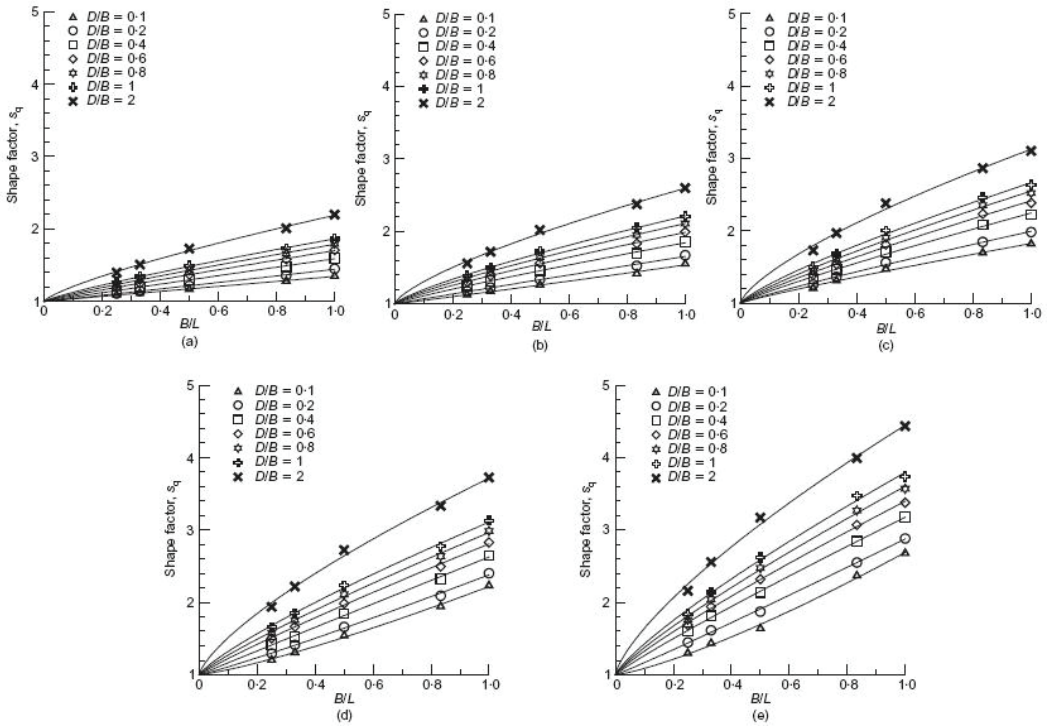

Figure 28: Shape factor s_q against B/L for various D/B ranging from 0.1 to 2 and: (a) φ = 25°; (b) φ = 30°; (c) φ = 35°; (d) φ = 40°; (e) φ = 45° (Lyamin et al., 2007).

One of the most recent publications about the bearing capacity factors Nq and $N\gamma$ and the shape factors s_q and s_γ has been done by Loukidis and Salgado (2009). In the study the FE code SNAC (Abbo and Sloan, 2000) was used. It helped to determine the vertical bearing capacity of strip and circular footings resting on a sand layer. The analyses used unstructured meshes consisting of 15-noded triangular elements and an elastic-perfectly plastic model following the Mohr-Coulomb failure criterion. Two series of analyses were performed, one using an associated flow rule and one using a non-associated flow rule.

The Equation 45 and Equation 46 show the proposals made by Loukidis and Salgado (2009) for the shape factors s_γ and s_q for circular footings. They follow the simplification assumed traditionally in foundation engineering where a square foundation (or square loaded area) can be approximated by the solution for a circular one, which is much easier to obtain because of the axial symmetry of the problem (Loukidis and Salgado, 2009). The resulting shape factor values were compared to the shape factor values based on limit analysis (Lyamin *et al.*, 2007) and the method of characteristics (Martin, 2003).

$$s_\gamma^{circ} = 1 + 0.26 * \frac{1+sin\varphi}{1-sin\varphi} - 0.73 \tag{45}$$

$$s_q^{circ} = 1 + 2.9 * tan^2\varphi \tag{46}$$

Loukidis and Salgado (2009) pointed out that the earlier proposals for the shape factor s_γ done by De Beer (1970) based on footing model tests and suggesting that s_γ is independent of the friction angle, predicts shape factor values that are always below unity, with $s_\gamma = 0.6$ for square or circular footings. In reality, the bearing capacity of square and circular footings with zero embedment is smaller than the bearing capacity of strip footings, although theoretical methods assuming a simple Mohr-Coulomb failure criterion suggest the opposite. This is because of the fact that the peak friction angle of the sand is lower in triaxial conditions (square/circular footings) than in plane strain conditions (strip footings), according to Meyerhof (1963) and discussed by Lyamin *et al.* (2007) and Salgado (2008). For that reason, Meyerhof (1963) suggested that, for the determination of the bearing capacity of strip footings, the peak friction angle value used in the calculations should be 10% higher than the peak friction angle for triaxial conditions.

It was concluded by Loukidis and Salgado (2009) that there is good agreement between the Finite Element results, rigorous limit analysis bounds and the method of characteristics solutions regarding the shape factors for circular footings. The factors s_q and s_γ always increase with increasing friction angle. However, equations for s_q and s_γ used in current practice seem to underestimate the rate of increase of these factors with φ.

2.3. Shape factors used in the general geotechnical engineering practice

Following the Norwegian approach of the bearing capacity analysis, Emdal and Grande (2006) affirm that for a foundation with limited length, L; the bearing capacity will increase slightly because there will be involved larger shear areas to contribute to the bearing capacity at the ends of the foundation. Also, the change from a strip footing to a square footing increases the kinematic freedom to form shear failure modes.

Theoretically, for an effective stress analysis the bearing capacity for square/circular footings caused by attraction, a, and the effective overburden, p', outside the foundation (the Nq part) may increase up to 20% for vertical load cases. However, there are indications that the bearing capacity caused by soil weight (the $N\gamma$ part) decreases for non-strip loads and a 30% reduction is proposed for pure vertical loading (Emdal and Grande, 2006). The authors proposed to use conservative values for the $N\gamma$ part equation for all geometry cases and not to apply any geometry corrections.

The Eurocode 7 proposes to adopt the shape factor equations for s_q (Equation 21) and s_c (Equation 22) recommended by Brinch-Hansen (1970) and Vesić (1973), respectively. For the shape factor s_γ (Equation 23), the value of 0.4 that multiplies the B/L factor should be changed to 0.3 in cases when $B/D \leq 1$ (Bond and Harris, 2008).

Finally, Sieffert and Bay-Gress (2000) compared the bearing capacity calculation methods for shallow foundations used by the European countries, concerning the formulations of bearing capacity factors, depth and shape

factors, load inclination and eccentricity factors, among others. They concluded that evaluated bearing capacity depends highly on the method used, and therefore on the country. Only the eccentricity correction is accepted unanimously; however, this does not mean that this correction is more accurate. The results calculated with Eurocode 7 stay in the high mean of results found from the European methods used. For that reason, Sieffert and Bay-Gress (2000) say that the bearing capacity needs to be better understood using new parametric and numerical analyses.

Chapter 3

The relative footing dimension in the bearing capacity problem: numerical simulations

The FEM can be used to predict the bearing capacity of surface with confidence (Griffiths, 1982). Also, it can model localization of deformation in shear bands for associated and non-associated flow rule. Furthermore, it predicts the failure of granular materials provided a proper type of element is selected, like the 15-noded triangle, and provided that a sound numerical procedure is employed, for example, it embodies equilibrium iterations within each loading step (de Borst and Vermeer, 1984).

It has been commented in previous chapters that many researchers have investigated experimental and theoretically the vertical bearing capacity of square, rectangular and circular shallow foundations on different types of soils that follow the Mohr-Coulomb failure criterion. For instance: Golder (1941), Meyerhof (1963), Brinch-Hansen (1970), De Beer (1970), Bolton and Lau (1993), Michalowski (2001), Michalowski and Dawson (2002a), Michalowski and Dawson (2002b), Erickson and Drescher (2002) and Lyamin *et al.* (2007).

Furthermore, many researchers have investigated the vertical bearing capacity of shallow foundations using Finite Elements (FE) or Finite Differences (FD). For example: Griffiths (1982), de Borst and Vermeer (1984), Manoharan and Dasgupta (1995), Frydman and Burd (1997), Potts and Zdravkovic (2001), Yin *et al.* (2001), Erickson and Drescher (2002), Salgado *et al.* (2004), Hjiaj *et al.*, (2005), Zhu and Michalowski (2005), Lyamin *et al.* (2007), Zhao and Wang (2009), Loukidis and Salgado (2009) and Puzakov *et al.* (2009).

In particular, Manoharan and Dasgupta (1995) affirm that the FEM applied in shallow foundations has the advantage of idealizing the material behaviour of soil, which is non-linear with plastic deformations, in a more rational manner.

In the present work, computations of bearing capacity factors has been carried out using the FEM for strip, circular/square and rectangular footings with a rough base. The following chapter summarize the results of: the bearing capacity factors Nq and Nγ, and the shape factors s_q and s_γ for circular/square and rectangular footings. The analyses were performed for the associated flow rule ($\psi = \varphi$) and for the non-associated flow rule ($\psi < \varphi$). The constitutive model used for the soil is an elastic-perfectly plastic model following a Mohr-Coulomb failure criterion. The effect of the soil lying above footing base level is represented only as overburden load. The contributions of the upper portion of the slip surface above the footing base level (depth factors) are not considered.

Finally, the results of bearing capacity factors and shape factors are compared with predictions from the empirical and semi-empirical formulas from previous studies employing other methods of analysis.

3.1. Mesh discretization and boundary conditions

The Finite Element analyses were performed using three codes:

- PLAXIS 2D V9 for the plane strain (strip footings) and axisymmetrical (circular footings) analyses, using unstructured meshes consisting of 15-noded triangular elements and 6-noded triangular elements. One half of the footing was modelled taking advantage of one plane of symmetry.
- PLAXIS 3D Foundations V2.1 for the three-dimensional (3D) analyses (rectangular and square footings) for the associated and the non-associated flow rule (when $\varphi < 30°$), using unstructured meshes in the horizontal plane and structured meshes in the two vertical planes, as a result of the 15-noded wedge elements. One quarter of the footing was modelled due to the two planes of symmetry.
- PLAXIS 3D Tunnel V2.4 for the 3D analyses (rectangular and square footings) for the non-associated flow rule (when $\varphi \geq 30°$), using an unstructured mesh in one of the vertical planes and structured meshes in the horizontal and the other vertical plane, as a result of 15-noded wedge

elements. One quarter of the footing was modelled as a result of the two planes of symmetry.

The 2D calculations with 15-noded triangular elements were done in order to get more accurate results and find the overshooting when the 3D analyses were performed. On the other hand, the use of 6-noded triangular elements made the results of two dimensions (2D) comparable to the corresponding cases in the 3D analyses.

The planes of symmetry of the footings allowed modeling of one half (for 2D analyses) and one quarter (for 3D analyses) of the footings; however, it is discussed in Chapter 4 some cautions about this assumption.

According to Potts and Zdravkovic (2001), unstructured meshing allows efficient element arrangement and refinement of the element in the vicinity of the corners of the footing, which is crucial for the accurate prediction of the collapse load. In Chapter 4 is discussed an interesting finding of the present study related to this fact.

As a result of the different results that can be obtained when 15-noded elements or 6-noded elements are used in 2D analysis; and furthermore, when the 3D analysis is done for 15-noded wedge elements (which are comparable to 6-noded elements for 2D), a mesh calibration of the model was done.

The mesh calibration provides an overview of the number of elements and the average size of the element that a model in 3D needs to calculate a similar failure load that has been obtained in a previous 2D analysis. The failure load calculated in 3D for a footing of 3x20m (taken as a strip footing) should be ±10% different from the 2D solution for a strip footing (in plane strain). The main idea is to calibrate the calculation overshooting of the 3D results. The 3D results for 3x20m are used as comparative values for the other footings sizes. It is not possible to use the 2D solution as the comparative value for 3D solutions because the element mesh distribution is not similar.

For the mesh of the 2D model (plane strain conditions – strip footing), the 15-noded triangle was used. It provides a fourth order interpolation for displacements and the numerical integration involves 12 Gauss points (stress points) (Figure 29). The mesh generation in this case is based on a robust

triangulation procedure, which result in "unstructured" meshes (Brinkgreve *et al.*, 2008).

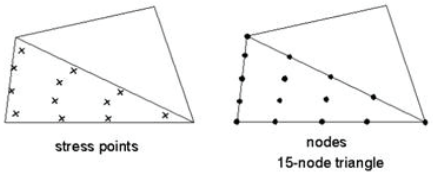

Figure 29: Position of nodes and stress points in soil elements
(Brinkgreve et al. 2008).

For the mesh of the 3D model, the basic 15-noded wedge elements were used. They are composed of 6-noded triangles in horizontal direction and 8-noded quadrilaterals in vertical direction (Figure 30) for PLAXIS 3D Foundation. In PLAXIS 3D-Tunnel, the 6-noded triangle is in one vertical plane and the 8-noded quadrilateral is in the horizontal and vertical plane left. The accuracy of the 15-noded wedge element is comparable with the 6-noded triangular element in PLAXIS 2D (Brinkgreve and Swolfs, 2007).

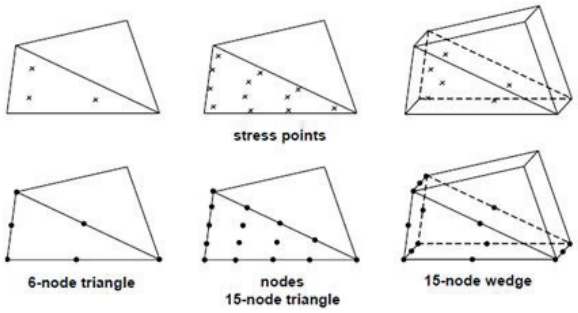

Figure 30: Comparison of 2D and 3D soil elements
(Brinkgreve and Swolfs, 2007).

As in the 2D model, the 2D mesh generator in the 3D model is based on a robust triangulation procedure, which results in "unstructured" meshes. Then, the 3D mesh is based on a system of horizontal and pseudo-horizontal planes in which the 2D mesh is used (for PLAXIS 3D Foundation). The same applies

to PLAXIS 3D-Tunnel, but changing to vertical and pseudo-vertical planes in which the 2D mesh is used.

The results got for the mesh calibration are shown in Figure 31 for two cases: (a) the exceedance of the 3D-15-noded wedge element from 2D-15-noded triangle element, (b) the exceedance of the 3D-15-noded wedge element from 2D-6-noded triangle element. Each case is sub-divided in three different curves. The first curve was obtained using a lower stiffness value in the 3D-footing respect to the 2D-footing stiffness and a complete model, which mean that no symmetry was used. The second case corresponds to a correct footing stiffness value between the 2D- and 3D-footings and a complete model. And the third case is a simplification when only a quarter of the footing was modelled due to the two planes of symmetry.

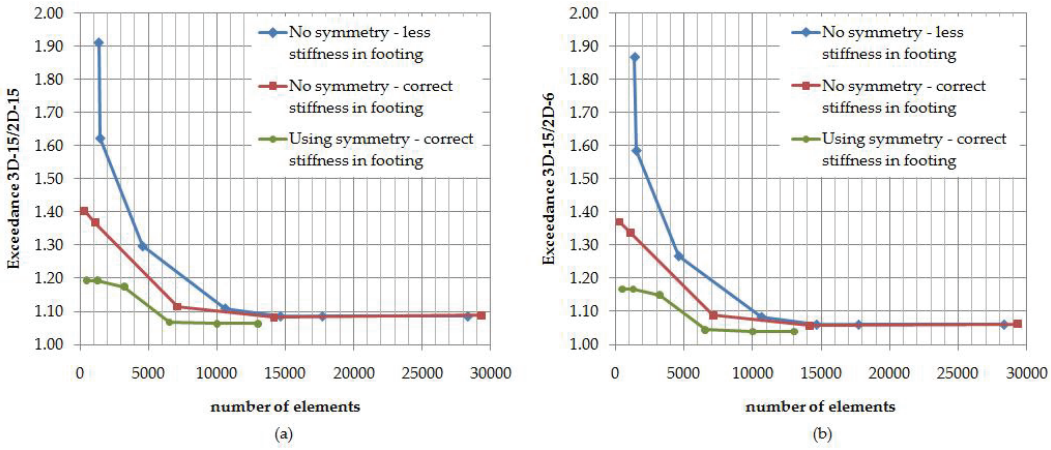

Figure 31: Variation of the overshooting 3D/2D with the number of elements in 3D-model: (a) exceedance of 3D-15-noded wedge element from 2D-15-noded triangle element, (b) exceedance of 3D-15-noded wedge element from 2D-6-noded triangle element.

The differences in the results are more noticeable for lower number of elements. The tolerance assumed for the overshooting (exceedance from 3D respect to 2D) is 1.10, which means that the 3D failure load should be maximum 10% different than the 2D failure load. Following that assumption, it can be seen in Figure 31 that for a complete model, in both cases (a) and (b),

the 3D model should contain at least 10000 elements. When the symmetry is used (only a quarter of the total footing size is modelled), this value reduces to 6500 elements.

Due to the sensitivity of the model to the number of elements, which is affected by the size of the model and the mesh chosen, another version of the overshooting 3D/2D varying with the 3D-average size element was analyzed (Figure 32).

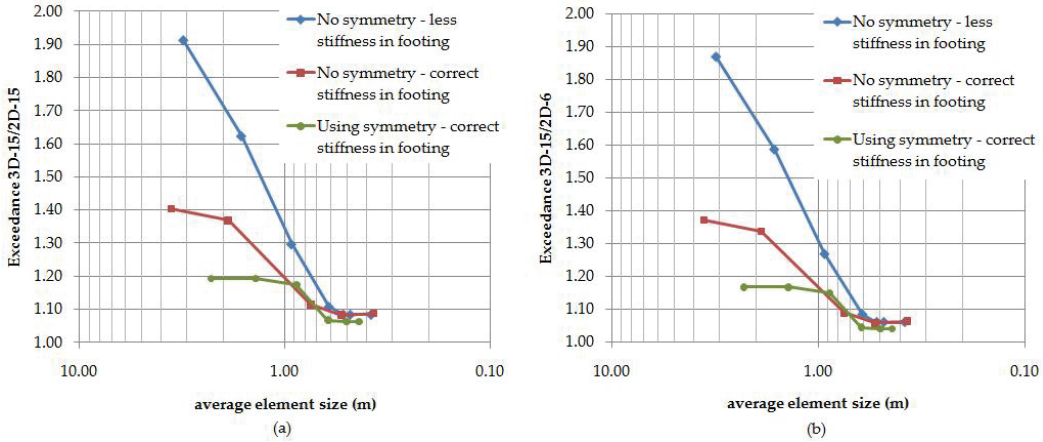

Figure 32: Variation of the overshooting 3D/2D with the average size of element in a 3D-model: (a) exceedance of 3D-15-noded wedge element from 2D-15-noded triangle element, (b) exceedance of 3D-15-noded wedge element from 2D-6-noded triangle element.

In Figure 32, an average element size of 0.60m obeys the assumption 10% of exceedance. In general, the number of elements in the model is not going to be the main factor that influences the overshooting. It will depend more on the average element size and the number of elements under the footing which was controlled to be from four to five elements). It seems that is more important how the elements are distributed in the model than a larger number of elements in it. The important effect is to capture the intense concentration of plastic shear strains with the elements in the areas that requires it.

From Figure 31 and 32, a lower asymptotic behaviour of the curves can be identified, showing that after a defined number or elements or average size of

element, the exceedance of 3D respect to 2D results will be the same, even though, these two variables increase.

It was suggested by Loukidis and Salgado (2009) that close to the footing edges the element size should be limited to 0.035-0.06B and 0.07-0.11B at the vicinity of the footing centre. Following this criteria, for a footing with B = 3 m, the local element size around the footing centre should be between 0.35-0.55 and for the footing edge between 0.175-0.3. In fact, the local element size around the footing without refinement reaches a value of 0.1785 which agrees with that criterion.

When in later calculations, refinements around the footing borders and corners were performed, the exceedance 3D/2D decreased from 4%-6% to 1.7%. Unfortunately, these refinements were part of some final sensitivity analyses and were not in the main calculation results. Future calculations must take account of this fact.

Figure 33, 34 and 35 show some examples of the Finite Element meshes used for the mesh discretization. It can be concluded that once that the number of elements and the average element size are under control, the local refinement has a good impact in the accuracy of the results..

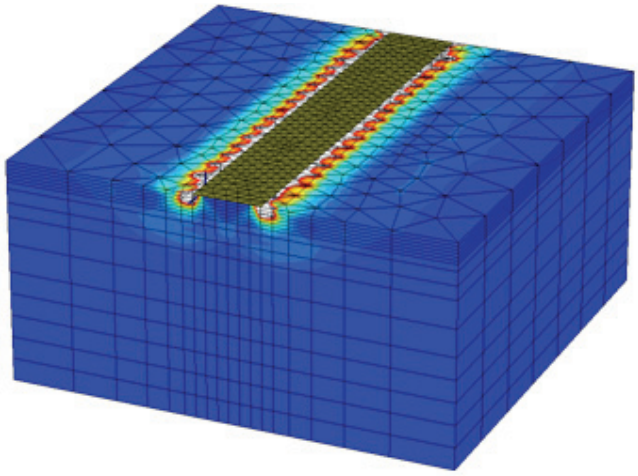

Figure 33: Finite Element mesh and failure mechanism as incremental shear strains: 14176 elements / 0.53m element average size / without using symmetry / 6 elements under the footing.

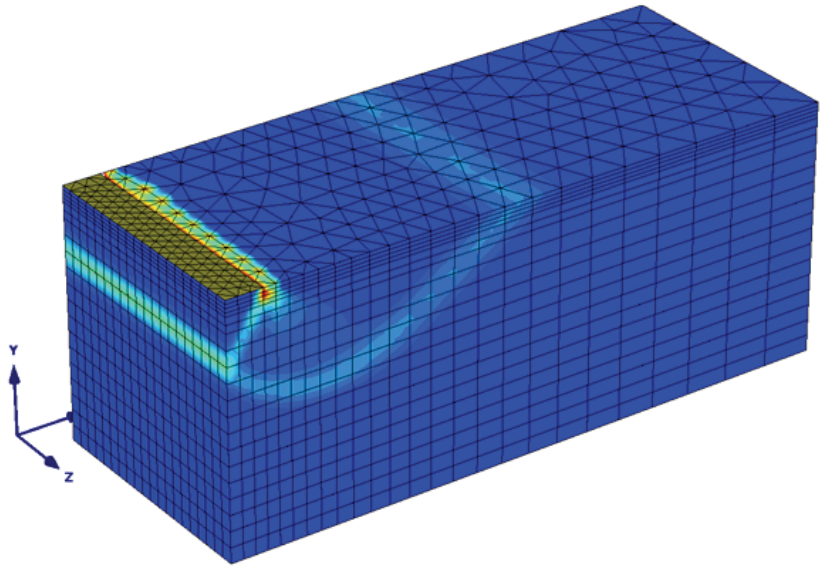

Figure 34: Finite Element mesh and failure mechanism as incremental shear strains: 10020 elements / 0.50m element average size / using two planes of symmetry / 6 elements under the footing (3 shown due to symmetry)

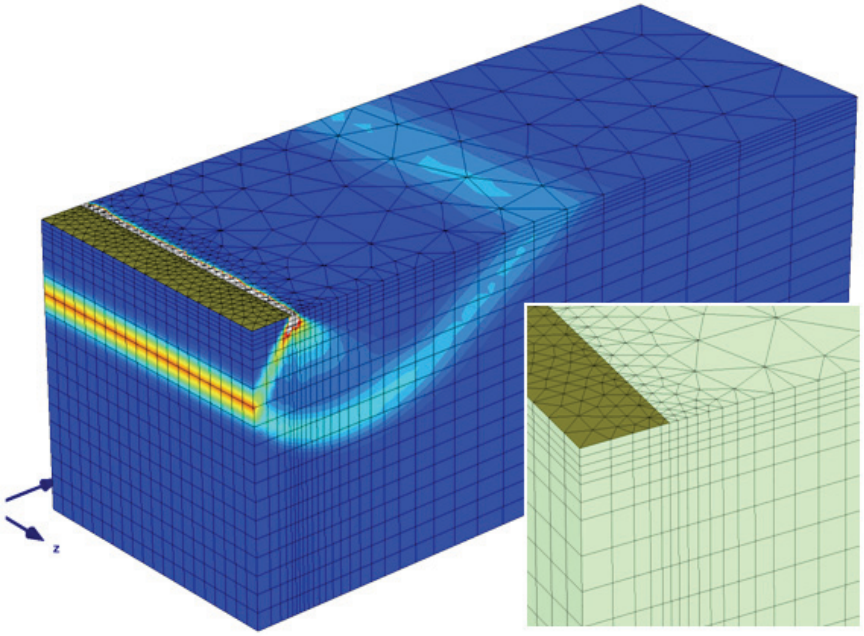

Figure 35: Finite Element mesh and failure mechanism as incremental shear strains when the corner and border of the footing have been refined.

On top of the model, a rough footing is placed to be loaded with a uniformly distributed load. Also, a overburden, p', equal to 11 kPa was uniformly distributed to simulate a footing embedment of D = 0.55m (for γ_{soil} = 20 kN/m^3), defining the footing as shallow (in a shallow footing D < 5B and in this case 0.55m < 5*3m). The boundaries of the model where sufficiently far from the footing avoiding to intersect the failure zone.

At the bottom boundary of the Finite Element mesh, the two horizontal and vertical degrees of freedom are fixed. At the lateral boundaries, only the horizontal degree of freedom, corresponding to the axis, is fixed. The distances of the bottom and lateral boundaries from the footing varied from analysis to analysis in order to ensure that the boundaries did not interfere with the development of the collapse mechanism while maintaining adequate mesh density close to the footing (Loukidis and Salgado, 2009). For that reason, a defined number of elements is not specified for all the analyses, there was a particular number for each case of analysis (detailed in Table 4 and Table 5). However, the general geometrical aspects that have been discussed in this section were followed.

Figure 36 shows the typical mesh and boundary conditions for footing simulations for the three different Finite Element codes used: (a) PLAXIS 2D V9, (b) PLAXIS 3D Foundations V2.1 and (c) PLAXIS 3D Tunnel V2.4.

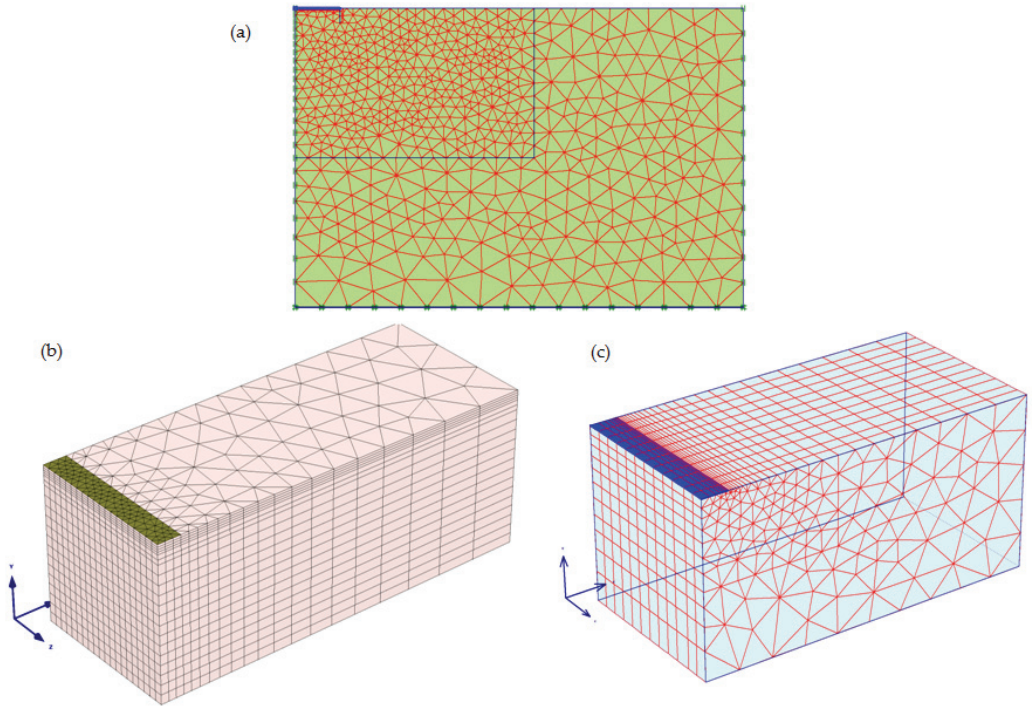

Figure 36: Typical mesh for footing simulations for the three different Finite Element codes used: (a) PLAXIS 2D V9, (b) PLAXIS 3D Foundations V2.1 and (c) PLAXIS 3D Tunnel V2.4.

3.2. Material model and parameters

The constitutive model used is an elastic-perfectly plastic model following the Mohr-Coulomb failure criterion. The stress-strain diagram consist of two straight lines idealizing a material with the property of continuing plastic flow at constant stress (Chen, 1975). The elastic-perfectly plastic assumption is based on the stress-strain behaviour of most real soils which is characterized by an initial linear portion and a peak of failure stress followed by softening to a residual stress (Figure 37).

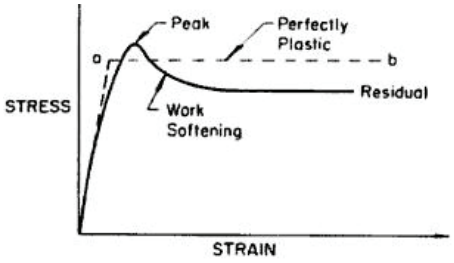

Figure 37: Stress-strain relationship for ideal and real soils (Chen, 1975).

According to de Borst and Vermeer (1984), the Mohr-Coulomb model is well able to provide accurate predictions of the ultimate bearing capacity of soil masses; particularly for problems where collapse is reached at relatively small strains, for instance the bearing capacity of shallow footings and the stability of slopes. In the numerical analysis of such problems, the stress field appears to converge to a particular state of limiting stress: all strains rates become plastic, so that a genuine limit load is obtained.

Several different soil parameters cases were used. They are specified in Table 1. Four different friction angles varying between 10°, 25°, 33° and 40° were analyzed with associated (cases A) and non-associated flow rule (cases B). This variation was of special interest to cover the range of friction angles that the soils can generally have; particularly when effective stress analyses are performed without any influence from ground water table ($\gamma_{unsaturated} = \gamma_{saturated}$), as was the case of the present study.

Table 1: Material parameters for the soil under the footing.

Case of study	Soil unit weight γ (kN/m³)	Young's modulus E_{ref} (MPa)	Poisson's ratio ν	Cohesion c (kPa)	Attraction a (kPa)	Friction angle φ (°)	Dilatancy angle ψ (°)
Set 1A	20	10	0.3	5	28.4	10	10
Set 1B	20	10	0.3	5	28.4	10	0
Set 2A	20	10	0.3	5	10.7	25	25
Set 2B	20	10	0.3	5	10.7	25	0
Set 3A	20	30	0.3	5	7.7	33	33
Set 3B	20	30	0.3	5	7.7	33	3
Set 4A	20	30	0.3	5	6.0	40	40
Set 4B	20	30	0.3	5	6.0	40	10

For the associated flow rule analyses (cases A), the friction angle φ was set equal to the dilatancy angle ψ. On the other hand, for the non-associated flow rule studies (cases B), when $\varphi < 30°$ the $\psi = 0°$ and when $\varphi \geq 30°$ the dilatancy angle was calculated using Equation 47 which is a relation generally adopted for sands (Nordal, 2007). Since it was assumed that the soil is perfectly plastic, the values reported in Table 1 represent peak friction angle and peak dilatancy angle values (Loukidis and Salgado, 2009).

$$\psi = \varphi - 30^0 \tag{47}$$

For the 3D analysis, five different footing sizes were studied. The width, B, was set equal to 3m for all the cases and the length, L, was varied every 5m starting at 20m and finishing with a square footing of 3x3m. The 3x20m footing in 3D was calibrated to be equivalent to the strip footing (B = 3m) in 2D analysis. On the on other hand, the square footing 3x3m was calibrated to be equivalent to the circular-axisymmetrical footing with a diameter of 3m. The Table 2 details the material parameters defined for the footings.

Table 2: Material parameters for the footings.

Footing size BxL (m)	Type of analysis	Structural element	Soil-footing interface	Stiffness parameters EI & EA or E	Thickness d (cm)
B = 3 strip	2D Plane strain	Plate	Rough	EI = $1x10^5$ kNm²/m EA = $1x10^7$ kN/m	34.6
3x20 "strip"(i)	3D	Floor	Rough	E = $30x10^6$ kPa	34.6
3x15	3D	Floor	Rough	E = $30x10^6$ kPa	34.6
3x10	3D	Floor	Rough	E = $30x10^6$ kPa	34.6
3x5	3D	Floor	Rough	E = $30x10^6$ kPa	34.6
3x3 square	3D	Floor	Rough	E = $30x10^6$ kPa	34.6
3x3 circular	2D Axisymmetric	Plate	Rough	EI = $1x10^5$ kNm²/m EA = $1x10^7$ kN/m	34.6

(i) A footing is considered strip if B/L < 0.2, in this case B/L = 3/20 = 0.15 < 0.2.

Results from all the sets will allow to study the variation for the bearing capacity factors, in terms of the friction angle, dilatancy angle and relative footing dimension.

3.3. Solution scheme

The general analysis of the shape factors involved in the bearing capacity problem for shallow foundations was divided in three fundamental calculations according to which part of the bearing capacity equation (Equation 38) was being investigated:

(a) Part A - Weightless soil with cohesion and friction: for the Nq part in Equation 38.

(b) Part B - Soil with self weight, cohesion and friction: for the complete Equation 38.

(c) Part C - Back-calculation of the soil-weight factor $N\gamma$: due to the conservative results of adding the factors of the bearing capacity equation (superposition principle) (Griffiths, 1982; Erickson and Drescher, 2002).

The calculation in Part A and Part B was organized in six steps for each set of soil material parameters specified in Table 1. The calculation steps are described below:

1. Theoretical calculation: The bearing capacity formula (Equation 38) was used to obtain the corresponding theoretical value of the ultimate load using the theoretical proposals for the values of Nq (Figure 18a) and the values of $N\gamma$ (Figure 18b), for a strip footing.

2. The 2D-15-strip footing analysis: a 2D plane strain FE calculation of a strip footing was performed with 15-noded elements to compare the results with the values got in step 1.

3. The 2D-6-strip footing analysis: a 2D plane strain FE calculation of a strip footing was performed with 6-noded elements to compare the results with the values got in step 2 (to know the error between them) and in step 4 for the 3x20m footing (to know the overshooting of 3D respect to 2D).

4. The 3D-analysis: 3D calculations were performed for the footing sizes specified in Table 2. The calculations were focused in getting the failure load and pattern.

5. The 2D-6-axisymmetric and the 2D-15-axisymmetric footing analyses: these 2D calculations were done with the objective of comparing (overshooting 3D/2D and error 3D/2D respectively) the results to the solution got for the square footing in the 3D analysis.

6. Finally, the shape factors were computed comparing the bearing capacity for the rectangular/square footing with that of a strip footing. This can be done if the Equation 38 is written as Equation 48, where Nq* and Nγ* are referred to as the modified bearing capacity factors. Then, the shape factors can then be defined as in Equation (49).

$$q_{ult} = (p' + a) * N_q^* + \tfrac{1}{2} * \gamma' * B * N_\gamma^* - a \tag{48}$$

$$s_q = \frac{N_q^*}{N_q}\,;\, s_\gamma = \frac{N_\gamma^*}{N_\gamma} \tag{49}$$

3.3.1. Study of Nq (Part A)

To isolate the N_q term in the equation of the bearing capacity, a weightless soil ($\gamma = 0$) was considered and the bearing capacity was derived from a uniform overburden p'. The initial stress state attributed to the soil was therefore p' in the vertical direction and K_o*p' in each of the two horizontal directions. The at rest earth pressure coefficient K_o was calculated according to the formula $K_0 = 1\text{-}\sin\varphi$, where φ is the friction angle given.

The target value for each calculation was the ultimate load that was read from the load-displacement curve plot for the middle point of the footings. Then, the N_q value was obtained by Equation 50 and the corresponding shape factor using Equation 49.

$$N_q = \frac{q_{ult-N_q} + a}{p' + a} \tag{50}$$

3.3.2. Total bearing capacity study (Part B) and back-calculation of Nγ (Part C)

The first approach followed for the study of the N_γ term was to consider a cohesionless (c = 0) self weight soil ($\gamma \neq 0$). However, the results obtained were not good due to difficulties that the program showed when zero cohesion (or a small value) was given. For instance, tension points close to the surface not allowing a clear failure surface. Respect to that, Griffiths (1982) mentions that the bearing capacity factor N_γ has no closed form solution. The problem with N_γ is that a frictional cohesionless soil in which self weight is included has an initial shear strength that increases with depth from zero at the ground surface. This has the effect of making curved the parts of the Hill and Prandtl mechanisms that were previously straight (Chen, 1975). Also, Zhu and Michalowski (2005) mention that purely frictional material led to numerical difficulties with convergence.

For that reason, it was decided to back-calculate the N_γ term in the bearing capacity equation estimating the complete bearing capacity and subtracting the N_q term as is shown in Equation 51.

$$N_\gamma = \frac{q_{ult-total} - ((p' + a) * N_q - a)}{0.5 * \gamma * B} = \frac{q_{ult-total} - q_{ult-Nq}}{0.5 * \gamma * B} \quad (51)$$

For the three parts of analysis (A, B and C), the calculation phases were defined with a tolerate error of 0.01. All the analyses started from an initial stage in which the geostatic stress field is established in the FE mesh (which corresponds to the K_0 procedure that follows Jaky's formula $K_0 = 1\text{-}\sin\varphi$). The next phase was the geometry and material setting in the model, ending with the incremental application of the load until the failure was got.

The loading procedure was defined as incremental multipliers for the 2D analysis using the code PLAXIS 2D and for the 3D analysis using the code PLAXIS 3D-Tunnel. In the case of the 3D analysis with the code PLAXIS 3D Foundation, the loading procedure was defined as stage construction, in which a slightly lower load compared to the failure load was applied, and then, a c-phi reduction was performed to get a multiplier for the initial load applied. The failure load results from the product of the initial load applied

and the multiplier from the c-phi reduction. This was the strategy due to the absence of incremental multipliers algorithm in the program PLAXIS 3D Foundation.

The calculations were performed for the set of soil parameters shown in Table 1 and footing parameters from Table 2. The Table 4 (for the Nq-study) and Table 5 (for the Total study and Nγ-back calculation) specify the number of elements, type of element, number of nodes, average element size, FEM code used and the target parameter for each case of analysis; as a summary of the procedure followed for the calculation of the shape factors variation with the relative footing dimension.

In Table 4 and Table 5, the target parameter refers to the main result of each simulation that will be used for estimation of the shape factors. The corresponding target parameters for the bearing capacity analysis are the failure loads (q_{ult}). The nomenclature used is explained in the following form: $q_{ult\text{-}i\text{-}j\text{-}k\text{-}m}$; where each sub-index corresponds to a particular meaning detailed in Table 3.

Table 3: Nomenclature used for the target parameter: $q_{ult\text{-}i\text{-}j\text{-}k\text{-}m}$.

Sub-index	Value	Meaning
i	Nq	Nq-study
	Total	Total-study
j	1A or 1B	Soil parameters Set1A or Set1B (Table 1)
	2A or 2B	Soil parameters Set2A or Set2B (Table 1)
	3A or 3B	Soil parameters Set3A or Set3B (Table 1)
	4A or 4B	Soil parameters Set4A or Set4B (Table 1)
k	2Ds	Analysis in 2D for strip footing (Table 2)
	3D3x20	Analysis in 3D for rectangular footing of 3x20m (Table 2)
	3D3x15	Analysis in 3D for rectangular footing of 3x15m (Table 2)
	3D3x10	Analysis in 3D for rectangular footing of 3x10m (Table 2)
	3D3x5	Analysis in 3D for rectangular footing of 3x5m (Table 2)
	3D3x3	Analysis in 3D for rectangular footing of 3x3m (Table 2)
	2Dc	Analysis in 2D for circular footing (Table 2)
m	15	Type of element: 15-noded triangular (2D analysis)
	6	Type of element: 6-noded triangular (2D analysis)
		Type of element: 15-noded wedge (3D analysis)

Table 4: Calculation details for each case of analysis in the Nq-study.

Case of study	Type of footing	Number of elements	Type of element	Number of nodes	Average element size	FEM code used	Target parameter
Set 1A	Strip	1190	15-noded	9742	0.355m	PLAXIS 2D V9	$q_{ult\text{-}Nq\text{-}1A\text{-}2Ds\text{-}15}$
	Strip	1190	6-noded	2492	0.355m	PLAXIS 2D V9	$q_{ult\text{-}Nq\text{-}1A\text{-}2Ds\text{-}6}$
	Rectangular	6940	15-noded wedge	20038	0.600m	PLAXIS 3D Foundation	$q_{ult\text{-}Nq\text{-}1A\text{-}3D3x20}$ $q_{ult\text{-}Nq\text{-}1A\text{-}3D3x15}$ $q_{ult\text{-}Nq\text{-}1A\text{-}3D3x10}$ $q_{ult\text{-}Nq\text{-}1A\text{-}3D3x5}$ $q_{ult\text{-}Nq\text{-}1A\text{-}3D3x3}$
	Circular	1190	15-noded	9742	0.355m	PLAXIS 2D V9	$q_{ult\text{-}Nq\text{-}1A\text{-}2Dc\text{-}15}$
	Circular	1190	6-noded	2492	0.355m	PLAXIS 2D V9	$q_{ult\text{-}Nq\text{-}1A\text{-}2Dc\text{-}6}$
Set 1B	Strip	1190	15-noded	9742	0.355m	PLAXIS 2D V9	$q_{ult\text{-}Nq\text{-}1B\text{-}2Ds\text{-}15}$
	Strip	1190	6-noded	2492	0.355m	PLAXIS 2D V9	$q_{ult\text{-}Nq\text{-}1B\text{-}2Ds\text{-}6}$
	Rectangular	6940	15-noded wedge	20038	0.600m	PLAXIS 3D Foundation	$q_{ult\text{-}Nq\text{-}1B\text{-}3D3x20}$ $q_{ult\text{-}Nq\text{-}1B\text{-}3D3x15}$ $q_{ult\text{-}Nq\text{-}1B\text{-}3D3x10}$ $q_{ult\text{-}Nq\text{-}1B\text{-}3D3x5}$ $q_{ult\text{-}Nq\text{-}1B\text{-}3D3x3}$
	Circular	1190	15-noded	9742	0.355m	PLAXIS 2D V9	$q_{ult\text{-}Nq\text{-}1B\text{-}2Dc\text{-}15}$
	Circular	1190	6-noded	2492	0.355m	PLAXIS 2D V9	$q_{ult\text{-}Nq\text{-}1B\text{-}2Dc\text{-}6}$

Case of study	Type of footing	Number of elements	Type of element	Number of nodes	Average element size	FEM code used	Target parameter
Set 2A	Strip	1190	15-noded	9742	0.355m	PLAXIS 2D V9	$q_{ult\text{-}Nq\text{-}2A\text{-}2Ds\text{-}15}$
	Strip	1190	6-noded	2492	0.355m	PLAXIS 2D V9	$q_{ult\text{-}Nq\text{-}2A\text{-}2Ds\text{-}6}$
	Rectangular	6940	15-noded wedge	20038	0.600m	PLAXIS 3D Foundation	$q_{ult\text{-}Nq\text{-}2A\text{-}3D3x20}$ $q_{ult\text{-}Nq\text{-}2A\text{-}3D3x15}$ $q_{ult\text{-}Nq\text{-}2A\text{-}3D3x10}$ $q_{ult\text{-}Nq\text{-}2A\text{-}3D3x5}$ $q_{ult\text{-}Nq\text{-}2A\text{-}3D3x3}$
	Circular	1190	15-noded	9742	0.355m	PLAXIS 2D V9	$q_{ult\text{-}Nq\text{-}2A\text{-}2Dc\text{-}15}$
	Circular	1190	6-noded	2492	0.355m	PLAXIS 2D V9	$q_{ult\text{-}Nq\text{-}2A\text{-}2Dc\text{-}6}$
Set 2B	Strip	1190	15-noded	9742	0.355m	PLAXIS 2D V9	$q_{ult\text{-}Nq\text{-}2B\text{-}2Ds\text{-}15}$
	Strip	1190	6-noded	2492	0.355m	PLAXIS 2D V9	$q_{ult\text{-}Nq\text{-}2B\text{-}2Ds\text{-}6}$
	Rectangular	6940	15-noded wedge	20038	0.600m	PLAXIS 3D Foundation	$q_{ult\text{-}Nq\text{-}2B\text{-}3D3x20}$ $q_{ult\text{-}Nq\text{-}2B\text{-}3D3x15}$ $q_{ult\text{-}Nq\text{-}2B\text{-}3D3x10}$ $q_{ult\text{-}Nq\text{-}2B\text{-}3D3x5}$ $q_{ult\text{-}Nq\text{-}2B\text{-}3D3x3}$
	Circular	1190	15-noded	9742	0.355m	PLAXIS 2D V9	$q_{ult\text{-}Nq\text{-}2B\text{-}2Dc\text{-}15}$
	Circular	1190	6-noded	2492	0.355m	PLAXIS 2D V9	$q_{ult\text{-}Nq\text{-}2B\text{-}2Dc\text{-}6}$

Case of study	Type of footing	Number of elements	Type of element	Number of nodes	Average element size	FEM code used	Target parameter
Set 3A	Strip	938	15-noded	7750	0.730m	PLAXIS 2D V9	$q_{ult\text{-}Nq\text{-}3A\text{-}2Ds\text{-}15}$
	Strip	938	6-noded	2000	0.730m	PLAXIS 2D V9	$q_{ult\text{-}Nq\text{-}3A\text{-}2Ds\text{-}6}$
	Rectangular	6940	15-noded wedge	20038	0.600m	PLAXIS 3D Foundation	$q_{ult\text{-}Nq\text{-}3A\text{-}3D3x20}$ $q_{ult\text{-}Nq\text{-}3A\text{-}3D3x15}$ $q_{ult\text{-}Nq\text{-}3A\text{-}3D3x10}$ $q_{ult\text{-}Nq\text{-}3A\text{-}3D3x5}$ $q_{ult\text{-}Nq\text{-}3A\text{-}3D3x3}$
	Circular	938	15-noded	7750	0.730m	PLAXIS 2D V9	$q_{ult\text{-}Nq\text{-}3A\text{-}2Dc\text{-}15}$
	Circular	938	6-noded	2000	0.730m	PLAXIS 2D V9	$q_{ult\text{-}Nq\text{-}3A\text{-}2Dc\text{-}6}$
Set 3B	Strip	938	15-noded	7750	0.730m	PLAXIS 2D V9	$q_{ult\text{-}Nq\text{-}3B\text{-}2Ds\text{-}15}$
	Strip	938	6-noded	2000	0.730m	PLAXIS 2D V9	$q_{ult\text{-}Nq\text{-}3B\text{-}2Ds\text{-}6}$
	Rectangular	3276	15-noded wedge	9844	0.247m	PLAXIS 3D Foundation (complete footing) PLAXIS 3D-Tunnel	$q_{ult\text{-}Nq\text{-}3B\text{-}3D3x20}$ $q_{ult\text{-}Nq\text{-}3B\text{-}3D3x15}$ $q_{ult\text{-}Nq\text{-}3B\text{-}3D3x10}$ $q_{ult\text{-}Nq\text{-}3B\text{-}3D3x5}$ $q_{ult\text{-}Nq\text{-}3B\text{-}3D3x3}$
	Circular	938	15-noded	7750	0.730m	PLAXIS 2D V9	$q_{ult\text{-}Nq\text{-}3B\text{-}2Dc\text{-}15}$
	Circular	938	6-noded	2000	0.730m	PLAXIS 2D V9	$q_{ult\text{-}Nq\text{-}3B\text{-}2Dc\text{-}6}$

Case of study	Type of footing	Number of elements	Type of element	Number of nodes	Average element size	FEM code used	Target parameter
Set 4A	Strip	938	15-noded	7750	0.730m	PLAXIS 2D V9	$q_{ult\text{-}Nq\text{-}4A\text{-}2Ds\text{-}15}$
	Strip	938	6-noded	2000	0.730m	PLAXIS 2D V9	$q_{ult\text{-}Nq\text{-}4A\text{-}2Ds\text{-}6}$
	Rectangular	9640	15-noded wedge	27151	0.602m	PLAXIS 3D Foundation	$q_{ult\text{-}Nq\text{-}4A\text{-}3D3x20}$ $q_{ult\text{-}Nq\text{-}4A\text{-}3D3x15}$ $q_{ult\text{-}Nq\text{-}4A\text{-}3D3x10}$ $q_{ult\text{-}Nq\text{-}4A\text{-}3D3x5}$ $q_{ult\text{-}Nq\text{-}4A\text{-}3D3x3}$
	Circular	938	15-noded	7750	0.730m	PLAXIS 2D V9	$q_{ult\text{-}Nq\text{-}4A\text{-}2Dc\text{-}15}$
	Circular	938	6-noded	2000	0.730m	PLAXIS 2D V9	$q_{ult\text{-}Nq\text{-}4A\text{-}2Dc\text{-}6}$
Set 4B	Strip	938	15-noded	7750	0.730m	PLAXIS 2D V9	$q_{ult\text{-}Nq\text{-}4B\text{-}2Ds\text{-}15}$
	Strip	938	6-noded	2000	0.730m	PLAXIS 2D V9	$q_{ult\text{-}Nq\text{-}4B\text{-}2Ds\text{-}6}$
	Rectangular	3276	15-noded wedge	9844	0.247m	PLAXIS 3D Foundation (diagonal footing) PLAXIS 3D-Tunnel	$q_{ult\text{-}Nq\text{-}4B\text{-}3D3x20}$ $q_{ult\text{-}Nq\text{-}4B\text{-}3D3x15}$ $q_{ult\text{-}Nq\text{-}4B\text{-}3D3x10}$ $q_{ult\text{-}Nq\text{-}4B\text{-}3D3x5}$ $q_{ult\text{-}Nq\text{-}4B\text{-}3D3x3}$
	Circular	938	15-noded	7750	0.730m	PLAXIS 2D V9	$q_{ult\text{-}Nq\text{-}4B\text{-}2Dc\text{-}15}$
	Circular	938	6-noded	2000	0.730m	PLAXIS 2D V9	$q_{ult\text{-}Nq\text{-}4B\text{-}2Dc\text{-}6}$

Table 5: Calculation details for each case of analysis in the Total and Nγ-back calculation.

Case of study	Type of footing	Number of elements	Type of element	Number of nodes	Average element size	FEM code used	Target parameter
Set 1A	Strip	1190	15-noded	9742	0.355m	PLAXIS 2D V9	$q_{ult\text{-}Total\text{-}1A\text{-}2Ds\text{-}15}$
	Strip	1190	6-noded	2492	0.355m	PLAXIS 2D V9	$q_{ult\text{-}Total\text{-}1A\text{-}2Ds\text{-}6}$
	Rectangular	6940	15-noded wedge	20038	0.600m	PLAXIS 3D Foundation	$q_{ult\text{-}Total\text{-}1A\text{-}3D3x20}$ $q_{ult\text{-}Total\text{-}1A\text{-}3D3x15}$ $q_{ult\text{-}Total\text{-}1A\text{-}3D3x10}$ $q_{ult\text{-}Total\text{-}1A\text{-}3D3x5}$ $q_{ult\text{-}Total\text{-}1A\text{-}3D3x3}$
	Circular	1190	15-noded	9742	0.355m	PLAXIS 2D V9	$q_{ult\text{-}Total\text{-}1A\text{-}2Dc\text{-}15}$
	Circular	1190	6-noded	2492	0.355m	PLAXIS 2D V9	$q_{ult\text{-}Total\text{-}1A\text{-}2Dc\text{-}6}$
Set 1B	Strip	1190	15-noded	9742	0.355m	PLAXIS 2D V9	$q_{ult\text{-}Total\text{-}1B\text{-}2Ds\text{-}15}$
	Strip	1190	6-noded	2492	0.355m	PLAXIS 2D V9	$q_{ult\text{-}Total\text{-}1B\text{-}2Ds\text{-}6}$
	Rectangular	6940	15-noded wedge	20038	0.600m	PLAXIS 3D Foundation	$q_{ult\text{-}Total\text{-}1B\text{-}3D3x20}$ $q_{ult\text{-}Total\text{-}1B\text{-}3D3x15}$ $q_{ult\text{-}Total\text{-}1B\text{-}3D3x10}$ $q_{ult\text{-}Total\text{-}1B\text{-}3D3x5}$ $q_{ult\text{-}Total\text{-}1B\text{-}3D3x3}$
	Circular	1190	15-noded	9742	0.355m	PLAXIS 2D V9	$q_{ult\text{-}Total\text{-}1B\text{-}2Dc\text{-}15}$
	Circular	1190	6-noded	2492	0.355m	PLAXIS 2D V9	$q_{ult\text{-}Total\text{-}1B\text{-}2Dc\text{-}6}$

Case of study	Type of footing	Number of elements	Type of element	Number of nodes	Average element size	FEM code used	Target parameter
Set 2A	Strip	938	15-noded	7750	0.730m	PLAXIS 2D V9	$q_{ult\text{-}Total\text{-}2A\text{-}2Ds\text{-}15}$
	Strip	938	6-noded	2000	0.730m	PLAXIS 2D V9	$q_{ult\text{-}Total\text{-}2A\text{-}2Ds\text{-}6}$
	Rectangular	6940	15-noded wedge	20038	0.600m	PLAXIS 3D Foundation	$q_{ult\text{-}Total\text{-}2A\text{-}3D3x20}$ $q_{ult\text{-}Total\text{-}2A\text{-}3D3x15}$ $q_{ult\text{-}Total\text{-}2A\text{-}3D3x10}$ $q_{ult\text{-}Total\text{-}2A\text{-}3D3x5}$ $q_{ult\text{-}Total\text{-}2A\text{-}3D3x3}$
	Circular	938	15-noded	7750	0.730m	PLAXIS 2D V9	$q_{ult\text{-}Total\text{-}2A\text{-}2Dc\text{-}15}$
	Circular	938	6-noded	2000	0.730m	PLAXIS 2D V9	$q_{ult\text{-}Total\text{-}2A\text{-}2Dc\text{-}6}$
Set 2B	Strip	938	15-noded	7750	0.730m	PLAXIS 2D V9	$q_{ult\text{-}Total\text{-}2B\text{-}2Ds\text{-}15}$
	Strip	938	6-noded	2000	0.730m	PLAXIS 2D V9	$q_{ult\text{-}Total\text{-}2B\text{-}2Ds\text{-}6}$
	Rectangular	6940	15-noded wedge	20038	0.600m	PLAXIS 3D Foundation	$q_{ult\text{-}Total\text{-}2B\text{-}3D3x20}$ $q_{ult\text{-}Total\text{-}2B\text{-}3D3x15}$ $q_{ult\text{-}Total\text{-}2B\text{-}3D3x10}$ $q_{ult\text{-}Total\text{-}2B\text{-}3D3x5}$ $q_{ult\text{-}Total\text{-}2B\text{-}3D3x3}$
	Circular	938	15-noded	7750	0.730m	PLAXIS 2D V9	$q_{ult\text{-}Total\text{-}2B\text{-}2Dc\text{-}15}$
	Circular	938	6-noded	2000	0.730m	PLAXIS 2D V9	$q_{ult\text{-}Total\text{-}2B\text{-}2Dc\text{-}6}$

Case of study	Type of footing	Number of elements	Type of element	Number of nodes	Average element size	FEM code used	Target parameter
Set 4A	Strip	938	15-noded	7750	0.730m	PLAXIS 2D V9	$q_{ult\text{-}Total\text{-}4A\text{-}2Ds\text{-}15}$
	Strip	938	6-noded	2000	0.730m	PLAXIS 2D V9	$q_{ult\text{-}Total\text{-}4A\text{-}2Ds\text{-}6}$
	Rectangular	9640	15-noded wedge	27151	0.602m	PLAXIS 3D Foundation	$q_{ult\text{-}Total\text{-}4A\text{-}3D3x20}$ $q_{ult\text{-}Total\text{-}4A\text{-}3D3x15}$ $q_{ult\text{-}Total\text{-}4A\text{-}3D3x10}$ $q_{ult\text{-}Total\text{-}4A\text{-}3D3x5}$ $q_{ult\text{-}Total\text{-}4A\text{-}3D3x3}$
	Circular	938	15-noded	7750	0.730m	PLAXIS 2D V9	$q_{ult\text{-}Total\text{-}4A\text{-}2Dc\text{-}15}$
	Circular	938	6-noded	2000	0.730m	PLAXIS 2D V9	$q_{ult\text{-}Total\text{-}4A\text{-}2Dc\text{-}6}$
Set 4B	Strip	938	15-noded	7750	0.730m	PLAXIS 2D V9	$q_{ult\text{-}Total\text{-}4B\text{-}2Ds\text{-}15}$
	Strip		6-noded			PLAXIS 2D V9	$q_{ult\text{-}Total\text{-}4B\text{-}2Ds\text{-}6}$
	Rectangular	3276	15-noded wedge	9844	0.247m	PLAXIS 3D-Tunnel	$q_{ult\text{-}Total\text{-}4B\text{-}3D3x20}$ $q_{ult\text{-}Total\text{-}4B\text{-}3D3x15}$ $q_{ult\text{-}Total\text{-}4B\text{-}3D3x10}$ $q_{ult\text{-}Total\text{-}4B\text{-}3D3x5}$ $q_{ult\text{-}Total\text{-}4B\text{-}3D3x3}$
	Circular	938	15-noded	7750	0.730m	PLAXIS 2D V9	$q_{ult\text{-}Total\text{-}4B\text{-}2Dc\text{-}15}$
	Circular	938	6-noded	2000	0.730m	PLAXIS 2D V9	$q_{ult\text{-}Total\text{-}4B\text{-}2Dc\text{-}6}$

3.4. Results and discussion

All analyses were performed for a footing with B = 3m. In some cases, just one quarter (B = 1.5m) of the total size of the footings (B = 3m) was modelled due to symmetrical conditions. Analyses for the complete size of the footing (without using symmetry) were also performed.

As it was said before, the simulations for Nq and s_q were done with $\gamma = 0$ and overburden p' = 11 kPa. In analyses for the determination of the total bearing capacity and the back-calculation of $N\gamma$ and s_γ, γ was set equal to 20 kN/m³.

According to Loukidis and Salgado (2009), the collapse load, q_{ult}, depends on the values considered for B, γ or p'; however, the values of the resulting bearing capacity equation factors are independent of these parameters when the soil friction angle and the dilatancy angle are always constant, which was the case of the present study for each individual material set of analysis.

3.4.1. Nq and s_q results

Figure 38, Figure 39, Figure 40 and Figure 41 show examples of the evolution of normalized footing load with normalized footing settlement w/B, illustrating that:

(a) The analyses with non-associated flow rule produce oscillation in the load-displacement curves when the collapse load is approached and after is reached. This is a characteristic, according to Loukidis and Salgado (2009) and mentioned in Chapter 1, observed in previous studies when the constitutive model of Mohr-Coulomb is used in combination with $\psi < \varphi$. The main reason for the oscillations is the apparent softening exhibited in shear bands when the energy is released and when the energy is transfered to the regions where the shear bands has not propagated yet. There is not a unique value of the failure load in this cases, it deviates from ±3% to ±6% from the mean value.

(b) The non-associated flow rule cases present lower values of Nq^*s_q than the associated cases. This is difference is more accentuated for higher friction angles.

(c) There is a close agreement between the 2D calculations for strip and circular footings with their respective equivalents results in 3D (3x20m footing and 3x3m footing). The agreement is better for lower friction angles; however, the general results are between the limit of ±10% of difference, for both types of elements: 6-noded and 15-noded triangle elements. See Annexe 3 for the specific values of the ultimate load.

(d) The normalized settlement when the collapse load (peak load) is reached, for the non-associated flow rule cases, is approximately two times higher than the one observed for the associated flow rule cases.

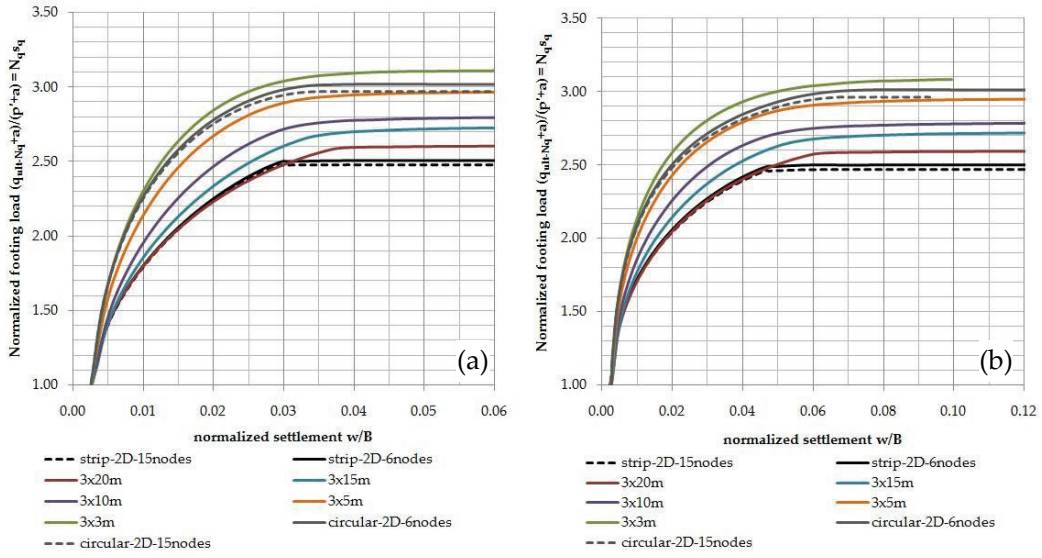

Figure 38: Load-settlement response from the analyses of footings in 2D and 3D for the determination of Nq^*s_q for a friction angle of 10°: (a) using associated flow rule $\psi = \varphi$ (Set 1A), and, (b) using non-associated flow rule $\psi < \varphi$ (Set 1B).

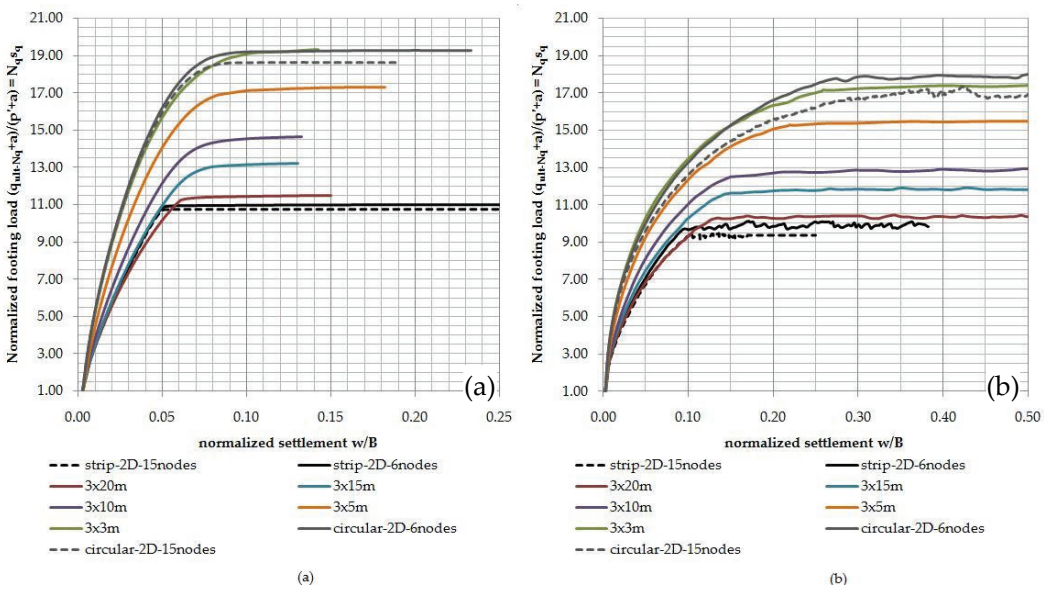

Figure 39: Load-settlement response from the analyses of footings in 2D and 3D for the determination of Nq^*s_q for a friction angle of 25°: (a) using associated flow rule $\psi = \varphi$ (Set 2A), and, (b) using non-associated flow rule $\psi < \varphi$ (Set 2B).

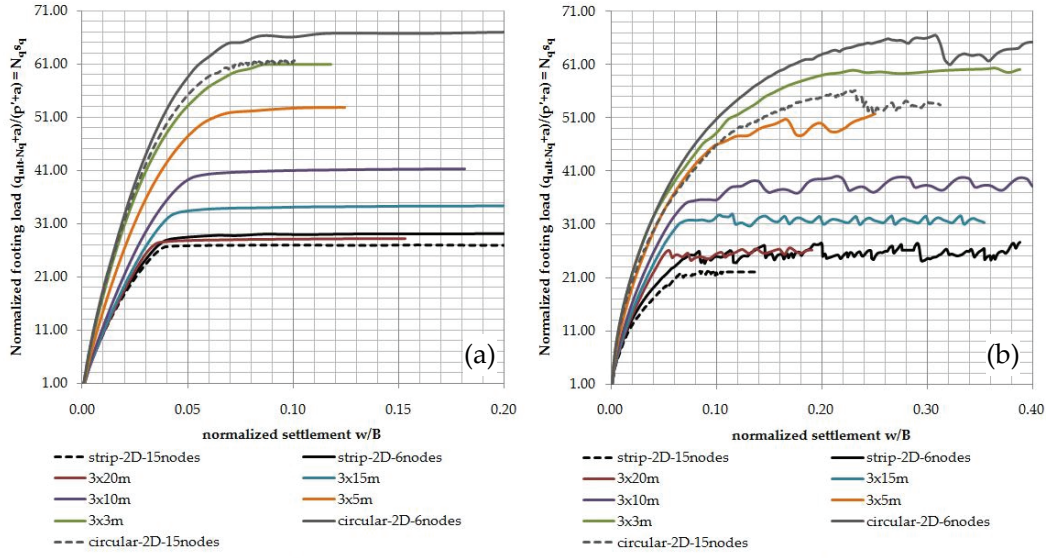

Figure 40: Load-settlement response from the analyses of footings in 2D and 3D for the determination of Nq^*s_q for a friction angle of 33°: (a) using associated flow rule $\psi = \varphi$ (Set 3A), and, (b) using non-associated flow rule $\psi < \varphi$ (Set 3B).

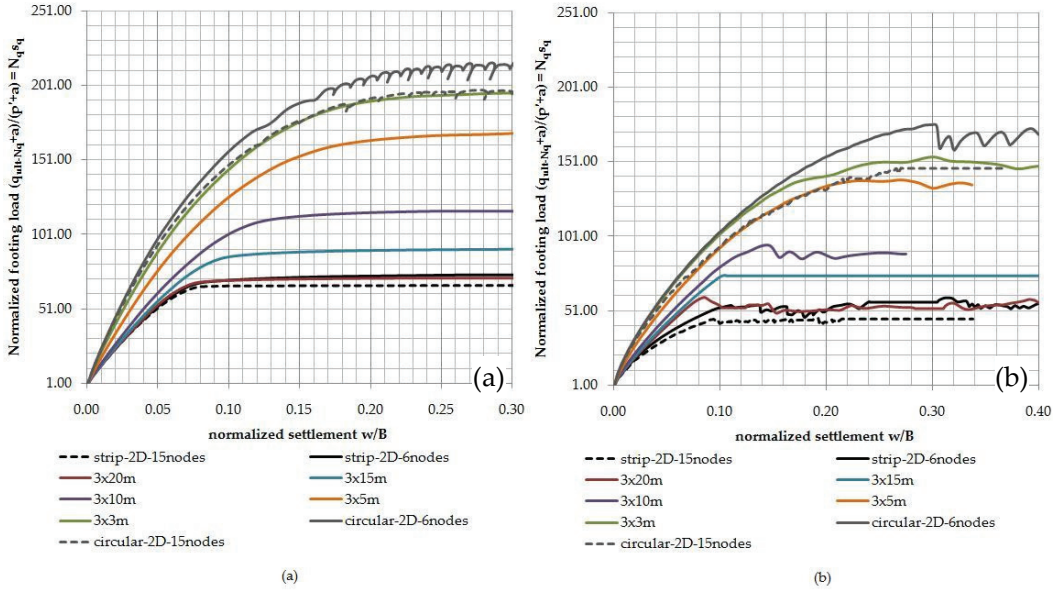

Figure 41: Load-settlement response from the analyses of footings in 2D and 3D for the determination of Nq^*s_q for a friction angle of 40°: (a) using associated flow rule $\psi = \varphi$ (Set 4A), and, (b) using non-associated flow rule $\psi < \varphi$ (Set 4B).

Figure 42, Figure 43 and Figure 44 show the collapse mechanisms for footings when $\gamma = 0$, $p' = 11$ kPa and $\varphi = 10°$; in cases of associated and non-associated flow rule.

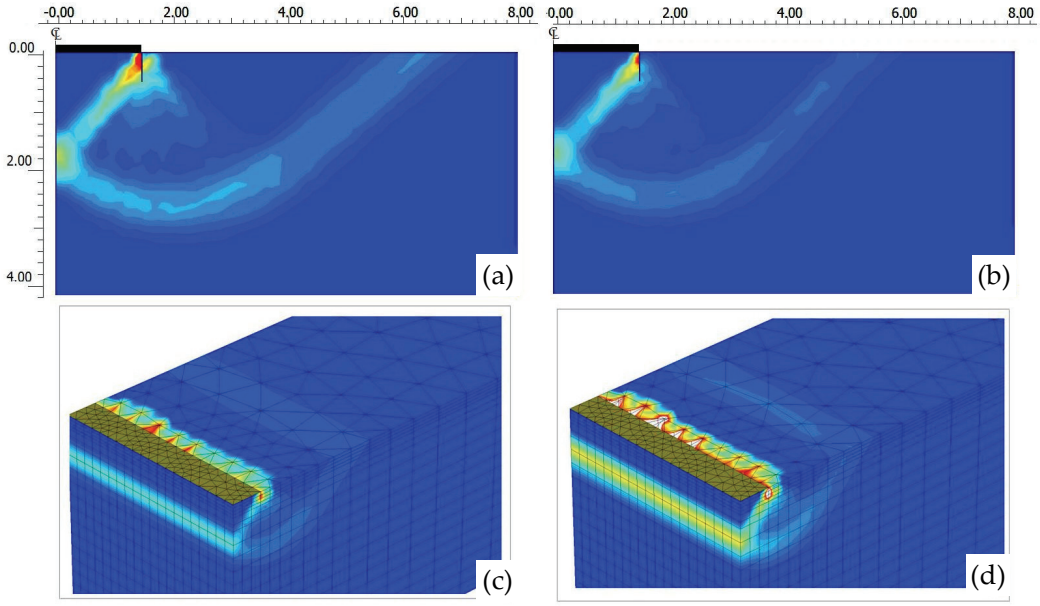

Figure 42: Collapse mechanisms (Nq-study) when $\varphi = 10°$ as depicted by incremental shear strains for: (a) strip footing in 2D and $\psi = \varphi$; (b) strip footing in 2D and $\psi < \varphi$; (c) 3x20m footing in 3D and $\psi = \varphi$; (d) 3x20m footing in 3D and $\psi < \varphi$.

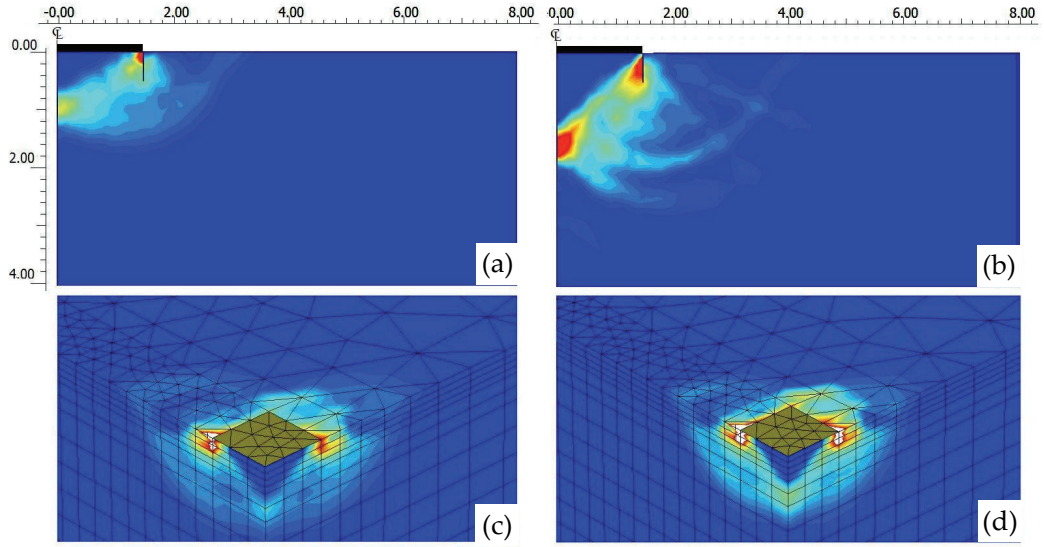

Figure 43: Collapse mechanisms (Nq-study) when $\varphi = 10°$ as depicted by incremental shear strains for: (a) circular footing in 2D and $\psi = \varphi$; (b) circular in 2D and $\psi < \varphi$; (c) 3x3m footing in 3D and $\psi = \varphi$; (d) 3x3m footing in 3D and $\psi < \varphi$.

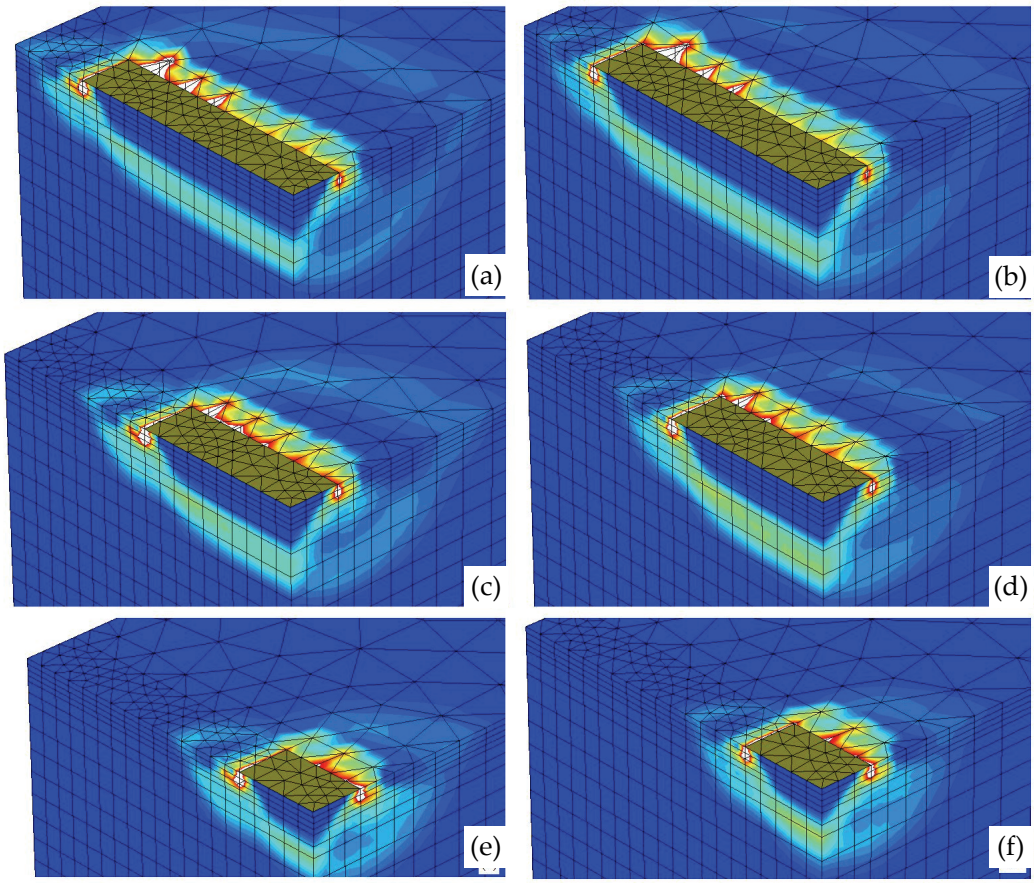

Figure 44: Collapse mechanisms (Nq-study) when $\varphi = 10°$ as depicted by incremental shear strains for: (a) 3x15m footing in 3D and $\psi = \varphi$; (b) 3x15m footing in 3D and $\psi < \varphi$; (c) 3x10m footing in 3D and $\psi = \varphi$; (d) 3x10m footing in 3D and $\psi < \varphi$; (e) 3x5m footing in 3D and $\psi = \varphi$; (f) 3x5m footing in 3D and $\psi < \varphi$.

Figure 45, Figure 46 and Figure 47 show the collapse mechanisms for footings for a weightless soil with a overburden of 11 kPa and a friction angle of 25°; in cases of associated flow rule and non-associated flow rule.

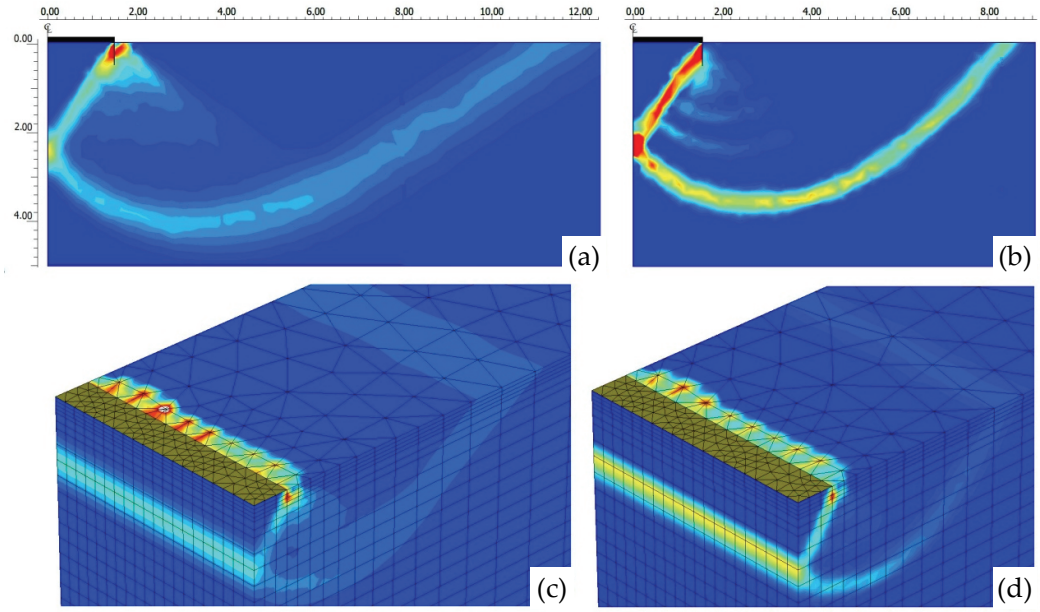

Figure 45: Collapse mechanisms (Nq-study) when $\varphi = 25°$ as depicted by incremental shear strains for: (a) strip footing in 2D and $\psi = \varphi$; (b) strip footing in 2D and $\psi < \varphi$; (c) 3x20m footing in 3D and $\psi = \varphi$; (d) 3x20m footing in 3D and $\psi < \varphi$.

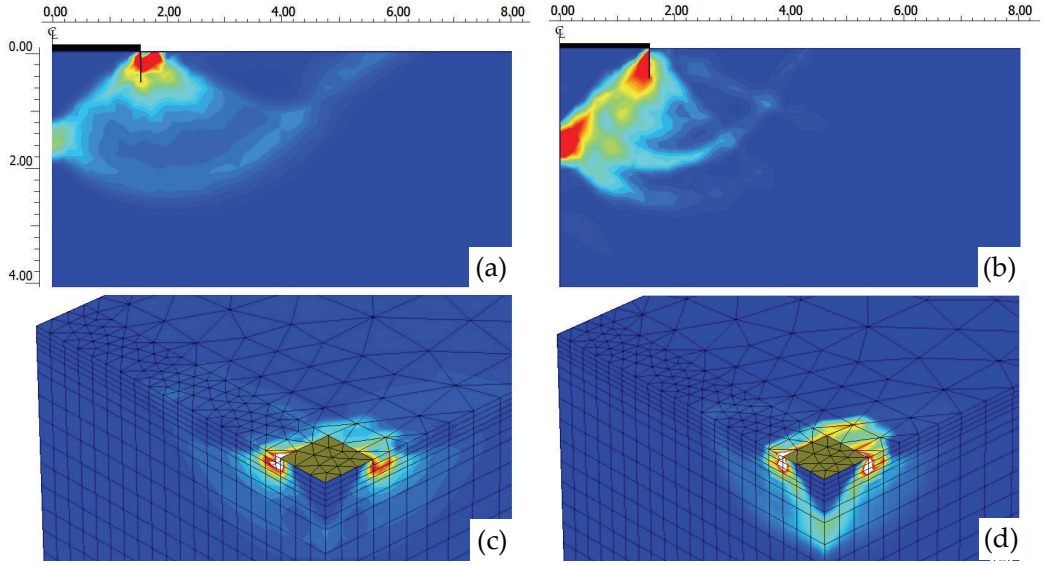

Figure 46: Collapse mechanisms (Nq-study) when $\varphi = 25°$ as depicted by incremental shear strains for: (a) circular footing in 2D and $\psi = \varphi$; (b) circular in 2D and $\psi < \varphi$; (c) 3x3m footing in 3D and $\psi = \varphi$; (d) 3x3m footing in 3D and $\psi < \varphi$.

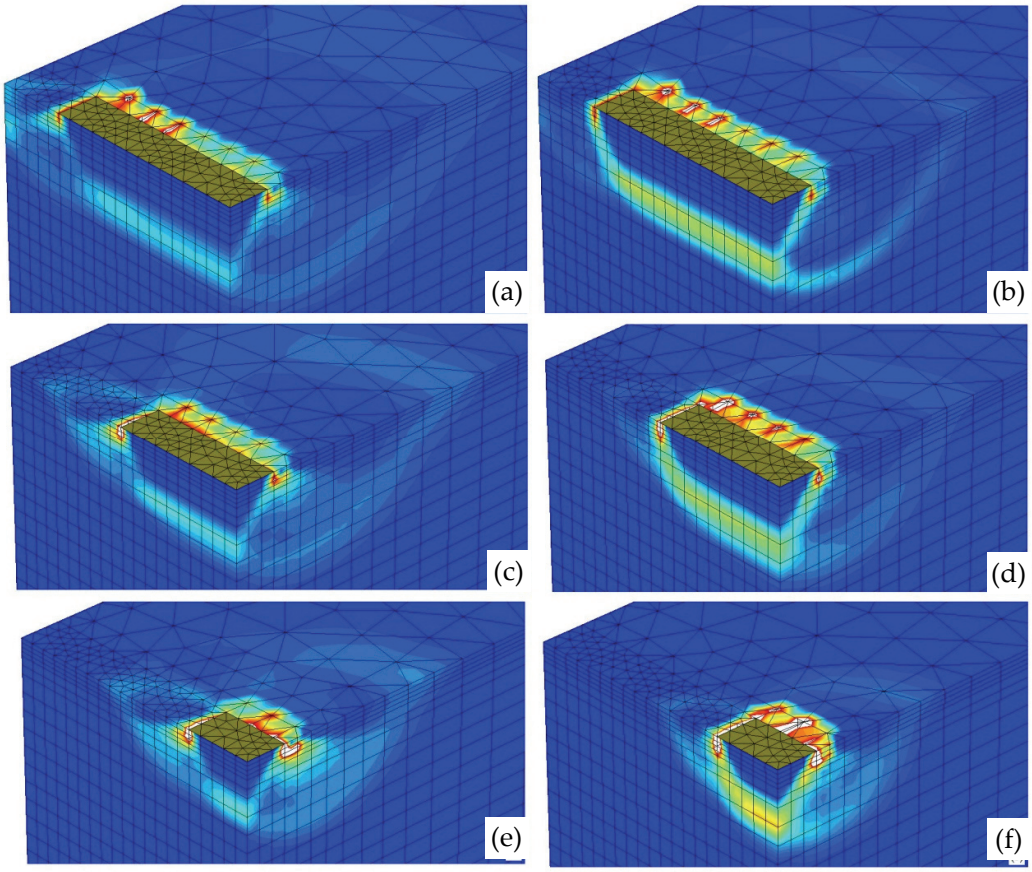

Figure 47: Collapse mechanisms (Nq-study) when $\varphi = 25°$ as depicted by incremental shear strains for: (a) 3x15m footing in 3D and $\psi = \varphi$; (b) 3x15m footing in 3D and $\psi < \varphi$; (c) 3x10m footing in 3D and $\psi = \varphi$; (d) 3x10m footing in 3D and $\psi < \varphi$; (e) 3x5m footing in 3D and $\psi = \varphi$; (f) 3x5m footing in 3D and $\psi < \varphi$.

Figure 48, Figure 49 and Figure 50 show the collapse mechanisms for footings for a weightless soil with a overburden of 11 kPa and a friction angle of 33°; in cases of associated flow rule and non-associated flow rule.

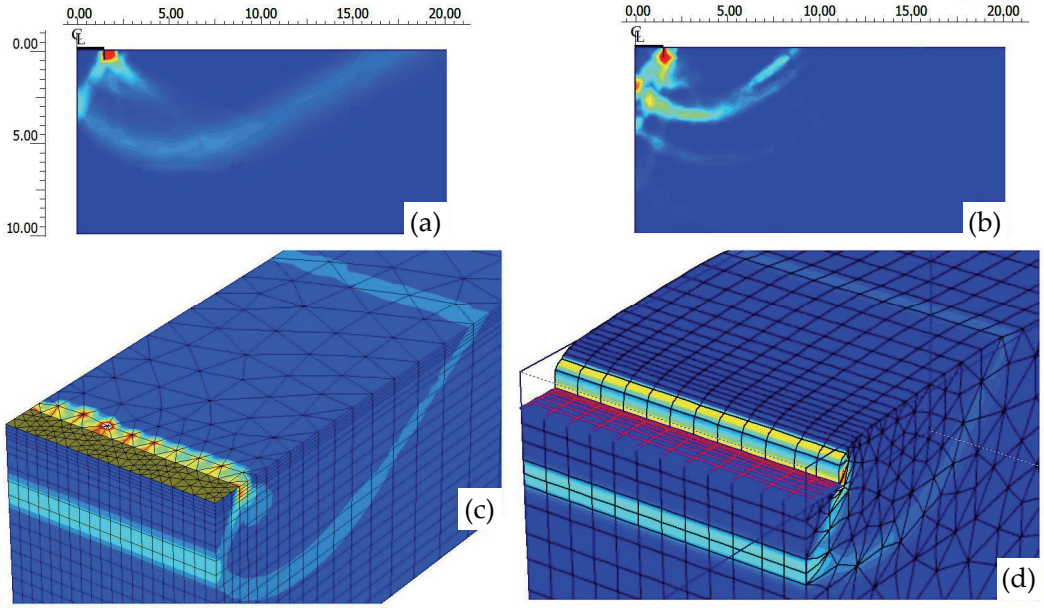

Figure 48: Collapse mechanisms (Nq-study) when φ = 33° as depicted by incremental shear strains for: (a) strip footing in 2D and ψ = φ; (b) strip footing in 2D and ψ < φ; (c) 3x20m footing in 3D and ψ = φ; (d) 3x20m footing in 3D and ψ < φ.

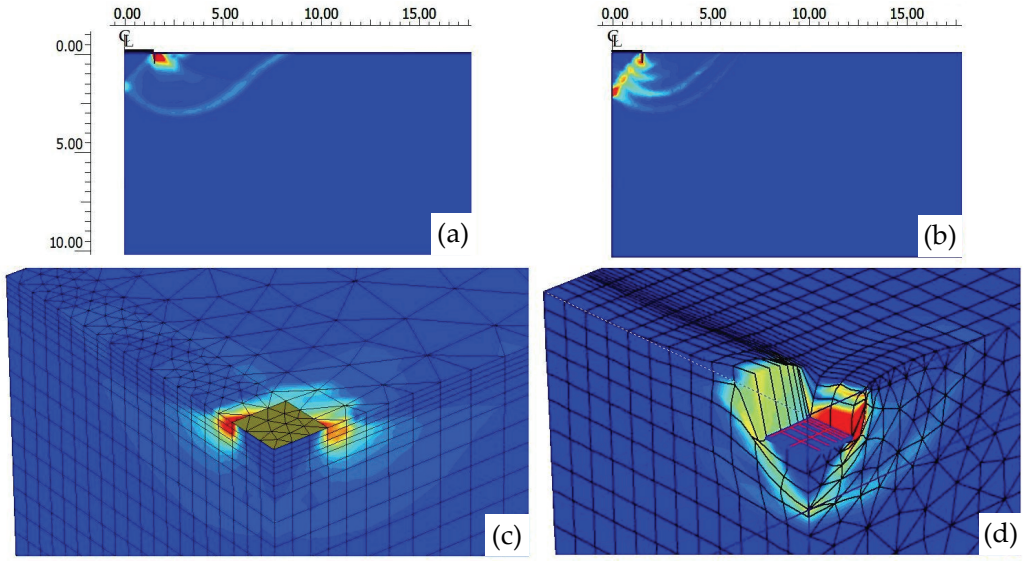

Figure 49: Collapse mechanisms (Nq-study) when φ = 33° as depicted by incremental shear strains for: (a) circular footing in 2D and ψ = φ; (b) circular in 2D and ψ < φ; (c) 3x3m footing in 3D and ψ = φ; (d) 3x3m footing in 3D and ψ < φ.

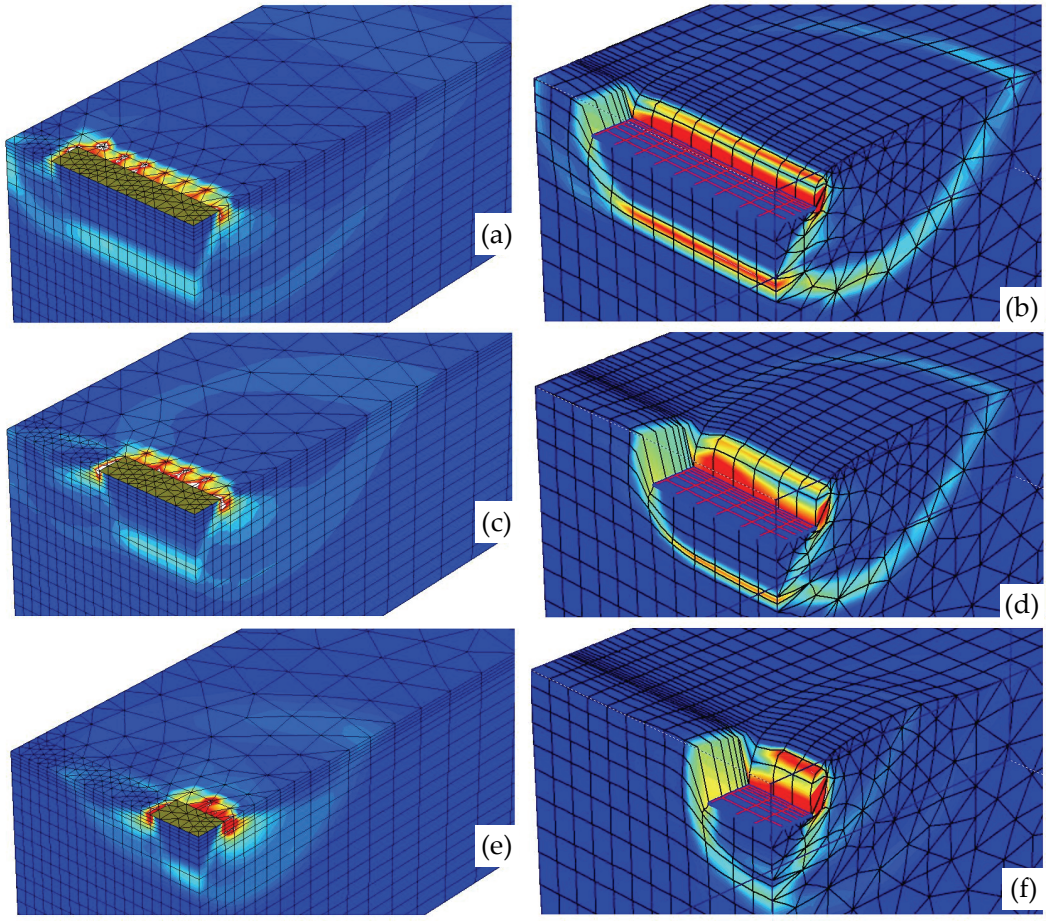

Figure 50: Collapse mechanisms (Nq-study) when $\varphi = 33°$ as depicted by incremental shear strains for: (a) 3x15m footing in 3D and $\psi = \varphi$; (b) 3x15m footing in 3D and $\psi < \varphi$; (c) 3x10m footing in 3D and $\psi = \varphi$; (d) 3x10m footing in 3D and $\psi < \varphi$; (e) 3x5m footing in 3D and $\psi = \varphi$; (f) 3x5m footing in 3D and $\psi < \varphi$.

Figure 51, Figure 52 and Figure 53 show the collapse mechanisms for footings for a weightless soil with a overburden of 11 kPa and a friction angle of 40°; in cases of associated flow rule and non-associated flow rule.

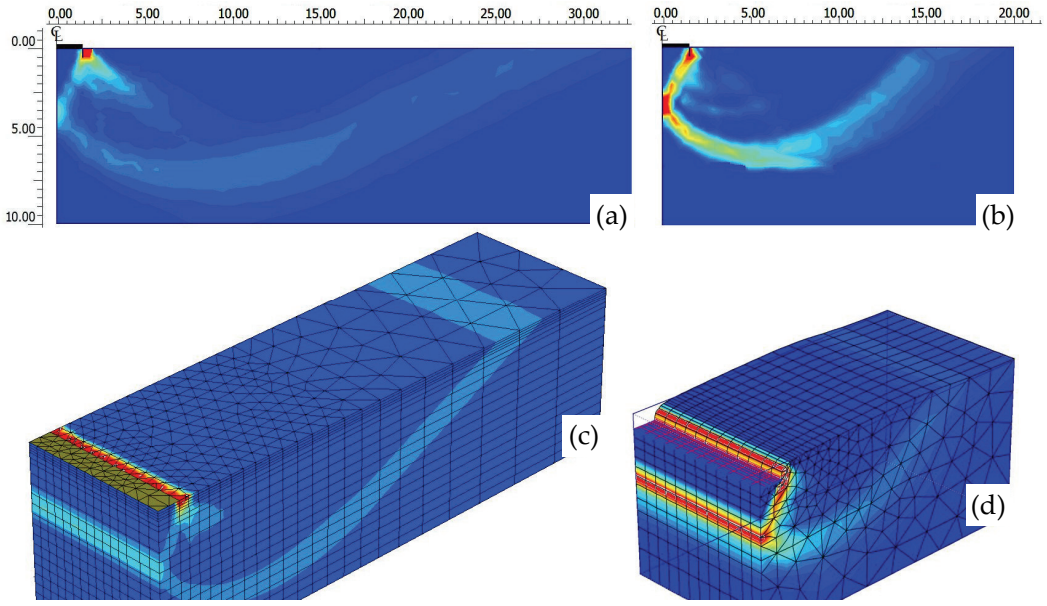

Figure 51: Collapse mechanisms (Nq-study) when φ = 40° as depicted by incremental shear strains for: (a) strip footing in 2D and ψ = φ; (b) strip footing in 2D and ψ < φ; (c) 3x20m footing in 3D and ψ = φ; (d) 3x20m footing in 3D and ψ < φ.

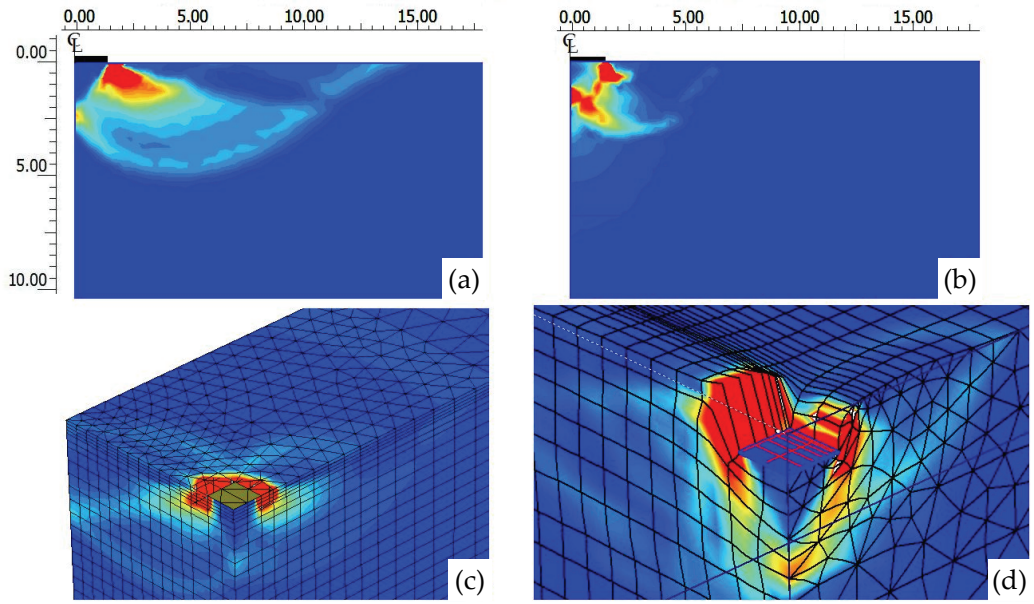

Figure 52: Collapse mechanisms (Nq-study) when φ = 40° as depicted by incremental shear strains for: (a) circular footing in 2D and ψ = φ; (b) circular in 2D and ψ < φ; (c) 3x3m footing in 3D and ψ = φ; (d) 3x3m footing in 3D and ψ < φ.

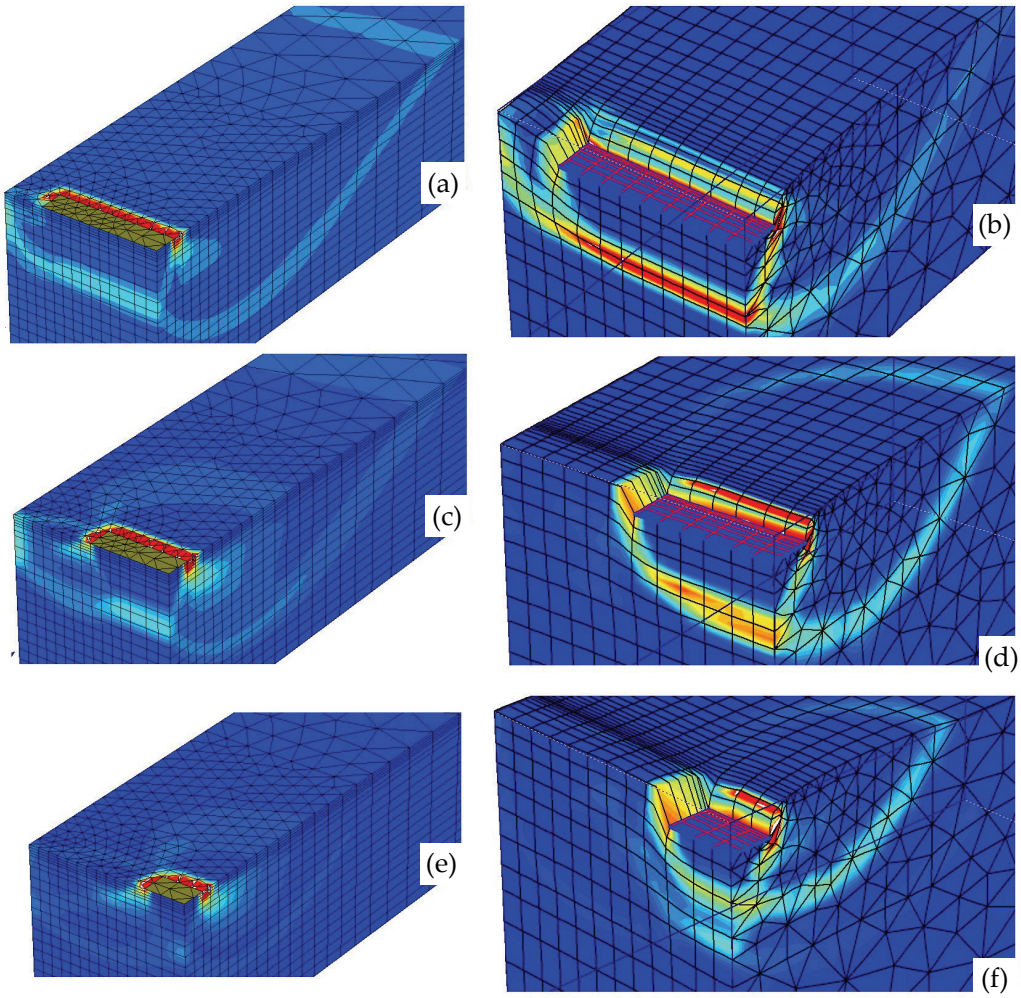

Figure 53: Collapse mechanisms (Nq-study) when $\varphi = 40°$ as depicted by incremental shear strains for: (a) 3x15m footing in 3D and $\psi = \varphi$; (b) 3x15m footing in 3D and $\psi < \varphi$; (c) 3x10m footing in 3D and $\psi = \varphi$; (d) 3x10m footing in 3D and $\psi < \varphi$; (e) 3x5m footing in 3D and $\psi = \varphi$; (f) 3x5m footing in 3D and $\psi < \varphi$.

In general, the collapse mechanisms developed with 2D and 3D Finite Element analyses agree well between them in shape and size, this can be compared taking the width of the footing as the comparative value (1.5m in all the cases). It should be aware that in the collapse mechanism, the scale colours does not

coincide between them, this is because the main interest of the plots was to show the failure pattern shape and not the strains level developed.

For the case of non-associated flow rule, the mechanism is more localized in shear bands due to the apparent softening and energy release exhibited by a material with $\psi < \varphi$. Also, as was observed in previous studies and pointed out by Loukidis and Salgado (2009), the collapse mechanism for the $\psi = \varphi$ cases is larger than the one for $\psi < \varphi$. This causes that the bearing capacity for non-associated flow rule is lower than for associated flow rule, which effect is more distinct for higher friction angles (the difference between the friction and dilatancy angle is higher).

The last behaviour can be illustrated with Figure 54 (for strip footings) and Figure 55 (for circular footings) which show the Nq bearing capacity factor normalized with respect to the corresponding value from the exact solution (Equation 2) for the associated and non-associated flow rule cases.

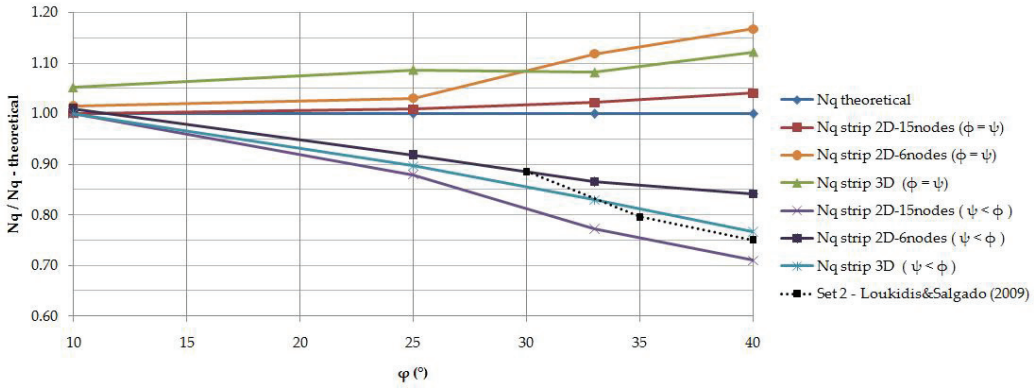

Figure 54: Bearing capacity factor Nq for strip footings normalized with respect to the corresponding value from the exact solution (Prandtl, 1921).

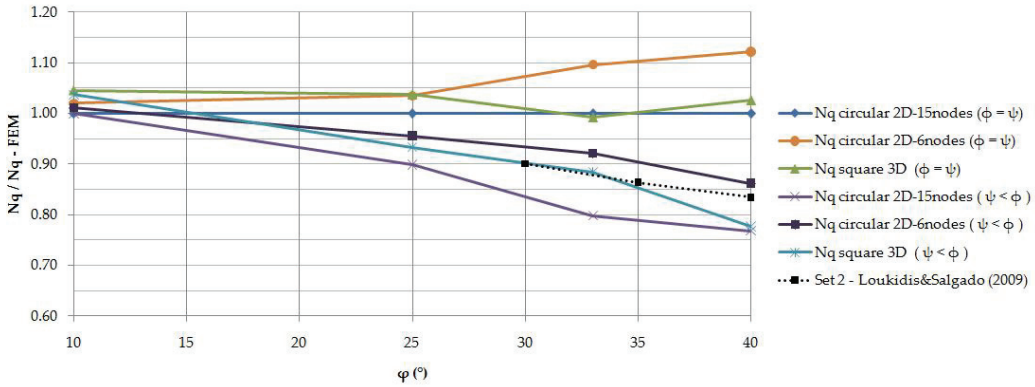

Figure 55: Bearing capacity factor Nq for circular footings normalized with respect to the corresponding value from the 2D Finite Element solution with 15-noded elements.

It can be seen in Figure 54 that the results for 15-noded elements are very close to the theoretical values, for that reason, they were used as the normalization values for the circular footings (Figure 55). The solutions for 6-noded elements deviate from the theoretical values in a little more than 15% for the highest friction angle. However, the 3D-FE solution for the strip footing (3x20m) lies between the two borders defined by the 15-noded (2D-FE) and 6-noded (2D-FE) solutions with a maximum deviation of around 10% (which was the value of tolerance defined as acceptable). These facts establish the validity of the present FE simulations. The values of the bearing capacity factor Nq for a soil with $\psi < \varphi$ values are clearly smaller than the Nq values for a material with an associated flow rule, this fact agrees with previous studies (de Borst and Vermeer, 1984; Manoharan and Dasgupta, 1995; Frydman and Burd, 1997; Yin *et al.*, 2001; Loukidis and Salgado, 2009). The solution for 3D-strip footings and $\psi < \varphi$ lies between the 2D-FE solutions for 6-noded and 15-noded elements and it is very close to the solutions obtained by Loukidis and Salgado (2009) for dilatancy angles 30° lower than the friction angles.

A similar behaviour is observed in Figure 55 for circular/square footings with the 3D-solutions, they are limited by the 2D-solutions (15-noded and 6-noded elements) and they have a close agreement with the solution for circular footings and $\psi < \varphi$ obtained by Loukidis and Salgado (2009). Also, the non-

associated flow rule cases show smaller Nq values than the $\psi = \varphi$ cases, especially, for higher friction angles.

In general, the results obtained in the present study agree with the findings of Manoharan and Dasgupta (1995) who mention that for lower friction angles, $\varphi < 25°$, both the flow rules, associated and non-associated, give the same result (or very similar like in the present case); and, as φ is increased further, Nq-values are overestimated with an associated flow rule.

Finally, the focus of this part of the present study is the shape factor s_q in the bearing capacity equation and how the bearing capacity factor Nq is affected by the relative footing dimension B/L. For that reason, Figure 56, Figure 57, Figure 58 and Figure 59 show the variations of the shape factor and the factor Nq^*s_q with the relative footing dimension B/L for the friction angles studied (10°, 25°, 33° and 40°) in the associated and non-associated flow rule cases. The results are also compared with the different theoretical proposals commented in Chapter 2.

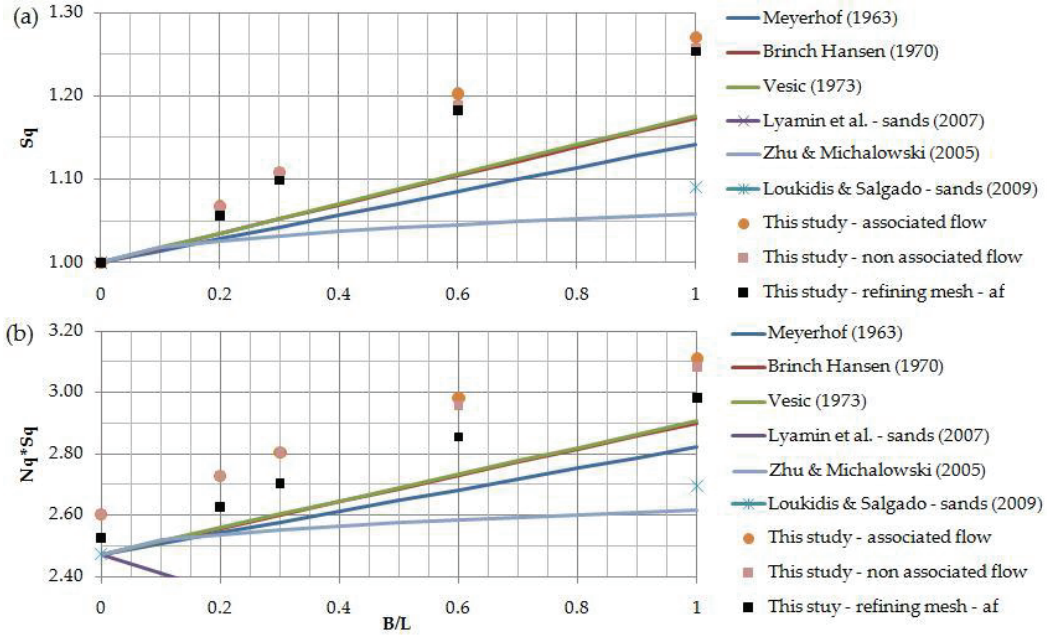

Figure 56: Comparison of results for $\varphi = 10°$ from various methods of analysis: (a) shape factor s_q and (b) factor Nq^*s_q, respect to the relative footing dimension B/L.

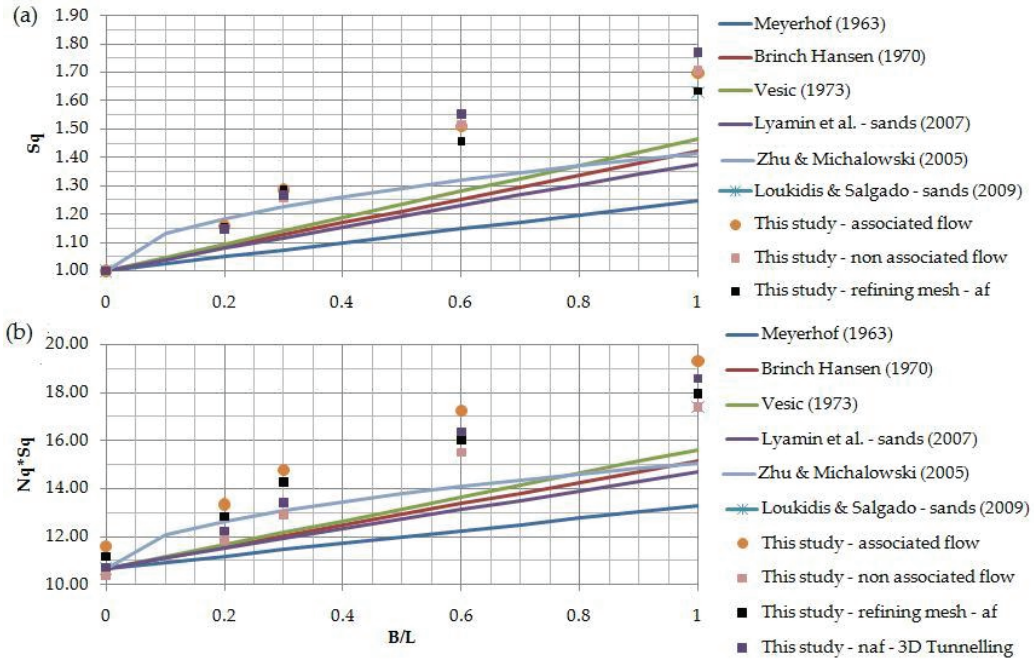

Figure 57: Comparison of results for φ = 25° from various methods of analysis: (a) shape factor s_q and (b) factor $N_q^* s_q$, respect to the relative footing dimension B/L.

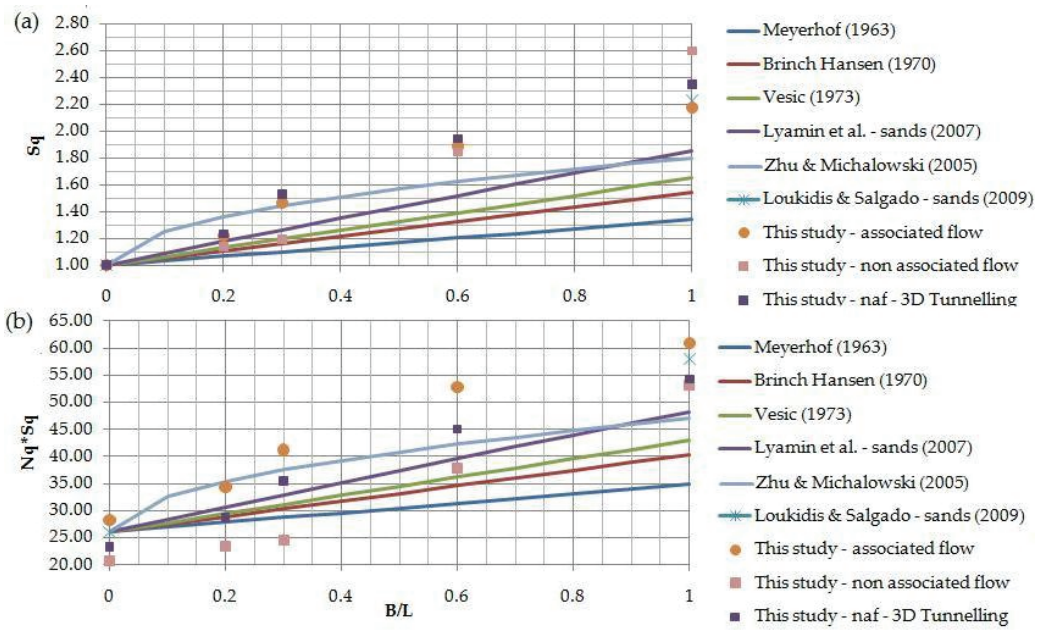

Figure 58: Comparison of results for φ = 33° from various methods of analysis: (a) shape factor s_q and (b) factor $N_q^* s_q$, respect to the relative footing dimension B/L.

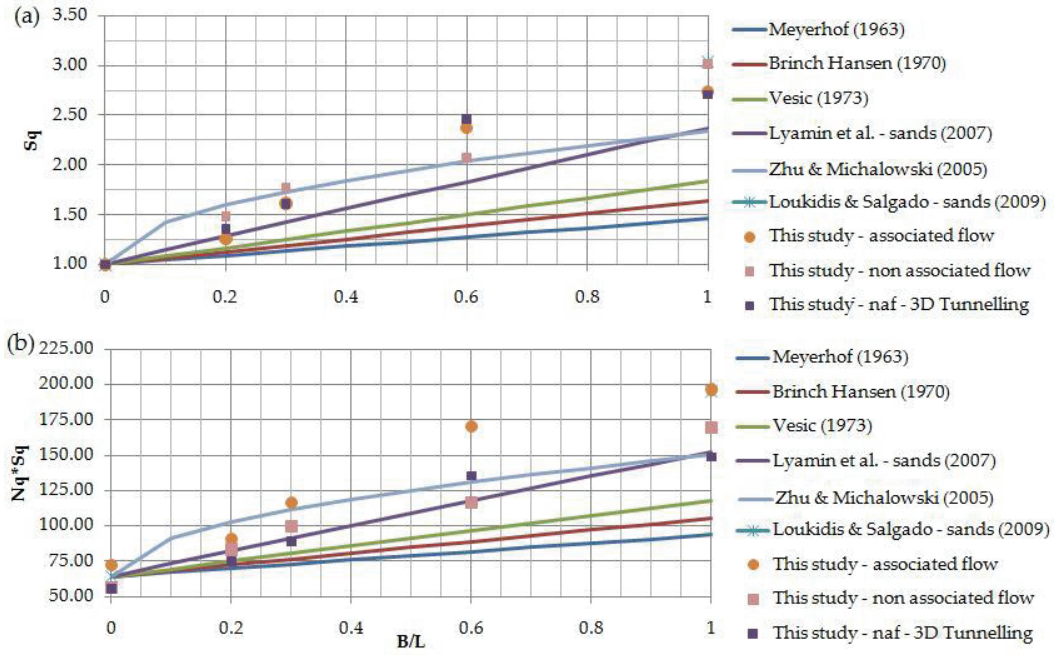

Figure 59: Comparison of results for $\varphi = 40°$ from various methods of analysis: (a) shape factor s_q and (b) factor Nq^*s_q, respect to the relative footing dimension B/L.

From Figure 56, Figure 57, Figure 58 and Figure 59 shown before, several aspects can be commented:

(a) The shape factor s_q increases when the relative footing dimension B/L increases from zero to one. That means that square/circular footings have higher bearing capacity factor (Nq^*s_q) than rectangular or strip footings. This fact coincides with what is proposed by previous studies; however, both the shape factor values and their rate of increase with φ are significantly smaller than those resulting from the Finite Element analyses.

(b) The associated and non-associated flow rule is not strongly affecting the shape factor s_q. The effect is more visible in the bearing capacity factor Nq^*s_q. When $\psi < \varphi$, Nq^*s_q reaches a lower value than the case when $\psi = \varphi$ and this difference is more evident for higher friction angles ($\varphi > 30°$). However, the bearing capacity factor Nq^*s_q in the non-associated case is

closer to the proposals given by previous studies, which mean than the last ones are still on the safe side.

(c) There is a close agreement between the results for square footings of the present study and the results of Loukidis and Salgado (2009) for circular footings, especially for $\varphi > 30°$. This fact establishes the validity of the present FE simulations, taking into account that the study of Loukidis and Salgado (2009) applies to sands.

(d) Mesh refining on the borders of the footings was done for the cases of $\varphi = 10°$ and $\varphi = 25°$ in $\psi = \varphi$ case. It was observed that the shape factors s_q and the Nq^*s_q factors were smaller and closer to the results proposed by previous studies. It seems that the refinement produces more accurate results.

(e) The FE simulations were performed using two planes of symmetry and not using them. When the symmetry was skipped, the results did not change for $\varphi < 30°$ and both cases of flow rule. However, when the two planes of symmetry were used, some problems (discussed in Chapter 4) were observed for analyses with $\varphi > 30°$ in combination with $\psi < \varphi$. These problems were related to low collapse loads due to localization of failure on the surface. Later, it was discovered the dependency between a structure mesh on the vertical plane and the failure localization.

(f) To overcome the problem related to the combined analyses of $\varphi > 30°$, non-associated flow rule and two planes of symmetry in the footing; it was proposed to perform analyses with other 3D Finite Element code which allowed the construction of an unstructured mesh in the vertical plane of the model. Analyses with PLAXIS 3D Tunnel were done for friction angles of 33° and 40° (also for $\varphi = 25°$ to validate the results) obtaining general failure mechanisms and good agreement with preliminary results and theories, especially with the ones proposed by Zhu and Michalowski (2005).

(g) Performing 2D simulations for 6-noded and 15-noded elements in strip (plane strain) and circular (axisymmetrical) footings agree in ± 10% from results for similar cases in 3D simulations (strip 3x20m footing and square

3x3m footing respectively). Annexe 3 details the values of the failure load results.

(h) In general, there is good agreement between the shape factor s_q results of the present study and the proposals of Zhu and Michalowski (2005) and Loukidis and Salgado (2009) for $\varphi > 25°$. It can be recommended to use these suggestions for s_q; even though they are approximate solutions: pseudo-upper-bound to the exact solutions according to Hjiaj *et al.* (2005). Lyamin *et al.* (2007) proposals have lower values. They come from an analysis that combines FEM and limit analysis which allows bracketing the exact solution. Therefore, they are highly recommended.

(i) For lower friction angles ($\varphi < 25°$), Vesić (1973) suggestions are recommended. They come from experimental studies and agree with the results of the present study.

(j) Meyerhof (1963) and Brinch-Hansen (1970) proposals for s_q are clearly lower than the values found in the present study. However, they are still on the safe side when they are compared to the results of the present study for non-associated flow rule.

(k) Finally, a good practice for shape factor can be to linearly interpolate between circular and strip solutions. It is in the conservative side.

3.4.2. $N\gamma$ and s_γ results

Figure 60, Figure 61 and Figure 62 show examples of the failure load with normalized footing settlement w/B, illustrating that:

(a) The analyses with $\psi < \varphi$ produce lower values of the ultimate load than the $\psi = \varphi$ cases. This difference is more notorious for higher friction angles, because ψ and φ are more deviated between them. There is not a unique value of the failure load, the oscillations in the load-displacement curve cause a deviation of ±3% to ±6% from the mean value.

(b) The 2D calculations for strip and circular footings agree with their respective equivalents results in 3D (3x20m footing and 3x3m footing respectively), especially for lower friction angles.

(c) The exception to (b) are the results for φ = 40° in associative and non-associative cases. The load-displacements curves are not clearly defined and the calculation time of the simulations was increased. This might be due to the high numerical work that a friction angle of 40° demands, especially in non-associative flow rule case.

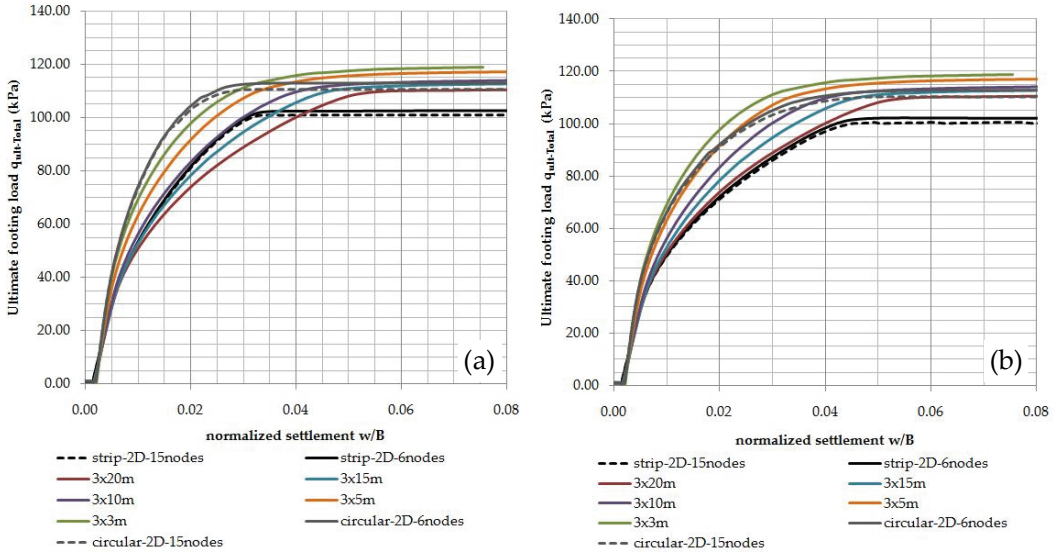

Figure 60: Load-settlement response from the analyses of footings in 2D and 3D for the determination of total bearing capacity (for Nγ back-calculation) for a friction angle of 10°: (a) using associated flow rule ψ = φ (Set 1A), and, (b) using non-associated flow rule ψ < φ (Set 1B).

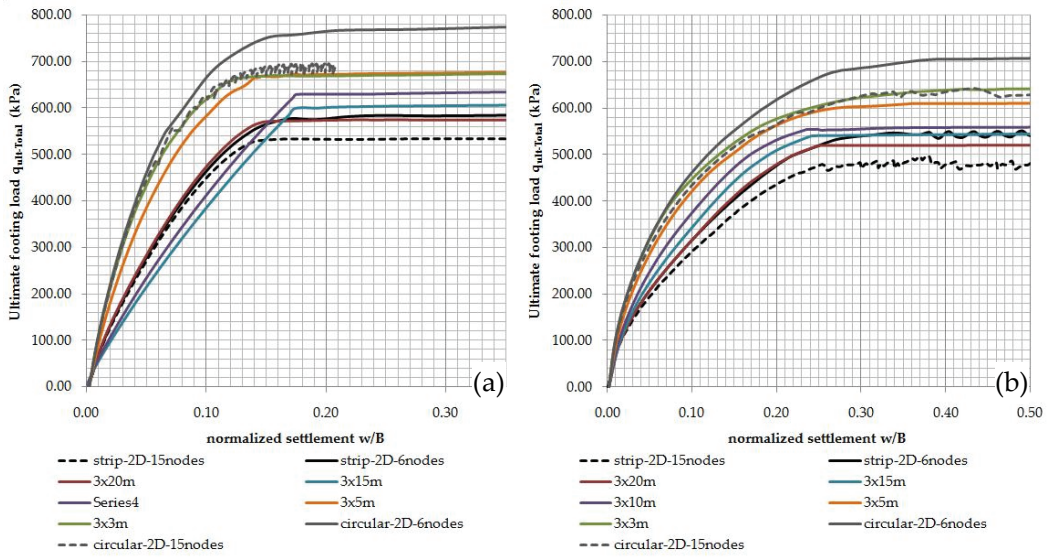

Figure 61: Load-settlement response from the analyses of footings in 2D and 3D for the determination of total bearing capacity (for Nγ back-calculation) for a friction angle of 25°: (a) using associated flow rule ψ = φ (Set 2A), and, (b) using non-associated flow rule ψ < φ (Set 2B).

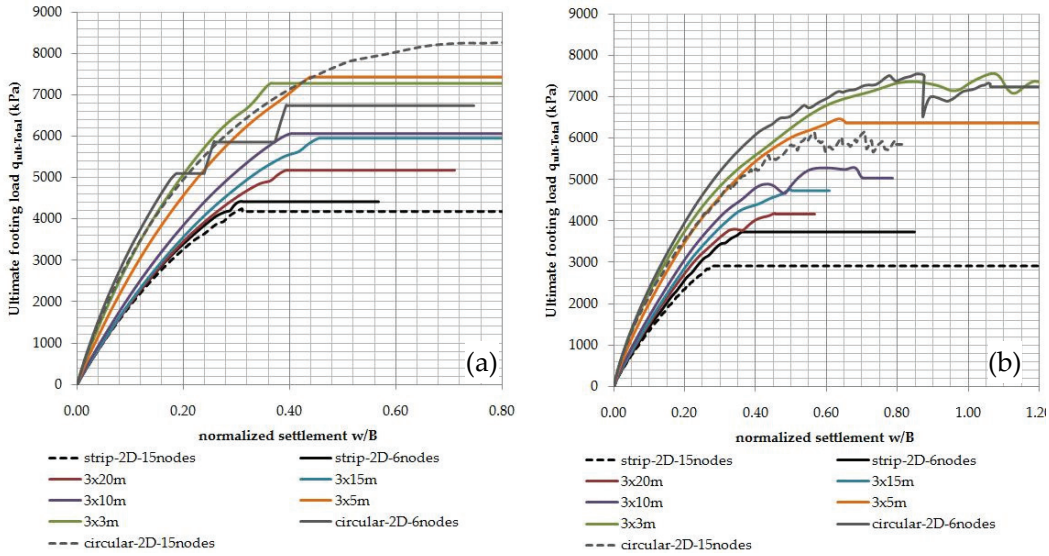

Figure 62: Load-settlement response from the analyses of footings in 2D and 3D for the determination of total bearing capacity (for Nγ back-calculation) for a friction angle of 40°: (a) using associated flow rule ψ = φ (Set 1A), and, (b) using non-associated flow rule ψ < φ (Set 1B).

Figure 63, Figure 64 and Figure 65 show the collapse mechanisms for footings when γ = 20 kN/m^3, p′ = 11 kPa and φ = 10°; in cases of associated and non-associated flow rule.

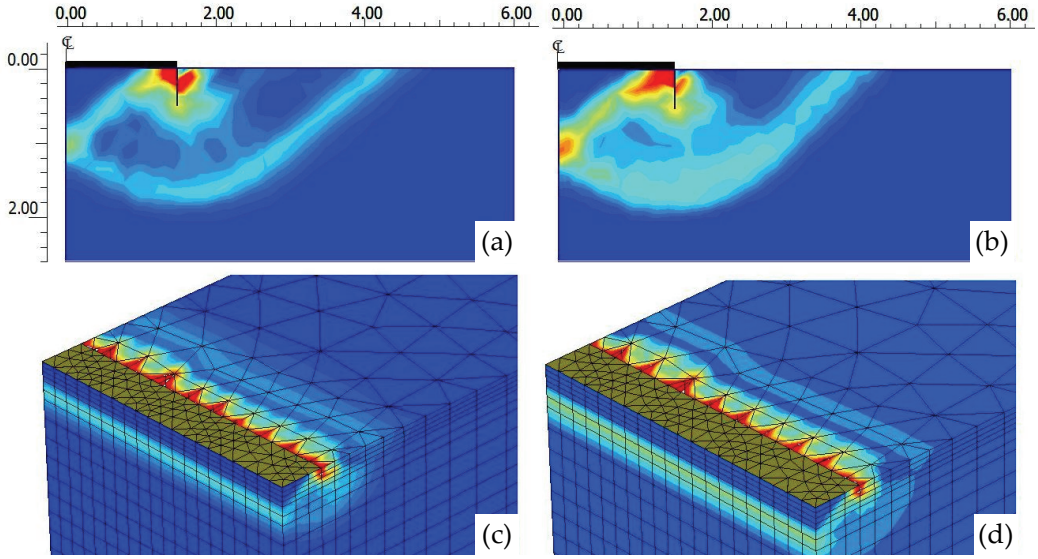

Figure 63: Collapse mechanisms (Nγ-back calculation) when φ = 10° as depicted by incremental shear strains for: (a) strip footing in 2D and $\psi = \varphi$; (b) strip footing in 2D and $\psi < \varphi$; (c) 3x20m footing in 3D and $\psi = \varphi$; (d) 3x20m footing in 3D and $\psi < \varphi$.

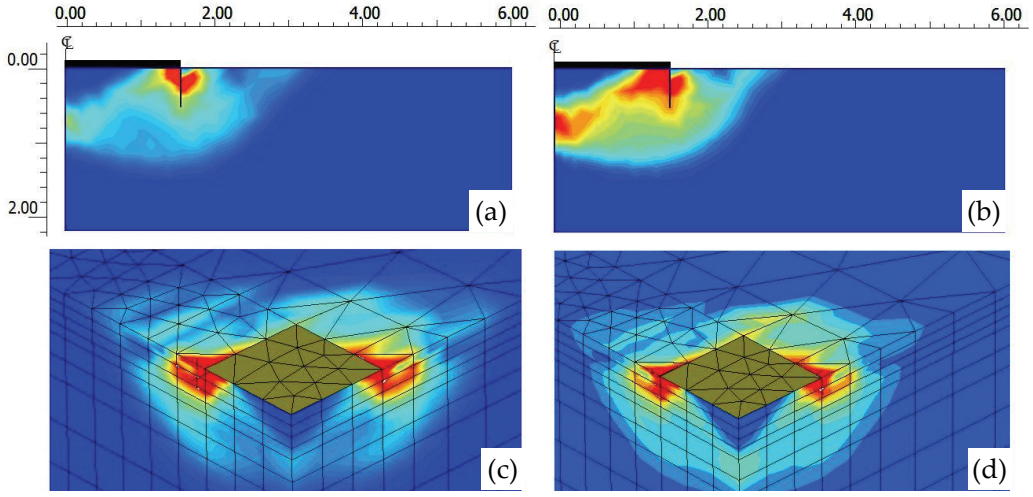

Figure 64: Collapse mechanisms (Nγ-back calculation) when φ = 10° as depicted by incremental shear strains for: (a) circular footing in 2D and $\psi = \varphi$; (b) circular in 2D and $\psi < \varphi$; (c) 3x3m footing in 3D and $\psi = \varphi$; (d) 3x3m footing in 3D and $\psi < \varphi$.

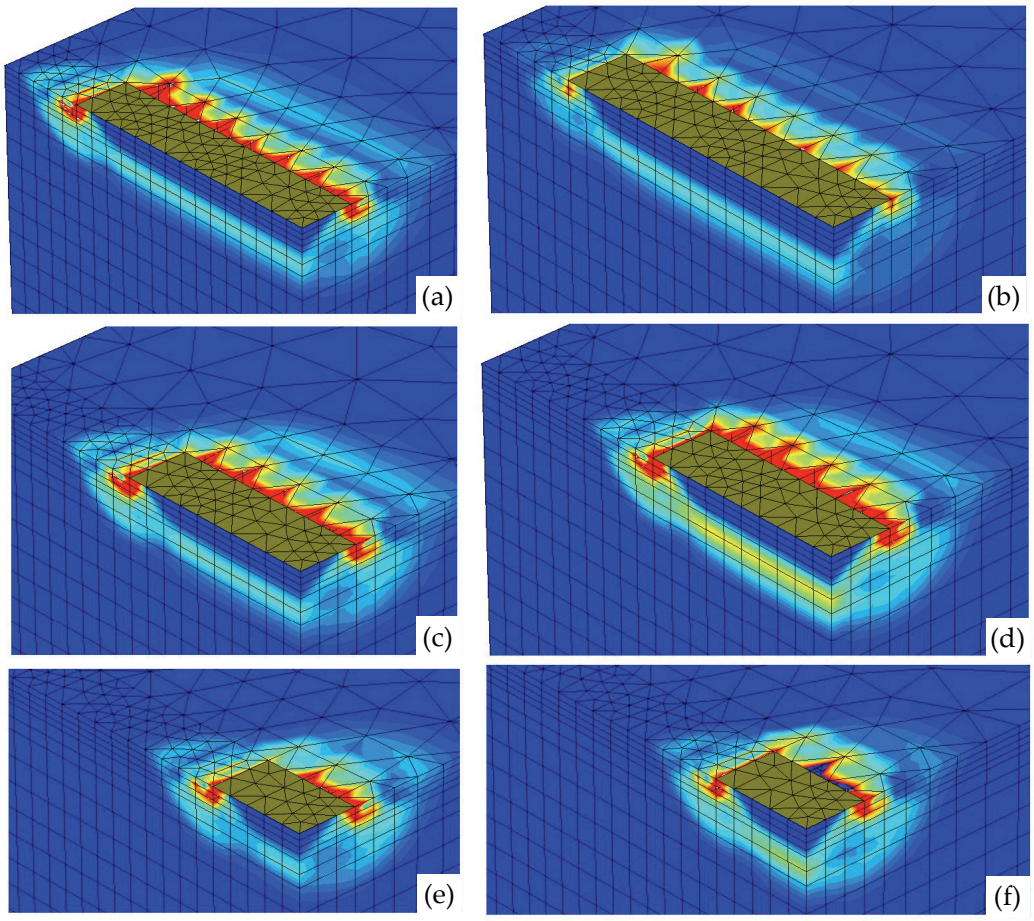

Figure 65: Collapse mechanisms (Nγ-back calculation) when φ = 10° as depicted by incremental shear strains for: (a) 3x15m footing in 3D and ψ = φ; (b) 3x15m footing in 3D and ψ < φ; (c) 3x10m footing in 3D and ψ = φ; (d) 3x10m footing in 3D and ψ < φ; (e) 3x5m footing in 3D and ψ = φ; (f) 3x5m footing in 3D and ψ < φ.

Figure 66, Figure 67 and Figure 68 show the collapse mechanisms for footings for a soil weight of 20 kN/m³ with a overburden of 11 kPa and a friction angle of 25°; in cases of associated flow rule and non-associated flow rule.

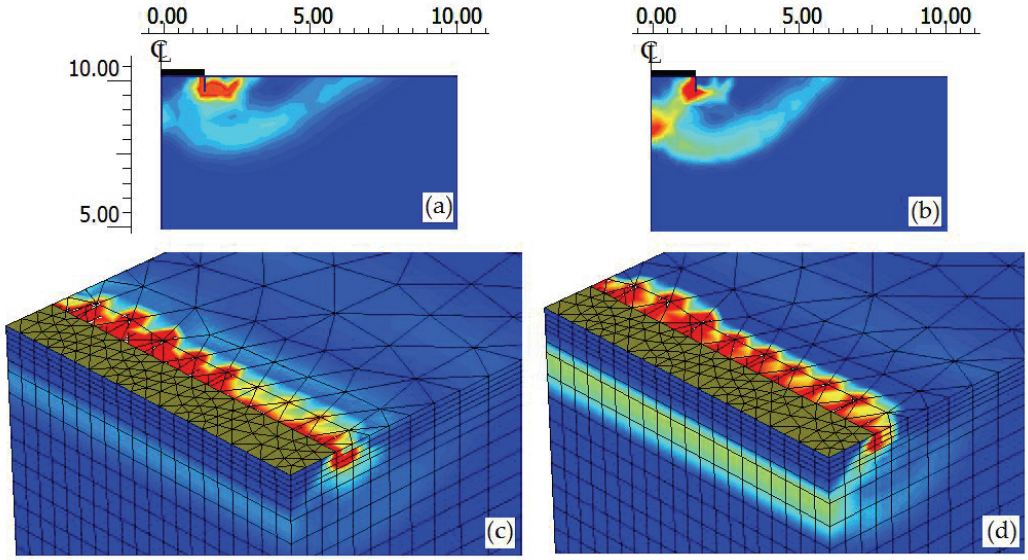

Figure 66: Collapse mechanisms (Nγ-back calculation) when φ = 25° as depicted by incremental shear strains for: (a) strip footing in 2D and ψ = φ; (b) strip footing in 2D and ψ < φ; (c) 3x20m footing in 3D and ψ = φ; (d) 3x20m footing in 3D and ψ < φ.

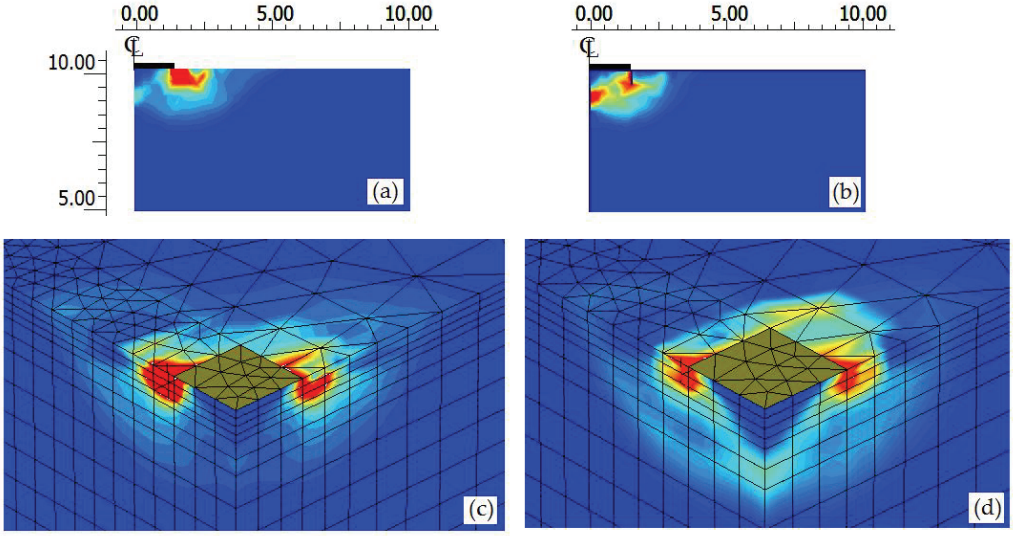

Figure 67: Collapse mechanisms (Nγ-back calculation) when φ = 25° as depicted by incremental shear strains for: (a) circular footing in 2D and ψ = φ; (b) circular in 2D and ψ < φ; (c) 3x3m footing in 3D and ψ = φ; (d) 3x3m footing in 3D and ψ < φ.

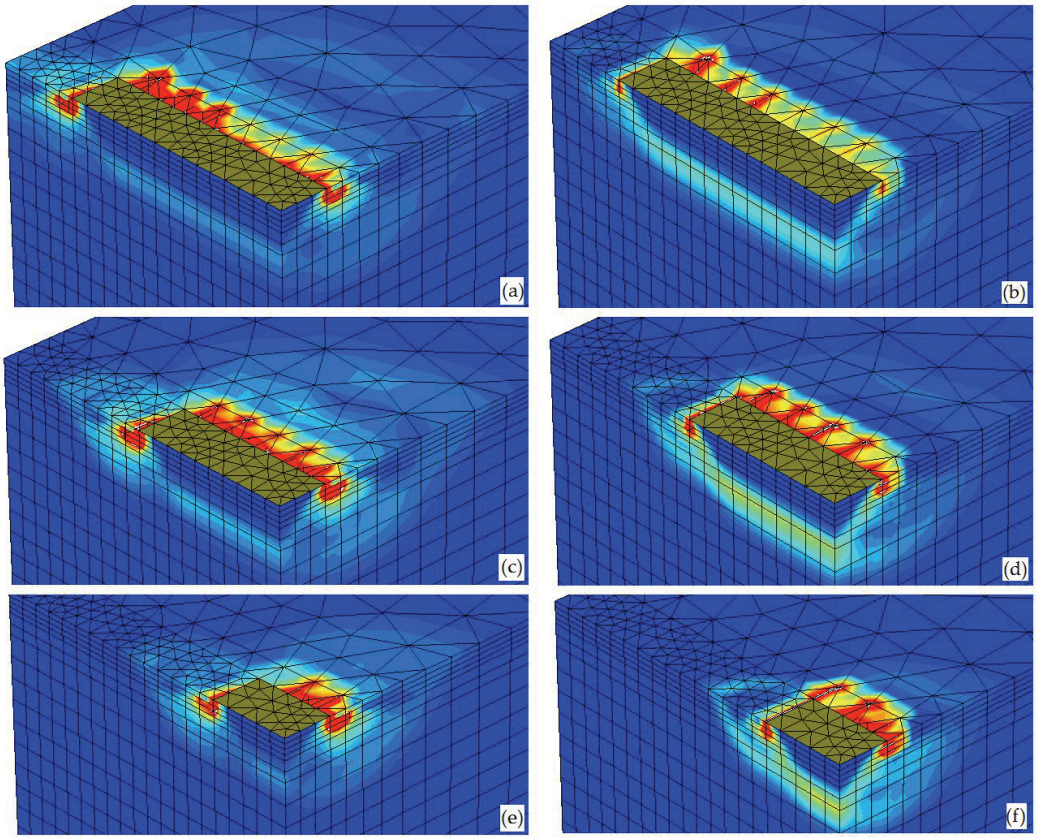

Figure 68: Collapse mechanisms (Nγ-back calculation) when φ = 25° as depicted by incremental shear strains for: (a) 3x15m footing in 3D and ψ = φ; (b) 3x15m footing in 3D and ψ < φ; (c) 3x10m footing in 3D and ψ = φ; (d) 3x10m footing in 3D and ψ < φ; (e) 3x5m footing in 3D and ψ = φ; (f) 3x5m footing in 3D and ψ < φ.

Figure 69, Figure 70 and Figure 71 show the collapse mechanisms for footings for a soil weight of 20 kN/m³ with a overburden of 11 kPa and a friction angle of 40°; in cases of associated flow rule and non-associated flow rule.

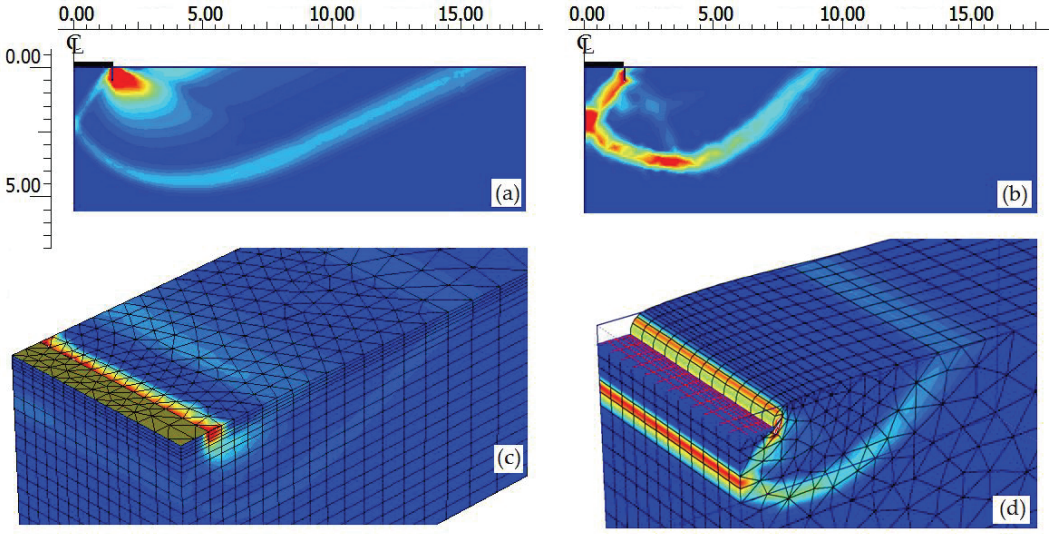

Figure 69: Collapse mechanisms (Nγ-back calculation) when φ = 40° as depicted by incremental shear strains for: (a) strip footing in 2D and ψ = φ; (b) strip footing in 2D and ψ < φ; (c) 3x20m footing in 3D and ψ = φ; (d) 3x20m footing in 3D and ψ < φ.

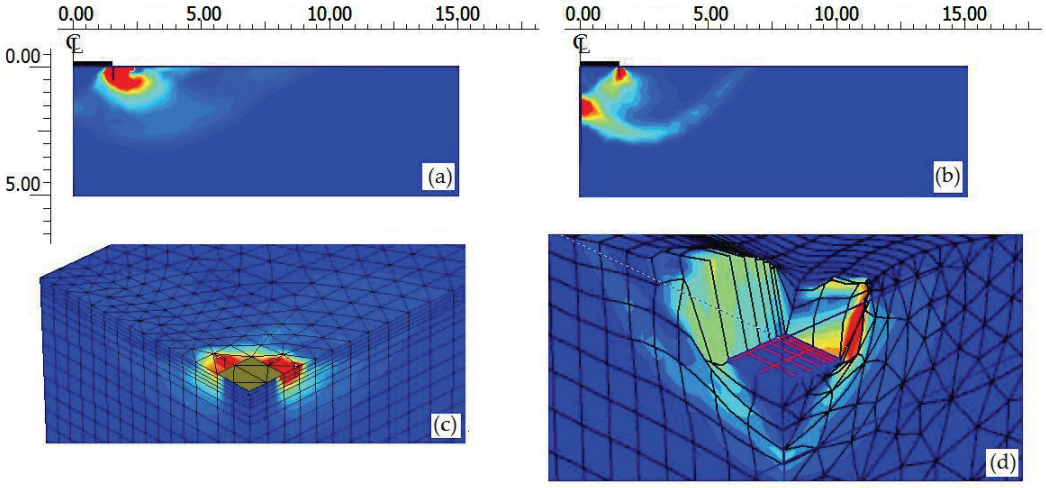

Figure 70: Collapse mechanisms (Nγ-back calculation) when φ = 40° as depicted by incremental shear strains for: (a) circular footing in 2D and ψ = φ; (b) circular in 2D and ψ < φ; (c) 3x3m footing in 3D and ψ = φ; (d) 3x3m footing in 3D and ψ < φ.

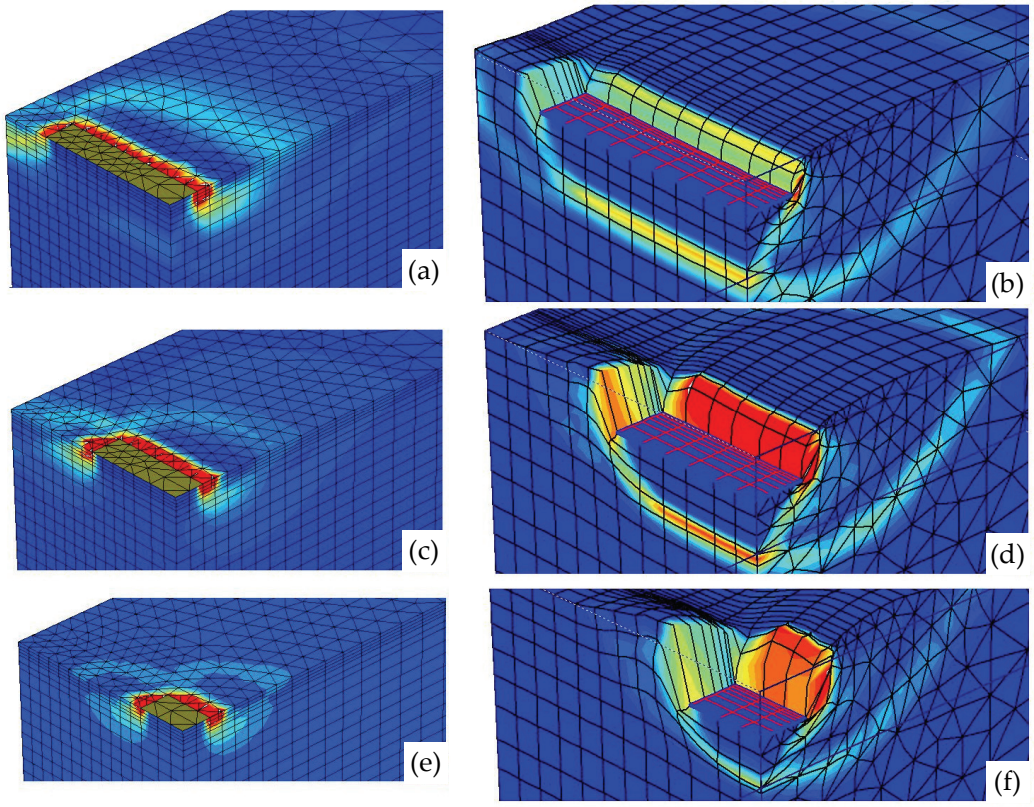

Figure 71: Collapse mechanisms (Nγ-back calculation) when φ = 40° as depicted by incremental shear strains for: (a) 3x15m footing in 3D and ψ = φ; (b) 3x15m footing in 3D and ψ < φ; (c) 3x10m footing in 3D and ψ = φ; (d) 3x10m footing in 3D and ψ < φ; (e) 3x5m footing in 3D and ψ = φ; (f) 3x5m footing in 3D and ψ < φ.

There is a good agreement in shape and size of the collapse mechanisms developed for 2D and 3D FE analyses. The size can be compared taking the width of the footing as the comparative value (1.5m for all the cases). The failure patterns do not follow the same scale colours because the main interest of the plots is to show the failure pattern shape and not the strains level developed on it.

For the case of non-associated flow rule, the mechanism is more localized in shear bands as was observed during the Nq study. The collapse mechanism

for the $\psi = \varphi$ cases is larger than the one for $\psi < \varphi$, causing lower values of bearing capacity, especially for high friction angles.

Figure 72 show the $N\gamma$ bearing capacity factor normalized with respect to the corresponding value from the exact solution (Martin, 2005) for the associated and non-associated flow rule cases analyzed in the present study. Even though there are various expression for $N\gamma$ in the literature, due to the different assumptions regarding the geometry of the collapse mechanism located immediately below the footing base, Martin (2005) proposed accurate results that were later proved by other authors to be exact (Smith, 2005; Hjiaj *et al.*, 2005; Lyamin *et al.*, 2007).

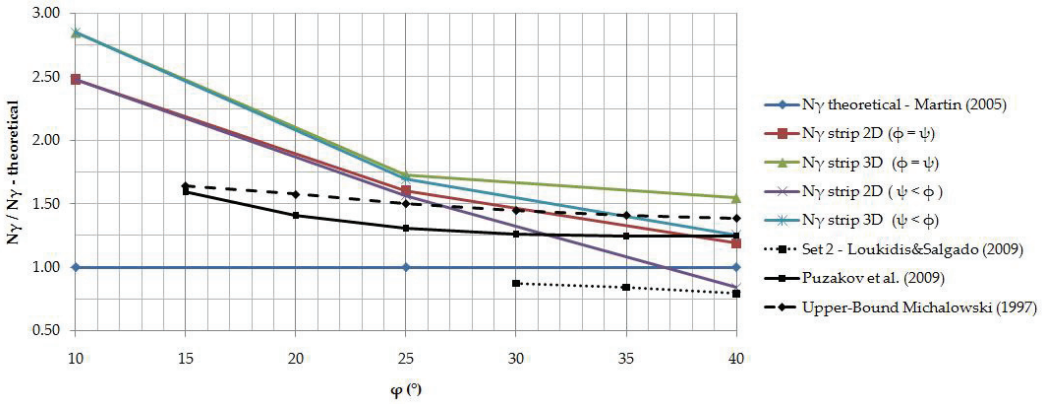

Figure 72: Bearing capacity factor $N\gamma$ for strip footings normalized with respect to the corresponding value from the exact solution (Martin, 2005).

It can be seen in Figure 72 that the $N\gamma$ results decrease with an increase in the friction angle, for associated and non-associated flow rule. However, the values of the bearing capacity factor $N\gamma$ for a soil with $\psi < \varphi$ are clearly smaller than the $N\gamma$ values for a material with an associated flow rule and this difference increases with increasing φ.

Comparing the results from the present study with Puzakov *et al.* (2009) and Michalowski (1997), they mostly agree for $\varphi > 25°$, with the exception of the non-associated flow rule result for $\varphi = 40°$ which surprisingly is very close to the one proposed by Loukidis and Salgado (2009). There is more dispersion in the results for low friction angles. Account must be taken of the many

uncertainties and assumptions affecting these results, they come from a back-calculation. However, this is a first step and effort in this type of analyses that should be re-studied in the future.

Finally, the focus of this part of the present study is the shape factor s_γ in the bearing capacity equation and how the bearing capacity factor $N\gamma$ is affected by the relative footing dimensions. For that reason, Figure 73, Figure 74, and Figure 75 show the variations of the factor $N\gamma^*s_\gamma$ (back-calculated according to Equation 51) with the relative footing dimension for the friction angles studied (10°, 25° and 40°) in the associated and non-associated flow rule cases. The results are also compared to the different theoretical proposals commented in Chapter 2.

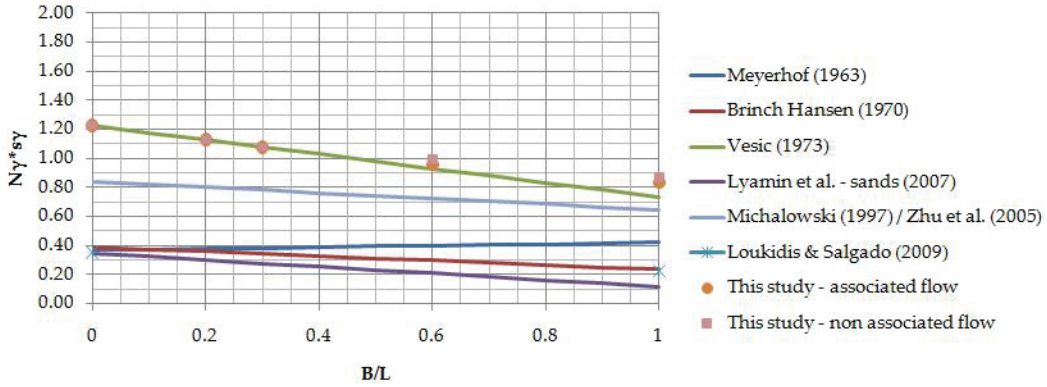

Figure 73: Comparison of results for φ = 10° from various methods of analysis: (a) shape factor s_γ and (b) factor $N\gamma^*s_\gamma$, respect to the relative footing dimension B/L.

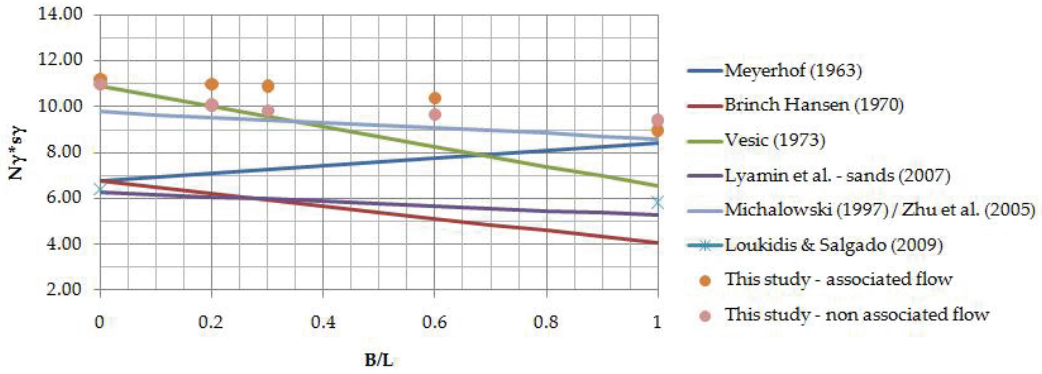

Figure 74: Comparison of results for φ = 25° from various methods of analysis: (a) shape factor s_γ and (b) factor $N\gamma^*s_\gamma$, respect to the relative footing dimension B/L.

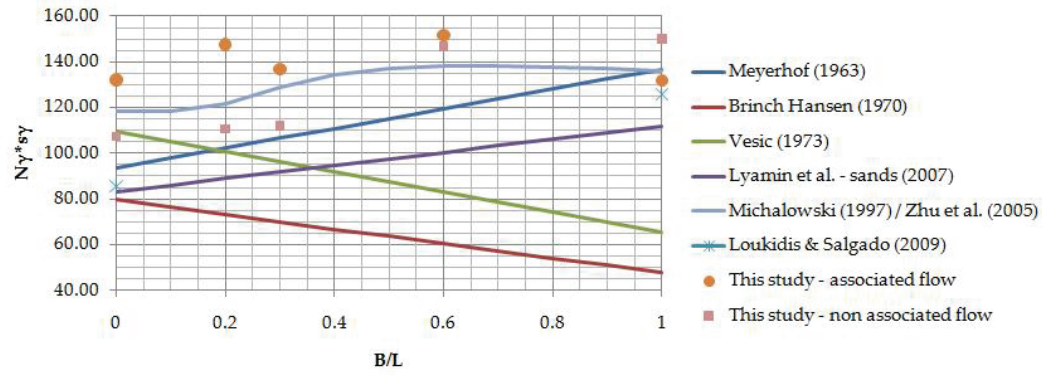

Figure 75: Comparison of results for φ = 40° from various methods of analysis: (a) shape factor s_γ and (b) factor $N\gamma^*s_\gamma$, respect to the relative footing dimension B/L.

From Figure 73, Figure 74 and Figure 75 shown above, several aspects can be commented:

(a) The shape factor s_γ (results from the present study) decreases when the ratio B/L increases from zero to one, for friction angles of 10° and 25°. For φ = 40°, the shape factor s_γ increases and then decreases for B/L closer to one; however, it is not clearly defined the tendency of the data.

(b) The fact mentioned in (a) coincides with what is proposed by previous studies for $\varphi = 10°$ and 25°. The tendency observed in $\varphi = 40°$ can be explained by the influence of triaxial conditions for sands. According to Loukidis & Salgado (2009), in reality, the bearing capacity of square and circular footings with zero embedment is smaller than the bearing capacity of strip footings, although theoretical methods assuming a Mohr-Coulomb failure criterion suggest the opposite. As pointed out by Meyerhof (1963), this is because of the fact that the peak friction angle of sand is lower in nearly triaxial conditions (square/circular footings) than in plane strain conditions (strip footings). Meyerhof (1963) suggested a 10% increment of the triaxial conditions peak friction angle for the determination of the bearing capacity of strip footings.

(c) The associated and non-associated flow rule is not strongly affecting the bearing capacity factor $N\gamma^* s_\gamma$ for small friction angles. The effect is more evident for higher friction angles (like $\varphi = 40°$).

(d) There is a close agreement between the results for $\varphi = 10°$ and the values proposed by Vesić (1973) based on experimental results of De Beer (1970). For $\varphi = 25°$ and $\varphi = 40°$, the agreement is with the proposals done by Michalowski (1997) and Zhu and Michalowski (2005), that were later corroborated by Puzakov *et al.* (2009).

(e) The agreement between the results for $\varphi = 10°$ and the values proposed by Vesić (1973) based on experimental results of De Beer (1970) could be attributed to the fact that in model tests the soil has reached the ultimate (critical) state characterized by incompressible plastic deformation. Therefore, the results of model test of De Beer seem reaffirming the material non-associativity (Erickson and Drescher, 2002). De Beer proposals are independent of the friction angle, that's why the results are much closer for low friction angles where more other important parameters (like cohesion/attraction) can influence the total bearing capacity.

(f) The effect observed in the results for $\varphi = 40°$, where s_γ increases and then slightly decreases with B/L closer to one was explained by Zhu and Michalowski (2005). They attributed this dependence to the effect of volumetric strain in plastically deforming material around the footing. For

elastic-perfectly plastic material model and $\psi = \varphi$, the larger the friction angle the more the material dilates, and the deforming zones along the footing width and length spread and interact in a complex fashion (Puzakov *et al.*, 2009).

(g) Performing 2D simulations for 6-noded and 15-noded elements in strip (plane strain) and circular (axisymmetrical) footings agree in ± 10% from results for similar cases in 3D simulations (strip 3x20m footing and square 3x3m footing). Annexe 4 details the values of the ultimate failure load results.

(h) In general, the proposals of Vesić (1973) for low friction angles and Zhu and Michalowski (2005) for high friction angles are recommended for strip, rectangular and circular footings analyses concerning shape factor s_γ. However, these are approximate solutions (pseudo-upper-bounds). Lyamin *et al.* (2007) proposals have lower values than the ones from the present study. They are highly recommended because they come from FE limit analysis which brackets the exact solution.

Chapter 4

Special features for three-dimensional Finite Element modeling of the bearing capacity problem

The determination of the bearing capacity of footings is of great practical importance in geotechnical engineering. Many analytical and numerical techniques can be used to calculate the vertical bearing capacity of a rigid strip footing (Martin, 2005). The common practice for calculation of collapse loads has been limit equilibrium methods. Nowadays, the Finite Element (FE) method is a powerful alternative in spite of it gives only approximate solutions.

In the present study, collapse loads FE calculations have been performed with the objective of finding the bearing capacity factors for strip footings and the corresponding shape factors for rectangular and circular/square footings. However, approaching the solution has not been straight forward. Many difficulties have been affronted and some solutions to overcome them have been tested.

The following paragraphs summarize two special features (SF) that must be taken into account when collapse loads are being calculated. They resulted from the difficulties that appeared during the numerical modeling of the bearing capacity problem when symmetry in the geometry of the model, non-associated flow rule and high friction angles ($\varphi > 30°$) in the soil material, were combined. Finally, previous published approaches are discussed.

4.1. SF #1: Structured vs. unstructured mesh for three-dimensional Finite Element bearing capacity calculations

A particular failure pattern was obtained when the symmetry of the footing (along its length L), the non-associative flow rule and $\varphi > 30°$, were combined in the different Nq-analyses (for all the footings lengths: 20m, 15m, 10m, 5m and 3m). In this section, the general problem is explained and the applied solutions to overcome it are presented.

In Chapter 3, it was mentioned that for the study of the bearing capacity factor Nq with PLAXIS 3D Foundation code, simulations were performed using symmetry (modeling just a quarter of the footing) and not using it. Any problem or difference in the results of the ultimate load and failure pattern was observed for friction angles lower than 30° in associated and non-associated flow rule cases. However, when friction angles higher than 30° (specifically, 33° and 40°) and non-associated flow rule were used, the failure loads were not closer to the expected theoretical values and the collapse pattern started to be localized in a type of punching failure. Specifically, the failure mechanism observed in this case had a "needle" shape going deeper around the FE elements border, especially when refinement on the footing borders was done (Figure 76).

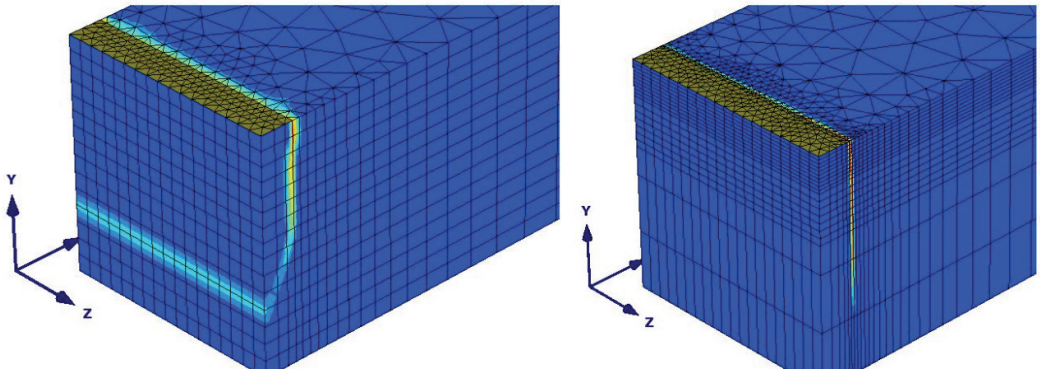

(a) (b)

Figure 76: "Needle" failure when $\varphi = 33°$ and $\psi = 3°$ modeling a quarter of a 3x20m footing (1.5x10m, two planes of symmetry) as a plot of incremental shear strains: (a) Mesh without being refined on border and (b) Mesh with refinement on the borders of the footing. It should be mentioned that the same behaviour was observed for $\varphi = 40°$ and $\psi = 10°$.

Two other simulations were performed using just one plane of symmetry for the footing. One plane along its short side B (B-symmetry, 3x10m footing) and the other one along its long side L (L-symmetry, 1.5x20m), which means that half of a 3x20m footing of was modelled for both cases. Figure 77 shows the results obtained. Surprisingly, the footing of 3x10m (Figure 77a) showed the failure pattern expected for the bearing capacity problem. On the other hand, the footing of 1.5mx20m (Figure 77b) shows a similar "needle" failure mechanism like the ones presented in Figure 76.

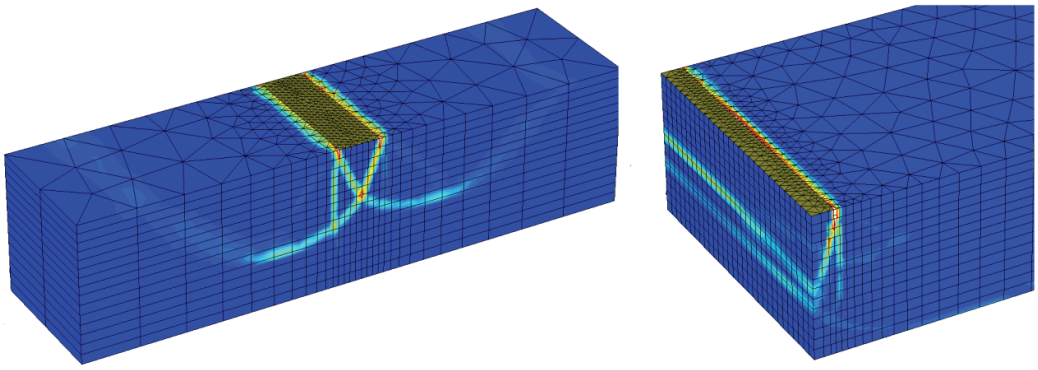

(a) (b)

Figure 77: Failure pattern when $\varphi = 33°$ and $\psi = 3°$ modeling using one plane of symmetry: (a) along the short side B (B-symmetry, footing of 3x10m) and (b) along the long side L (L-symmetry, footing of 1.5x10m). The same behaviour was observed for $\varphi = 40°$ and $\psi = 10°$.

These results seem to confirm that the use of symmetry along the footing length is affecting the final failure mechanism. In this case ($\varphi = 33°$ and $\psi = 3°$), the symmetry along the central length axis of the footing is restricting the deformation of the soil material in addition to the restriction of volume expansion caused by the low dilatancy angle in the non-associated flow rule. Therefore, to take the symmetry line along the length of the footing is not the best option because it suppresses the deformation flexibility of the elements in the vertical plane. Figure 78 shows an example of this deformation flexibility at failure when the elements along the central line (symmetry line) have a non-symmetric deformation when the full width of the footing is being modelled.

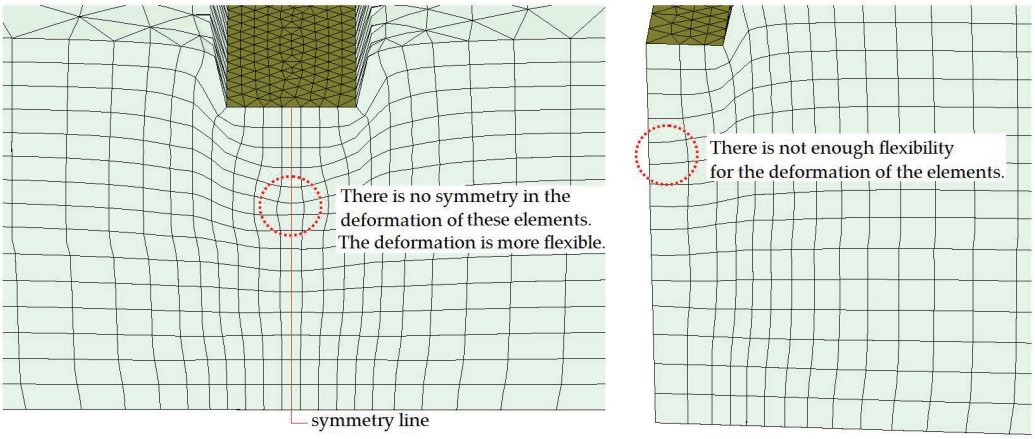

(a) (b)

Figure 78: Deformed mesh at failure when φ = 33° and ψ = 3° for: (a) Symmetry along the width B of the footing (B-symmetry) and (b) Symmetry along the length L of the footing (L-symmetry). The same behaviour was observed for φ = 40° and ψ = 10°.

It was demonstrated that the use or no use of L-symmetry plays an important role in the numerical determination of the bearing capacity for non-associated cases with friction angles higher than 30°. However, another important point was to find an explanation to which factors were causing such atypical failure mechanism (punching) when symmetry along the length of the footing was used.

As a result of the observation that the failure pattern was following the alignment of the mesh arrangement in the vertical plane, and, that the two vertical planes have a structured mesh in the FE code PLAXIS 3D Foundation; it was suggested by Professor Hans Peter Jostad to perform simulations in PLAXIS 2D with a structured mesh. To procure that, vertical lines were defined in a plane strain model for a coarse and very fine mesh as is shown in Figure 79a and 79b. As was expected, the results show that the "needle" failure pattern appeared also following the borders of the mesh elements (Figure 79c and 79d), even though, some small tendencies of following the log-spiral failure surface tried to be developed. However, these tendencies only respond to some unstructured mesh pattern that tries to be formed on the right side of the model as a result of the mesh refinement.

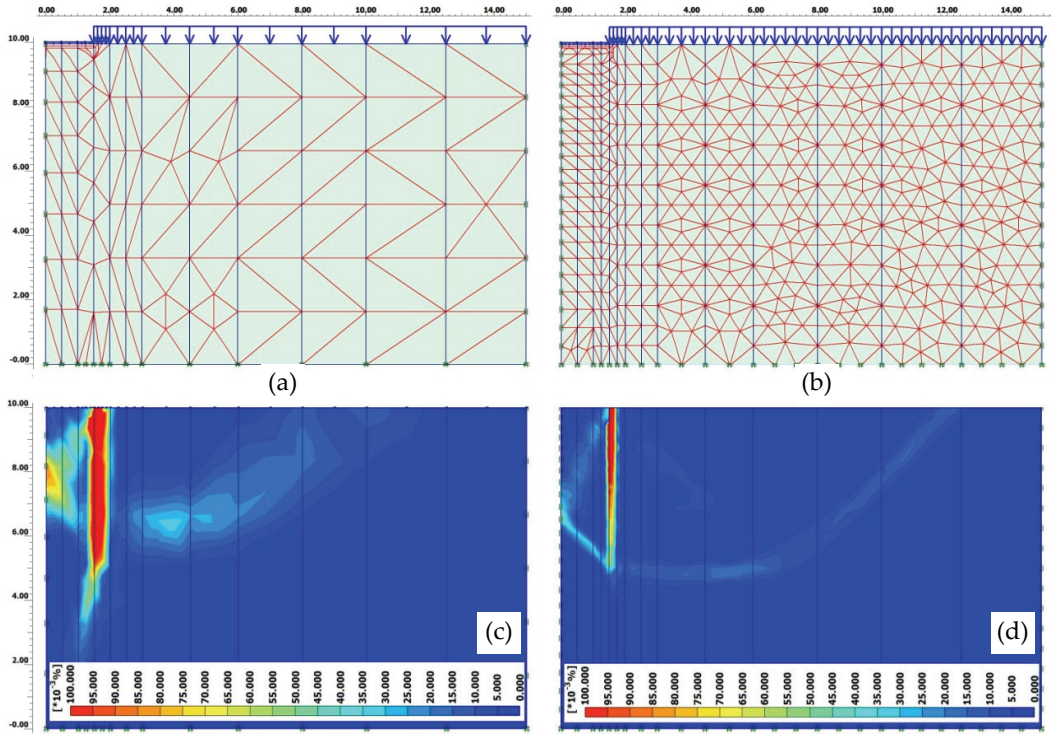

Figure 79: 2D simulations results with symmetry along the length of the footing and structured mesh when $\varphi = 33°$ and $\psi = 3°$: (a) Coarse structured mesh, (b) Very fine structured mesh, (c) Failure pattern as incremental shear strains for a coarse structured mesh, (d) Failure pattern as incremental shear strains for a very fine structured mesh. The same behaviour was observed for $\varphi = 40°$ and $\psi = 10°$ (Set 4B).

Having identified that the structured mesh in a vertical plane was the main factor causing the generation of the "needle" failure when the L-symmetry, a $\varphi > 30°$ and $\psi < \varphi$ were combined in the analysis; the following alternatives for approaching to the FE solution were analyzed: the use of another FE code that allowed the generation of an unstructured mesh in the vertical plane and the diagonal geometrical location of the footing respect to the general geometry of the model (which is discussed in Annexe 5).

For the proposal of using another FE code that allowed the generation of an unstructured mesh in the vertical plane, the FE code PLAXIS 3D Tunnel was chosen. Simulations were performed for the non-associated flow rule cases

with the friction angles of 33° (Set 3B, Table 1) and 40° (Set 4B, Table 1) (which were the ones giving difficulties), and also for $\varphi = 25°$ (Set 2B, Table 1) to make sure that the results with PLAXIS 3D Tunnel were not out of the range got with PLAXIS 3D Foundation. All the footings sizes were tried (3x20m, 3x15m, 3x10m, 3x5m and 3x3m) and good results were obtained when refers to shapes of the failure mechanisms and ultimate load values (and corresponding shape factors for rectangular footings). In Chapter 3, the collapse mechanism have been shown in Figure 48, Figure 49 and Figure 50 for $\varphi = 33°$; and in Figure 51, Figure 52 and Figure 53 for $\varphi = 40°$. Also, the results got for $\varphi = 25°$ and $\psi = 0°$ (Set 2B) are very close to the ones obtained with PLAXIS 3D Foundation (Figure 57) when refers to shape factor and Nq-bearing capacity factors. This gives more validity to the simulations with the code PLAXIS 3D-Tunnel.

Another positive point about the use of the FE code PLAXIS 3D Tunnel is that the result for the failure load tends to be more stable due to incremental multipliers algorithm for the loading input.

When PLAXIS 3D Tunnel is used, the number of FE under the footing in the plane where the structured mesh is being used should be controlled, because too few elements can overpredict failure loads values especially when small footings are being studied.

4.2. SF #2: Associated vs. non-associated flow rule for three-dimensional Finite Element bearing capacity calculations

Chen (1975) gives a geometrical interpretation of the flow rule. Figure 80a shows a layer of dense granular material under the action of two forces: a normal force Pn and a horizontal force Pt. Pn remains constant while Pt is gradually increases from zero to a value when sliding occur. At this point, Pt has overcome the cohesion, the surface friction (between the contact surfaces of adjoining particles) and the interlocking friction (by the interference of the particles themselves to changes of their relative position). As a result of the interlocking friction, a displacement upward additional to the horizontal

sliding will appear. Therefore, the displacement vector must make an angle θ to the slip plane. Setting out along the axes of (σ,τ) stress coordinates (Figure 80b) another set of coordinates corresponding to the plastic deformations ($\dot{\varepsilon}^P$, $\dot{\gamma}^P$) known as plastic normal strain rates and plastic shear strain rates, correspondingly; the direct consequence of the flow rule is that the plastic strain rate vector must be normal to the yield curve (in this case, Mohr-Coulomb) when their corresponding axes are superimposed. From Figure 80b, it can be seen that this is equivalent to assuming θ = φ in Figure 80a. For that reason, the volume expansion is a necessary complement to shearing deformation according to these idealizations.

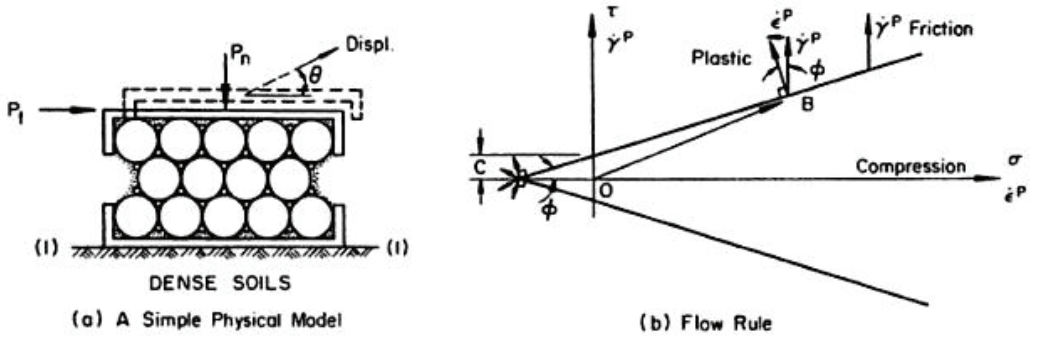

Figure 80: Plastic strain rate is normal to yield curve for perfectly plastic theory, but parallel to τ-axis for frictional theory. (Chen, 1975).

What happens in a frictional material is that the interlocking friction is ignored (θ = 0). Therefore, the deformation occurs by the slide of adjacent surfaces of the material points and there is no normal deformation. If the plastic strain rate vector is superimposed to the Coulomb yield curve (Figure 80b), the normality does not apply anymore (Chen, 1975) and now what applies is a non-associated flow rule.

Several authors that have studied the influence of the non-associativity on the bearing capacity of strip and circular footings have been mentioned in previous pages. Most of them agree in a general observation: the ultimate bearing capacity is influenced by the dilation angle ψ. This effect is significant for higher values of the friction angle when ψ is small compared to φ. Some have reported that the bearing capacity factors Nc, Nq and Nγ can decrease

up to about 40% with the decrease in ψ (increase in non-associativity) for strip and circular footings (Yin *et al*., 2001; Erickson and Drescher, 2002; Zhao and Wang, 2009; Loukidis and Salgado, 2009).

The most recent approaches done by Krabbenhøft *et al.* (2010) and Loukidis and Salgado (2009) state that for frictional materials, the assumption of $\psi = \varphi$ for bearing capacity calculations using FE can produce unconservative results for strip and circular footings.

The present study agrees with the literature findings. Nq values for strip (Figure 54) and circular footings (Figure 55), and, $N\gamma$ values for strip footings (Figure 72) derived from the FE calculations were lower for cases when $\psi < \varphi$. In other words, the consideration of associativity for the soil material overestimates the bearing capacity especially when high friction angles are considered.

However, the associated and non-associated flow rule is not strongly affecting the shape factors by itself (Figure 56, Figure 57, Figure 58 and Figure 59). Respect to this, Zhu and Michalowski (2005) said that the shape factors are ratios of the bearing capacity of rectangular footings to that of a strip footing, and they are likely to be less dependent on the dilatancy angle.

4.3. Some comments about other methods for determination of collapse loads

There are useful tools for testing the accuracy of FEM simulations, even though, all failure load solutions are not exact. A summarize of some types of failure load solutions are presented below emphasizing in its relevance for the bearing capacity problem. Furthermore, some other methods that have been used by other authors for calculating collapse loads are described.

4.3.1. Analytical techniques for determination of collapse loads

Based on the solution techniques, the analytical solutions can be classified into three groups, namely: (a) slip-line method or method of characteristics (MOC), (b) limit equilibrium method, and, (c) limit analysis.

(a) The slip-line method or method of characteristics (MOC)

This method is based on a numerical solution of the basic differential equations for the slip-line network derived using the equilibrium of stresses and yield conditions, everywhere in the fully plastified zones.

The Coulomb yield criterion is combined with the equations of equilibrium to give a set of differential equations of plastic equilibrium which, together with the stress boundary conditions, can be used to investigate the stresses in the soil beneath a footing at the point of incipient failure. The solution proceeds by constructing two intersecting families of curvilinear slip-lines (α-lines and β-lines) from known stresses at the boundary (Hjiaj *et al.*, 2005).

The solutions with this method are generally not exact boundary (Hjiaj *et al.*, 2005); however, they often provide the best estimate that can be obtained (Nordal, 2007). On the other hand, the flow rule is not taken into account in this method and its application is restricted to a set of boundary conditions.

Slip–line equations for plane deformation were first derived by Kötter (1903). A closed-form solution to the differential equations of the slip-line network for a footing on an imponderable soil was obtained by Prandtl (1921) which later was applied by Reissner (1924) and Novotortsev (1938).

However, for problems involving soil weight, the analytical solution procedure is more complicated due to the introduction of a hyperbolic set of partial differential equations that must be integrated numerically to obtain the ultimate load. Some of the investigators applying this method for estimation of the bearing capacity factors are Sokolovskii (1965), Lundgren and Mortensen (1953), Brinch-Hansen (1970), Booker (1969), Bolton and Lau (1993), Kumar (2003), Smith (2005) and Martin (2005).

(b) The limit equilibrium method

This solution is based on the equilibrium of a soil body above a potential sliding surface. In other words, an approximate failure surface of various simple shapes is assumed and a critical failure surface is found.

Terzaghi (1943) and Meyerhof (1951) solutions are based on this method. It was presented in previous chapters that the failure surface assumed by Terzaghi is a logarithmic spiral composed of a rigid active wedge, a radial shear zone and a rigid passive wedge. Meyerhof extended this theory for embedded footing. Narita and Yamaguchi (1992) made a three-dimensional analysis of bearing capacity of square and rectangular footings by use of method of slices.

In the limit equilibrium method, only global equilibrium is enforced and the shape of the failure mechanism is assumed a priori. Moreover, the kinematics of the problem is ignored in the sense that no strain rate field is defined and the flow rule is not invoked (Hjiaj *et al.*, 2004).

(c) The limit analysis: upper- lower-bound theorems

The basic theorems of limit analysis give upper and lower bounds on the collapse loads. The lower-bound theorem defines the lower limit to the collapse load by satisfying the equilibrium equations, stress boundary conditions and nowhere violates the yield criterion. On the other hand, collapse load by the upper–bound theorem is determined by equating the external rate of work to the internal rate of dissipation of a kinematically admissible velocity field, which satisfy the velocity boundary conditions, flow rule, strain and velocity compatibility conditions (Manoharan and Dasgupta, 1995).

A major advantage of the limit theorems is that the collapse load can be bracketed between two values, thus providing an inbuilt estimate of the error in the solution. Furthermore, the theory is rigorous, since it is based on the equations of continuum mechanics (Hjiaj *et al.*, 2004).

Authors like Drescher and Detournay (1993) and Michalowski (1997) have used the limit analysis for estimation of the failure mechanism and bearing

capacity factors for associated and non-associated flow rule. Also, Michalowski and Dawson (2002a) applied it for three-dimensional analysis of bearing capacity for square footing. More recently, the lower- and upper bound theorems have been combined with the Finite Element or Finite Difference method for evaluation of collapse loads. These approaches are discussed in the next section.

Finally, Krabbenhøft *et al.* (2005) affirm that the duality between the two theorems is well defined: the lower-bound theorem operates with stresses and a load multiplier, whereas the upper bound method involves velocities and plastic multipliers. The variables of the two problems are coupled by the flow rule stating that the strain rate vector is proportional to the gradient of the yield function, and by the condition that the plastic multipliers can be non-negative only at points where the yield function is equal to zero.

However, Krabbenhøft and Damkilde (2003) mention that the lower-bound method has the advantage over the upper-bound method that the computed collapse loads are always on the safe side. Hjiaj *et al.* (2005) say that although an upper bound solution is often a good estimate of the collapse load; a lower bound solution is more valuable in engineering practice as it results in a safe design.

4.3.2. Numerical techniques for determination of collapse loads

The last three decades have witnessed a growing use of the numerical modeling tools in almost all areas of geotechnical engineering, including shallow foundations stability. The most popular one is the FEM. However, some other tools like the Finite Difference method have been used alone or in combination with analytical solutions.

(a) The Finite Element Method (FEM)

The displacement FEM can be used to derive approximate estimates of the bearing capacity factors. The name *displacement method* corresponds to the fact

that forces or loads are put on the soil body and the response is studied in terms of displacements or deformations.

The soil volume is divided into elements which behaviour is described by equations in terms of an element stiffness matrix. Then, the global stiffness matrix is assembled integrating the entire element matrix. An incremental load is applied and the global equation system is solved to get a displacement increment. With the displacement increments, the strains increments are found for each element. These strains are used to find stress increments in the integration points of each element. If there is too high unbalanced forces (difference between the applied external load vector and the internal force vector integrated from the internal soil stresses), the load increment and/or iterations are modified until the results are converging. Finally, the results are updated adding increments of deformation and stress to form the total deformations and total stress. New load increments are repeatedly added until the specified external load is reached or failure occurs.

Some authors have attempted to apply FEM to predict bearing capacity of strip footings (Sloan and Randolph, 1982; Griffiths, 1982; Manoharan and Dasgupta, 1995; Frydman and Burd, 1997; Zhu and Michalowski, 2005; Loukidis and Salgado, 2009).

Griffiths (1982) represented the soil by an elastic-plastic model with a Mohr-Coulomb yield condition and used a viscoplastic initial strain method (Zienkiewicz, 1975) as the solution algorithm. More than 10 years later, Griffiths' work was extended to circular footings by Manoharan and Dasgupta (1995) who also used the viscoplastic technique. This technique consists in permitting large load increments, when they exceed the yield limit; they are redistributed by successive time integrations until the yield condition is satisfied. In both studies, a coarse mesh composed of 8-noded quadrilateral isoparametric elements with 2x2 reduced quadrature was used to model the soil mass.

Frydman and Burd (1997) considered the effect of friction angles on the bearing capacity by doing calculations with the program OXFEM. It was based on the displacement method using unstructured meshes of 6-noded isoparametric triangles with three Gauss points, a tangent stiffness approach

and the Matsuoka yield function (with plane strain Mohr-Coulomb corresponding parameters) for the elasto-plastic soil model.

According to Hjiaj *et al.* (2005), the FE calculations of Griffiths (1982), Manoharan and Dasgupta (1995) and Frydman and Burd (1997), constitute, at best, a pseudo-upper bound to the exact solutions, because a rigorous upper bound solution requires the flow rule to be satisfied everywhere and not only at the Gauss points.

Zhu and Michalowski (2005) used the FE system ABAQUS to arrive at the limit loads of square and rectangular footings. 20-noded quadratic brick elements with a reduced integration scheme were used to discretize the model and the soil was modelled as an isotropic elasto-perfectly plastic continuum with yielding described by Mohr-Coulomb function.

Loukidis and Salgado (2009) performed the analysis with the code SNAC using unstructured meshes of 15-noded triangular elements with 12 and 16 Gauss-quadrature points, respectively to plain strain and axisymmetrical elements. The constitutive model used was an elastic-perfectly plastic following the Mohr-Coulomb failure criterion.

In this study, as it was said, the FEM codes used for the analysis were PLAXIS 2D, PLAXIS 3D Tunnel and PLAXIS 3D Foundation. In all of them, the constitutive model used was an elastic-perfectly plastic following the Mohr-Coulomb failure criterion. PLAXIS 2D uses Gaussian integration within the triangular elements based on three sample points for the 6-noded triangular elements and 12 sample points for the 15-noded triangular elements. PLAXIS 3D Tunnel and PLAXIS 3D Foundation use Gaussian integration within the 15-noded wedge elements based on six sample points; the integration is a mixture between the 3-point integration of a 6-noded triangular element and the 4-point integration of an 8-noded quadrilateral element.

(b) The Finite Difference method (FDM)

The Finite Difference method (FDM) is a technique to convert a governing partial differential equation into a set of N algebraic equations involving N unknowns at N predetermined points in the problem. The medium is divided

into a finite difference mesh of quadrilateral elements and internally the program, like FLAC (Fast Lagrangian Analysis of Continua), subdivides each element into two overlayed set of constant-strain triangular elements.

Frydman and Burd (1997) considered the effect of friction angles on the bearing capacity by doing calculations with the finite-difference code FLAC. It is an explicit, time-marching method to solve the governing field equations in which every derivative is replaced by an algebraic expression written in terms of the field variables (stress or displacement) at discrete points in space (Frydman and Burd, 1997). In general, the calculations take the equation of motion to derive new velocities and displacements from stresses and forces. Then strain rates are derived from velocities and new stresses from strain rates. A conventional elastic-perfectly plastic frictional model based on Mohr-Coulomb yield criterion was used to represent the soil.

Yin *et al.* (2001) used this approach to examine the bearing capacity of strip footings by the numerical solution of the equations governing elastic-plastic soils with a non-associative flow rule. The three bearing capacity factors were obtained using FLAC. The explicit Lagrangian calculation scheme and the mixed discretization zoning technique in this code ensure that plastic collapse load and continued plastic flow could be modelled accurately (Yin *et al.*, 2001). Again, the elastic-plastic model with the Mohr-Coulomb failure criterion was used in the finite-difference modeling. Zhao and Wang (2009) extended Yin *et al.* (2001) work to circular footings.

Erickson and Drescher (2002) performed numerical computations using FLAC to evaluate the collapse load for circular footings taking into account the non-associativity of the soil. They pointed out that the use of a finite-difference program is most suitable for analyzing nonlinear behaviour of materials and related instability and failure phenomena. The elastic-perfectly plastic non-associative Mohr-Coulomb model was used for the numerical simulations.

Michalowski and Dawson (2002a) used the finite difference code FLAC3D with a mesh composed of 8-noded brick elements, subdivided into two overlapping sets of constant-strain tetrahedral elements. The code was used to calculate the bearing capacity of square footings for an elasto-plastic soil and compare them to upper-bound limit solutions. The results indicated that assumptions made in 3D limit analysis provided significant restrictions on the

velocity fields. Consequently, numerical results based on the FLAC3D code provided significantly lower and therefore more accurate, limit loads.

Puzakov *et al.* (2009) made a numerical evaluation of the bearing capacity factor s_γ for square and rectangular footings on granular soils (governed by the associative flow rule) using the finite-difference code FLAC3D. 8-noded brick elements were used with the objective of investigating if the peculiar effect found by Zhu and Michalowski (2005) in the function s_γ was caused by the method used or was originating from the mechanics of the problem. It was confirmed that for φ values of 35° and higher, there is a peak in the s_γ function at some aspect ratio.

(c) Combination FEM or FDM + limit analysis (lower- and upper-bound theorems)

The upper theorem states that the load (or the load multiplier), determined by equating the internal power dissipation to the power expended by the external loads in a kinematically admissible velocity field, is not less than the actual collapse load (Hjiaj *et al.,* 2005). On the other hand, the lower bound theorem states that the load, determined from a stress field that satisfies equilibrium within the domain and on its boundary, and does not violate the yield condition, are not greater that the actual collapse load (Hjiaj *et al.,* 2005). Therefore, they constitute a powerful tool to bracket the collapse load from above and below.

According to Hjiaj *et al.* (2005), practical application of these theorems usually requires a numerical method, since analytical solutions are available only for a few problem involving simple geometries and basic loading conditions. Also, care has to be taken to keep the bounding properties during the numerical treatment of these theorems. The FEM is probably the most flexible numerical method because it allows considering problems with complex geometries, non-homogenous material properties, anisotropy and various loading conditions at the same time.

Lysmer (1970) proposed an alternative method of computing lower bounds, which used FE and linear programming. In this procedure the soil mass is discretized into a collection of 3-noded triangular elements with the nodal variables being the unknown stresses that are also variables for the linear yield

criterion. Statically admissible stress discontinuities are permitted to occur at the interfaces between adjacent triangles. Sloan (1988) affirms that the major advantage of the numerical formulation of the lower bound theorem is that complex loadings and geometries can be dealt with. However, the principal disadvantage of the technique is that significant amounts of time may be necessary to solve the resulting linear programming problem. Sloan (1988) proposes a strategy to solve this problem based on Bottero *et al.* (1980) formulation (Figure 81).

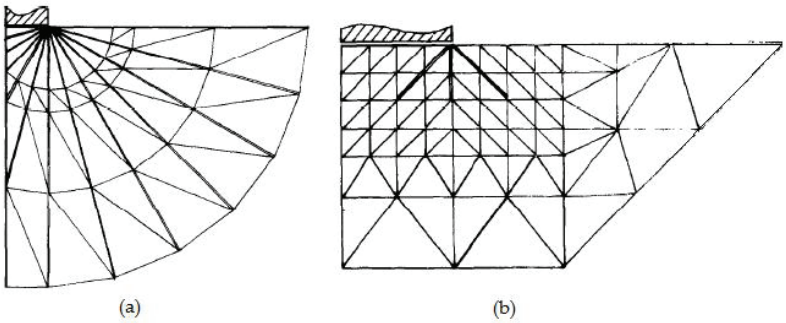

Figure 81: Examples of: (a) static (lower-bound) and (b) kinematic (upper-bound) strip footing mesh for FEM (Bottero *et al.*, 1980).

Ukritchon *et al.* (2003) got numerical upper- and lower-bound solutions of the $N\gamma$ bearing capacity factor of a surface strip footing on a frictional soil following the Mohr-Coulomb failure envelope with associated flow rule. The analyses were by linear programming and finite-element spatial discretization based on Sloan and Kleeman (1995) and Sloan (1998), respectively.

Yang *et al.* (2003) computed lower bound limit loads of smooth rectangular surface footings. A perfectly rigid-plastic soil model was assumed. The numerical procedure computed a statically admissible stress field via FEM together with a non-linear optimization procedure. The stress field was constructed using linear 4-noded tetrahedrons. In the non-linear optimization process, the maximum value of the objective function was searched. The objective function was the bearing capacity of footing subjected to the stress boundary condition, stress discontinuity equilibrium condition, stress equilibrium condition and yield condition.

Hjiaj *et al.* (2005) applied numerical limit analyses to evaluate the soil weight bearing capacity factor $N\gamma$ for a rigid surface footing with a smooth or rough interface in a cohesionless frictional Mohr–Coulomb material. Assuming an associated flow rule, the true collapse load was bracketed within 3.42% by computing rigorous lower and upper bound solutions using limit analysis methods (Lyamin and Sloan, 2002a and 2002b). The numerical formulations of both the upper and the lower bound theorems were obtained by FE and solved using non-linear mathematical programming schemes. The yield criterion was used in its native non-linear form according to the formulation of Lyamin and Sloan (2002b) that uses a two-stage quasi-Newton solver (full details of the formulation and references to earlier works are found in Lyamin and Sloan, 2002b).

Salgado *et al.* (2004) and Lyamin *et al.* (2007) made two- and three-dimensional rigorous bearing capacity calculations based on finite element analyses for strip, square, circular and rectangular foundations in clays and sands, respectively. The results of the analyses propose rigorous, definitive values of the shape and depth factors for foundations in clays. For the case of sands, the results propose values of the shape and depth factors for calculation of the bearing capacity and also, a different form of the bearing capacity Equation that does not considered separately the effects of shape and depth for Nq and $N\gamma$. Both studies were possible because of the development of efficient algorithms for optimization of stress fields for lower-bound analysis (using non-linear programming) and velocity fields for upper-bound analysis. These algorithms are detailed in Lyamin (1999) and Lyamin and Sloan (2002b) for the lower-bound case; and in Lyamin and Sloan (2002a), Lyamin *et al.* (2005a) and Krabbenhøft *et al.* (2005) for the upper-bound case.

(d) Innovative approaches applied to the solution of the bearing capacity of footings

Lyamin *et al.* (2005b) presented an adaptive remeshing technique procedure for lower bound limit analysis with application to the bearing capacity of a rigid strip footing. Unlike conventional finite element meshes, a lower bound grid incorporates statically admissible stress discontinuities between adjacent elements. These discontinuities permit large stress jumps over an infinitesimal distance and reduce the number of elements needed to predict the collapse

load accurately. Eight mesh adaptive schemes were tested. It was found that the accuracy of the analysis is more dependent on the number of discontinuities originating from the stress singularity at the footing edge, rather than on the element size distribution over the problem domain. The mesh around a singular point should be governed by a fan-like stress field. For that reason, optimal-mesh-adaptive procedure, based on the magnitude of the Lagrange multipliers, appears to be the most suitable option for lower bound computations.

Jahanandish *et al.* (2010) applied the theory of the Zero Extension Lines (ZEL) for the determination of the bearing capacity of strip shallow foundations considering stress level effect. The basic concept of ZEL method is that for any state of strain, two perpendicular directions of compressive and tensile strains exist and therefore, there are two directions along which linear axial strain increments are zero. Comparisons were made with existing experimental data and the good agreement showed that the ZEL method can be employed to consider the stress level dependency of soil strength in the bearing capacity computation of foundations.

4.4. Final suggestions for three-dimensional Finite Element numerical computation of collapse loads

After the 3D numerical computation of the bearing capacity factors and the corresponding shape factors for rectangular and square footings in associated and non-associated materials, some general remarkable points are listed as cares that should be taken when these types of analyses are done:

- The Mohr-Coulomb yield criterion is suitable for the analysis. It provides accurate predictions of the ultimate bearing capacity of soil masses; particularly for problem where collapse is reached at relatively small strains.
- The accuracy of the analysis is more dependent on the number of FE under the footing and at the footing edge, rather than on the element size

distribution over the problem domain. For that reason, mesh refining on the borders of the footing is highly recommended.

- The FE distribution in the vertical plane (perpendicular to the footing length L) of the 3D model really matters for calculation of the bearing capacity (especially for $\varphi > 30°$ and $\psi < \varphi$). There is strong influence of the structure mesh in the vertical plane when using symmetry along the length of the footing. It gives local punching failure problem. Solutions for this problem can be to avoid the use of symmetry in the problem (there is more flexibility in the deformation for vertical elements) or to use another FE code that allows the construction of unstructured meshes on a vertical plane (for example PLAXIS 3D-Tunnel).
- A 3D-FE code that allows the construction of unstructured meshes on a vertical plane gives good results when the bearing capacity calculation is done using footing symmetry along its length, a non-associated flow rule for the soil material and friction angles higher than 30°. However, it can also be used for friction angles lower than 30° not changing the results. Furthermore, the same FE code well applies for associated flow rule bearing capacity cases. Care must be taken of having enough elements under the footing on the plane where the structured mesh is being used; it can overpredict values if too few elements are under the footing.
- When using symmetry for calculation of bearing capacity, at least, one vertical plane of unstructured mesh should be used. Otherwise, it is not recommendable to use symmetry in the model.
- For frictional materials ($\psi < \varphi$), the FE bearing capacity calculation must be done taking into consideration the non-associated flow rule. This will give more realistic values for the ultimate failure load and the bearing capacity factors that can be derived from them. However, the shape factors won't be strongly affected by this aspect.

Conclusions

The present study was developed in two main areas regarding: the theoretical description of the bearing capacity problem for strip, rectangular and square/circular footings; and, the numerical modeling of the bearing capacity problem using FEM codes in two dimensions-2D (for plane strain-strip footings and axi-symmetrical conditions-circular footings) and three dimensions-3D (for rectangular footings).

The aim was oriented to the detailed study of the FE calculation of the bearing capacity problem in order to defined: a) the influence of the relative footing dimension in the bearing capacity factors for associative and non-associative materials, b) the shape factors when rectangular and square footings were analyzed, and, c) special features that should be taken into account when the numerical computing of ultimate loads is tried.

Respect to how the bearing capacity factors (Nq and $N\gamma$) are influenced by the relative footing dimension (B/L), it was seen that square/circular footings have higher Nq bearing capacity factor than rectangular or strip footings. On the other hand, the $N\gamma$ factor decreases when the ratio B/L increases from zero to one, for friction angles of 10° and 25°. For $\varphi = 40°$, the value of $N\gamma$ increases and then decreases when B/L is closer to one. These results coincide with the tendencies proposed in previous studies, especially, to those that use upper-bound limit analysis approaches.

The associated and non-associated flow rule is not strongly affecting the shape factor s_q and s_γ. The effect is more visible in the corresponding bearing capacity factor for the footing shape. When $\psi < \varphi$, $Nq*s_q$ and $N\gamma*s_\gamma$ reaches lower values than the cases when $\psi = \varphi$. This difference is more evident for higher friction angles ($\varphi > 30°$). Consequently, the associated flow rule ($\varphi = \psi$) overestimates the bearing capacity factors and the corresponding ultimate failure loads.

Regarding the shape factors when rectangular and square footings were analyzed, it was said that they are not highly affected by the associated and the non-associated flow rule. There was good agreement between the results

of the present study and the results obtained by authors using the upper-bound limit solution, this confirms what was said by Hjiaj *et al.* (2005) about bearing capacity FE simulations: they are pseudo-upper bound to the exact solutions, because a rigorous upper bound solution requires the flow rule to be satisfied everywhere and not only at the Gauss points. Several proposals about the shape factors formulas have been recommended; however, to use the ones proposed by Eurocode 7 are on the safe side and can be quite conservative. A good practice can be to linearly interpolate between the shape factors for circular and strip solutions, it is also in the conservative side.

Concerning special features, which should be taken into account when the 3D numerical computing of ultimate loads is tried, are related to the symmetry of the model, the mesh in the FE code and the non-associated plasticity of the soil material.

In general, when 3D-FE analysis is tried it is highly recommended to model the full geometry of the footing, without any symmetrical simplification. However, if symmetry is required in the model in order to refine areas that can lead to problems without increasing the calculation time, an unstructured mesh should be present in one of the vertical planes of the model. This is a healthy practice when non-associated materials are studied. Actually, the use of non-associated flow rule is a must in the bearing capacity calculations. It will give more realistic values for the ultimate failure load and the bearing capacity factors that can be derived from them.

Finally, in most recent studies, the analysis of the bearing capacity problem has been done by combination of FEM with limit analysis (upper- and lower-bound theorems). This is a powerful tool because the upper- and lower-bound solutions allow bracketing the collapse load from above and below, and, the FEM allows considering problems with complex geometries, non-homogenous material properties, anisotropy and various loading conditions at the same time. The solution algorithms for this type of analyses are oriented to optimization and non-linear programming techniques.

This innovative approach opens a new interesting dimension for the study of the bearing capacity problem.

Future work in this field about 3D-numerical modeling of the bearing capacity problem should be oriented in finding the nature of the problems observed during the present work. The nature of this difficulties behaviour should be clearly recognize and described deeply. Even though the bearing capacity problem has been widely study, there are many new tools that must be tested to clearly understand the bearing phenomenon, and therefore, performing better design of foundations.

References

Abbo, A.J. and Sloan W.C. 2000. *SNAC, User manual, Version 2.0*. Department of Civil, Surveying and Environmental Engineering. University of Newcastle, Callaghan, Australia.

Biarez, J., Burel, M. and Wack, B. 1961. Contribution à l'étude de la force portante des foundations. *Proceedings V International Conference on Soil Mechanics and Foundation Engineering.* Paris, France: Vol. 1, pp. 603.

Bolton, M.D. and Lau, K. 1993. Vertical bearing capacity factors for circular and strip footings on Mohr Coulomb soil. *Canadian Geotechnical Journal.* Vol. 30, No. 4, pp. 1024-1033.

Bond, A. and Harris, A. 2008. *Decoding the Eurocode 7*. Great Britain: Taylor & Francis.

Booker, J.R. 1969. *Application of theories of plasticity to cohesive frictional soils*. PhD thesis, Sidney University, Australia.

Bottero, A.; Negre, R.; Pastor, J. and Turgeman, S. 1980. Finite Element method and limit analysis theory for soil mechanics problems. *Computer Methods in Applied Mechanics and Engineering.* Vol. 22, pp.131-149.

Brinch-Hansen, J. 1961. A general formula for bearing capacity. *Danish Geotechnical Institute Bulletin*. Vol. 11, pp. 38-46.

Brinch-Hansen, J. 1970. A revised and extended formula for bearing capacity. *Danish Geotechnical Institute Bulletin*. Vol. 28, pp. 5-11.

Brinkgreve, R.B.J., and Broere, W. 2004. *PLAXIS 3D Tunnel – Version 2.0: Reference Manual*. Delft, Netherlands.

Brinkgreve, R.B.J., and Swolfs, W.M. 2007. *PLAXIS 3D Foundation – Version 2.0: Reference Manual*. Delft, Netherlands.

Brinkgreve, R.B.J.; Broere, W. and Waterman, D. 2008. *PLAXIS 2D – Version 9.0: Reference Manual*. Delft, Netherlands.

Chen, W.F. 1975. *Limit analysis and soil plasticity*. New York: Elsevier Publishing Co.

Coduto, D.P. 2000. *Foundation design: principles & practices*. 2 ed. Prentice Hall.

Das, B.M. 2009. *Shallow foundations: Bearing capacity and settlement*. Boca Raton: Taylor & Francis Group, LLC.

De Beer, E.E. 1970. Experimental determination of the shape factors and the bearing capacity factors of sand. *Géotechnique.* Vol. 20, No. 4, pp. 387-411.

de Borst, R. and Vermeer, P.A. 1984. Possibilities and limitations of Finite Element for limit analysis. *Géotechnique.* Vol. 34, No. 2, pp. 199-210.

Drescher, A. and Detournay, E. 1993. Limit load in translational failure mechanisms for associative and non –associative materials. *Géotechnique.* Vol. 43, No. 3, pp. 443-456.

Drucker, D.C. and Prager, W. 1952. Soil mechanics and plastic analysis of limit design. *Quarterly of Applied Mathematics*. Vol. 10, No. 2, pp. 157-165.

Emdal, A. and Grande, L. 2006. *TBA5100 Theoretical Soil Mechanics Handouts*. Geotechnical Division. Department of Civil and Transport Engineering. Norwegian University of Science and Technology. Trondheim, Norway.

Erickson, H.L. and Drescher, A. 2002. Bearing capacity of circular footings. *Journal of Geotechnical and Environmental Engineering*. Vol. 128, No. 1, pp. 38-43.

European Committee for Standardization. 2004. *Eurocode 7: Geotechnical design – Part 1: General rules*. NS-EN 1997-1:2004+NA:2008. Standard Norge.

Frydman, S. and Burd, H.J. 1997. Numerical studies of bearing-capacity factor $N\gamma$. *Journal of Geotechnical and Environmental Engineering.* Vol. 123, No. 1, pp. 20-29.

Golder, H.Q. 1941. The ultimate bearing pressure of rectangular footings. *Journal of the Institute of Civil Engineers.* Vol. 17, No. 2, pp. 161-174.

Griffiths, D.V. 1982. Computation of bearing capacity factors using Finite Element. *Géotechnique.* Vol. 32, No. 3, pp. 195-202.

Hjiaj, M., Lyamin, A.V. and Sloan, S.W. 2004. Bearing capacity of a cohesive-frictional soil under non-eccentric inclined loading. *Computers and Geotechnics.* Vol. 31, pp. 491-516.

Hjiaj, M., Lyamin, A.V. and Sloan, S.W. 2005. Numerical limit analysis solutions for the bearing capacity factor Nγ. *International Journal of Soils and Structures*. No. 42, pp. 1681-1704.

Jahanandish, M.; Veiskarami, M. and Ghahramani, A. 2010. Numerical bearing capacity computation and load-displacement behaviour of shallow foundations by stress level based ZEL method. *Proceedings 7th European Conference on Numerical Methods in Geotechnical Engineering*. Trondheim, Norway.

Kötter, F. 1903. Die bestimmung des druckes an gekrümmten gleitflächen, eine aufgabe aus der lehre vom erddruck. *Sitzungsberichte der Akademie der Wissenschaften*. Berlin, pp. 229-233.

Krabbenhøft, K. and Damkilde, L. 2003. A general non-linear optimization algorithm for lower bound limit analysis. *International Journal for Numerical Methods in Engineering*. Vol. 56, pp. 165-184.

Krabbenhøft, K., Lyamin, A.V., Hjiaj, M. and Sloan, S.W. 2005. A new discontinuous upper bound limit analysis formulation. *International Journal for Numerical Methods in Engineering*. Vol. 63, pp. 1069-1088.

Krabbenhøft, K., Lyamin, A.V. and Sloan, S.W. 2010. Associated plasticity for non-associated frictional materials. *Proceedings 7th European Conference on Numerical Methods in Geotechnical Engineering*. Trondheim, Norway.

Kumar, J. 2003. *Nγ for rough strip footing using the method of characteristics.* Canadian Geotechnical Journal. Vol. 40, No. 2, pp. 669-674.

Loukidis, D. and Salgado, R. 2009. Bearing capacity of strip and circular footings in sand using FE. *Computers and Geotechnics*. No. 36, pp. 871-879.

Lundgren, H. and Mortensen, K. 1953. Sur le terme de surface dans le calcul des foundations en milieu pulvurulent. *Proceedings III International Conference in Soil Mechanics and Foundation Engineering.* Zurich, Switzerland. Vol. 1, pp. 336.

Lyamin, A.V. 1999. *Three-dimensional lower bound limit analysis using nonlinear programming*. PhD thesis, Department of Civil, Surveying and Environmental Engineering. University of Newcastle, NSW.

Lyamin, A.V., Sloan, S.W., 2002a. Upper bound limit analysis using linear FE and nonlinear programming. *International Journal for Numerical and Analytical Methods in Geomechanics*. Vol. 26, No. 2, pp. 181–216.

Lyamin, A.V., Sloan, S.W., 2002b. Lower bound limit analysis using linear FE and nonlinear programming. *International Journal for Numerical Methods in Engineering*. Vol. 55, No. 5, pp. 573–611.

Lyamin, A.V., Krabbenhøft, K., Abbo, A.J. and Sloan, S.W. 2005a. General approach to modeling discontinuities in limit analysis. *Proceedings 11th International Conference of the International Association for Computer Methods and Advances in Geomechanics (IACMAG)*. Torino. Vol. 1, pp. 95–102.

Lyamin, A.V., Sloan, S.W., Krabbenhøft, K., and Hjiaj, M. 2005b. Lower bound limit analysis with adaptive remeshing. *International Journal for Numerical Method in Engineering*. Vol. 63, pp. 1961-1974.

Lyamin, A.V., Salgado, R., Sloan, S.W. and Prezzi, M. 2007. Two- and three-dimensional bearing capacity of footings in sand. *Géotechnique*. Vol. 57, No. 8, pp. 647-662.

Lysmer, J. 1970. Limit analysis of plane problems in soil mechanics. *Journal of Soil Mechanics and Foundations Division*. ASCE. Vol. 96, pp. 1311-1334.

Manoharan, N. and Dasgupta, P. 1995. Bearing capacity of surface footings by FE. *Computers & Structures*. Vol. 54, No. 4, pp. 563-586.

Martin, C.M. 2003. *User guide for ABC – Analysis of bearing capacity, version 1.0.* OUEL Report No.2261/03. Department of Engineering Science, University of Oxford.

Martin, C.M. 2005. Exact bearing capacity calculations using the method of characteristics. *Proceedings 11th International Conference IACMAG*. Turin, Vol. 4, pp. 441.

Meyerhof, G.G. 1951. The ultimate bearing capacity of foundations. *Géotechnique*. Vol. 2, pp. 301-331.

Meyerhof, G.G. 1963. Some recent research on the bearing capacity of foundations. *Canadian Geotechnical Journal.* Vol. 1, No. 1, pp. 16-26.

Michalowski, R.L. 1997. An estimate of the influence of soil weight on bearing capacity using limit analysis. *Soils and Foundations*. Vol. 35, No. 4, pp. 57-64.

Michalowski, R. 2001. Upper-bound load estimates on square and rectangular footings. *Géotechnique*. Vol. 51, No. 9, pp. 787-798.

Michalowski, R. and Dawson, E.M. 2002a. Three-dimensional analysis of limit loads on Mohr-Coulomb soil. *Foundations of Civil and Environmental Engineering (FCEE)*. Poznan University of Technology. Vol. 1, pp.137-147.

Michalowski, R. and Dawson, E.M. 2002b. Ultimate loads on square footings. *Proceedings of the 8th International Symposium on Numerical Models in Geomechanics (NUMOG VIII).* Rome, Balkema, Rotterdam, The Netherlands, pp. 415-418.

Mizuno, E., and Chen, W.F. 1990. Cap models for clay strata to footing loads. *Computers & Structures*. No. 17, pp. 511-528.

Narita, K. and Yamaguchi, H. 1992. Three-dimensional bearing capacity analysis of foundations by use of a method of slices. *Soils and Foundations*. Vol. 32, No. 4, pp. 143-155.

Nordal, S. 2007. *TBA 4115 Finite Element in geotechnical engineering: lecture notes*. Geotechnical Division. Norwegian University of Science and Technology.

Novotortsev, V.I. 1938. Application of the theory of plasticity to problems of determining the bearing capacity of building foundations. *Izv. VNIG*. Vol. 22, pp. 22.

Prandtl, L. 1921. Uber die eindringungsfestigkeit plastisher baustoffe und die festigkeit von schneide. *Zeitschrift für angewandte mathematik und mechanik*, Basel, Switzerland. Vol. 1, No. 1, pp. 15-20.

Potts, D.M. and Zdravkovic, L. 1999. *Finite Element analysis in geotechnical engineering: applications*. London: Thomas Telford Ltd.

Poulos, H.G., Carter, J.P., and Small, J.C. 2001. Foundations and retaining structures – research and practice. *Proceedings 15th International Conference on Soil Mechanics and Foundation Engineering.* Istanbul, Turkey, Vol. 4, pp. 2527.

Puzakov, V., Drescher, A. and Michalowski, R. 2009. Shape factor s_γ for shallow footings. *Geomechanics and Engineering*. Vol. 1, No. 2, pp. 113-120.

Reissner, H. 1924. Zum erddruckproblem. *First International Conference on Applied Mechanics Proceedings,* Delft, Netherlands. pp. 295-311.

Salgado, R., Lyamin, A.V., Sloan, S.W. and Yu, S. 2004. Two- and three dimensional bearing capacity of foundations in clay. *Géotechnique*. Vol. 54, No. 5, pp. 297-306.

Salgado, R. 2008. *The engineering of foundations*. New York: McGraw-Hill.

Shield, R.T., and Drucker, D.C. 1953. The application of limit analysis to punch-indentation problems. *Journal of Applied Mechanics*. No. 20, pp. 453-460.

Sieffert, J.-G. and Bay-Gress, Ch. 2000. Comparison of European bearing capacity calculation methods for shallow foundations. *Proceedings Institute of Civil Engineers*. No. 143, pp. 65-74.

Sloan, S.W. 1988. Lower bound limit analysis using FE and linear programming. *International Journal for Numerical and Analytical Methods in Geomechanics.* Vol. 12, pp.61-77.

Sloan, S.W. and Kleeman, P.W. (1995). Upper bound limit analysis using discontinuos velocity fields. *Computer Methods in Applied Mechanics and Engineering.* Vol. 127, No. 1, pp. 293-314.

Smith, C.C. 2005. Complete limiting stress solutions fro the bearing capacity of strip footings on a Mohr-Coulomb soil. *Géotechnique*. Vol. 55, No. 8, pp. 607-612.

Sokolovskii, V.V. 1965. *Statics of soil media.* Oxford: Pergamon Press.

Terzaghi, K. 1943. *Theoretical soil mechanics.* New York: John Wiley.

Ukritchon, B.; Whittle, A.J. and Klangvijit, C. 2003. Calculations of bearing capacity factor $N\gamma$ using numerical limit analysis. *Journal of Geotechnical and Environmental Engineering.* Vol. 129, No. 6, pp. 468-474.

Vesić, A.S. 1963. Bearing capacity of deep foundations in sand. National Academy of Sciences, National Research Council. *Highway Research Record*. No. 39, pp. 112-153.

Vesić, A.S. 1973. Analysis of ultimate loads of shallow foundations. *Journal of the soil mechanics and foundations division*. ASCE. Vol. 99, No. 1, pp. 45-73.

Yin, J.-H., Wang, Y.-J. and Selvadurai, A.P.S. 2001. Influence of non-associativity on the bearing capacity of a strip footing. *Journal of Geotechnical and Environmental Engineering*. Vol. 127, No. 11, pp. 985-989.

Zhao, L. and Wang, J.-H. 2009. Influence of non-associativity on the bearing capacity factors of a circular footing. *Journal of Shanghai Jiaotong University (Science)*. Vol. 14, No. 4, pp. 429-434.

Zhu, M. and Michalowski, R.L. 2005. Shape factors for limit loads on square and rectangular footings. *Journal of Geotechnical and Geoenvironmental Engineering.* ASCE. Vol. 131, No. 2, pp. 223-231.

Zienkiewicz, O.C., Humpheson, C., and Lewis, R.W. 1975. Associative and non-associative visco-plasticity and plasticity in soil mechanics. *Géotechnique*. Vol. 25, No. 4, pp. 671-689.

List of symbols and abbreviations

Symbol / Abbreviation	Name / Meaning	Units
ν	Poisson's ratio	---
γ	Soil unit weight	kN/m^3
(σ,τ)	Stress coordinates (normal stress, shear stress)	kPa
$\dot{\boldsymbol{\gamma}}^p$	Plastic shear strain rate	---
$\dot{\boldsymbol{\varepsilon}}^p$	Plastic normal strain rate	---
a	attraction	kPa
aφ-analysis	Effective stress analysis	---
B	Width of the footing	m
B/L	Relative footing dimension	---
B-symmetry	Symmetry along the width B of the footing	---
c	Cohesion	kPa
c*	Drescher and Detournay (1993) new cohesion	kPa
D	Foundation depth of the footing	m
d	Thickness of the footing	cm
EA	Stiffness parameter for the footing	kN/m
EI	Stiffness parameter for the footing	kNm^2/m
E_{ref} or E	Young's modulus	MPa-kPa
FDM	Finite Difference method	---
FE	Finite Elements	---
FEM	Finite Element Method	---
K_o	At rest earth pressure coefficient	---
$K_{p\gamma}$	Passive earth pressure coefficient resulting from the minimum value of the passive force contribution obtained by trial and error	---
L	Length of the footing	m
L/B	Aspect ratio	---
L-symmetry	Symmetry along the length L of the footing	---
MOC	Method of characteristics	---
$N\gamma$	Non-dimensional bearing capacity factor for soil weight contribution	---
Nc	Non-dimensional bearing capacity factor for cohesion contribution	---
Nq	Non-dimensional bearing capacity factor for overburden contribution	---
Nq^*s_q	Normalized footing load for Nq study	---
$N\gamma^*s_\gamma$	Normalized footing load for $N\gamma$ back-calculation	---

Symbol / Abbreviation	Name / Meaning	Units
N_q^*	Modified non-dimensional bearing capacity factor for overburden contribution and rectangular footings	---
N_γ^*	Modified non-dimensional bearing capacity factor for soil weight contribution and rectangular footings	---
Pn	Normal force	kN
$P_{p\gamma}$	Minimum value of the passive force contribution obtained by trial and error when $\varphi \neq 0$, $\gamma \neq 0$, $p' = 0$, $c = 0$	kN
P_{pc}	Passive force contribution obtained when $\varphi \neq 0$, $\gamma = 0$, $p' = 0$, $c \neq 0$	kN
P_{pq}	Passive force contribution obtained when $\varphi \neq 0$, ⊚ = 0, $p' \neq 0$, $c = 0$	kN
Pt	Horizontal force	kN
q or p′	Overburden	kPa
q_o or q_{ult}	Maximum load which the foundation can support. Ultimate load. Collapse load.	kPa
s_c	Shape factor for the Nc bearing capacity factor	---
s_q	Shape factor for the Nq bearing capacity factor	---
s_γ	Shape factor for the $N\gamma$ bearing capacity factor	---
θ	Angle of the displacement vector to the slip plane	°
σ'_v	Foundation stress	kPa
φ	Friction angle	°
$\varphi = \psi$	Associated flow rule	---
φ^*	Drescher and Detournay (1993) new friction angle	kPa
ψ	Dilatancy angle	°
$\psi < \varphi$	Non-associated flow rule	---
w/B	Normalized footing settlement	---
2D	Two geometrical dimensions	---
3D	Three geometrical dimensions	---

Annexe 1

Equations for calculating the bearing capacity factors

Author	Nq	Nc	Nγ
Prandtl (1921) and Reissner (1924)	$tan^2(\frac{\pi}{4}+\frac{\varphi}{2}) * e^{\pi * tan\varphi}$	$(N_q-1) * cotan\varphi$	---
Terzaghi (1943)	$\frac{e^{2*(\frac{3*\pi}{4}-\frac{\varphi}{2})*tan\varphi}}{2*cos^2(45+\frac{\varphi}{2})}$	$(N_q-1) * cotan\varphi$	$\frac{1}{2}K_{p\gamma}tan^2\varphi - \frac{tan\varphi}{2}$ *$K_{p\gamma}$ is given in tables*
Meyerhof (1951) and (1963)	$\frac{1+sin\varphi}{1-sin\varphi} * e^{\pi * tan\varphi}$	$(N_q-1) * cotan\varphi$	$(N_q-1) * tan(1.4\varphi)$
Biarez *et al.* (1961)	---	---	$1.8 * (N_q-1) * tan\varphi$
Brinch-Hansen (1961) and (1970)	$tan^2(\frac{\pi}{4}+\frac{\varphi}{2}) * e^{\pi * tan\varphi}$	$(N_q-1) * cotan\varphi$	$1.5 * (N_q-1) * tan\varphi$
Vesić (1973)	$tan^2(\frac{\pi}{4}+\frac{\varphi}{2}) * e^{\pi * tan\varphi}$	$(N_q-1) * cotan\varphi$	$2 * (N_q+1) * tan\varphi$
Michalowski (1997)	---	---	$e^{0.66+5.11tan\varphi} * tan\varphi$
Poulos *et al.* (2001)	---	---	$0.1045 * e^{9.6\varphi}\ with\ \varphi\ in\ radians$
Hjiaj *et al.* (2005)	---	---	$e^{\frac{1}{6}*(\pi+3\pi^2 tan\varphi)} * (tan\varphi)^{\frac{2\pi}{5}}$
Salgado (2008)	---	---	$(N_q-1) * tan(1.32\varphi)$
Loukidis and Salgado (2009)	$\frac{1+sin\varphi}{1-sin\varphi} * e^{F(\varphi,\psi)*\pi*tan\varphi}$ $F(\varphi,\psi) = 1 - tan\varphi * (tan(0.8 * (\varphi-\psi)))^{2.5}$	---	$(N_q-1) * tan(1.34\varphi)$
Eurocode 7	$tan^2(\frac{\pi}{4}+\frac{\varphi}{2}) * e^{\pi * tan\varphi}$	$(N_q-1) * cotan\varphi$	$2 * (N_q-1) * tan\varphi$
Norway	$tan^2(\frac{\pi}{4}+\frac{\varphi}{2}) * e^{\pi * tan\varphi}$ or Figure 18a	$(N_q-1) * cotan\varphi$	Figure 18b

Annexe 2

Equations for calculating the shape factors for rectangular and circular/square footings

Author	s_q	s_c	s_γ
Terzaghi (1943)	1.0 square 1.0 circular	1.3 square 1.3 circular	0.4 square 0.4 circular
Meyerhof (1951) and (1963)	$1\, when\, \varphi = 0^o$ $1 + 0.1 * tan^2(\frac{\pi}{2} + \frac{\varphi}{2}) * B/L\, when\, \varphi = 10^o$	$1 + 0.2tan^2(\frac{\pi}{2} + \frac{\varphi}{2}) * B/L$	$1\, when\, \varphi = 0^o$ $1 + 0.1 * tan^2(\frac{\pi}{2} + \frac{\varphi}{2}) * B/L\, when\, \varphi = 10^o$
Brinch-Hansen (1961) & (1970)	$1 + sin\varphi * B/L$	$1 + N_q/N_c * B/L$	$1 - 0.4 * B/L$
Vesić (1973)	$1 + tan\varphi * B/L$	$1 + N_q/N_c * B/L$	$1 - 0.4 * B/L$
Zhu and Michalowski (2005)	$1 + 1.9 * tan^2\varphi * \sqrt{B/L}$	$1 + (1.8 * tan^2\varphi + 0.1) * \sqrt{B/L}$	$1 + (0.6 * tan^2\varphi - 0.25) * B/L\, when\, \varphi \leq 30^0$ $1 + (1.3 * tan^2\varphi - 0.5) * L/B^{1.5} * e^{-(L/B)}\, when\, \varphi > 30^0$
Salgado *et al.* (2004)	---	$1 + 0.12 * (B/L) + 0.17 * \sqrt{D/B}$	---
Lyamin *et al.* (2007)	$1 + (0.098\varphi - 1.64)(\frac{D}{B})^{0.7-0.01\varphi}(\frac{B}{L})^{1-0.16*\frac{D}{B}}$	---	$1 + (0.0336\varphi - 1) * (B/L)$
Loukidis and Salgado (2009)	$s_q^{circ} = 1 + 2.9 * tan^2\varphi$	---	$s_\gamma^{circ} = 1 + 0.26 * \frac{1+sin\varphi}{1-sin\varphi} - 0.73$
Eurocode 7	$1 + sin\varphi * B/L$	$1 + N_q/N_c * B/L$	$1 - 0.3 * B/L$
Norway	1.20 square	---	0.70 square

Annexe 3

Failure loads for each case of analysis in the Nq-study

Case of study		Value (kPa)		Case of study		Value (kPa)	
Set 1A	$q_{ult-Nq-1A-2Ds-15}$	69	69	Set 1B	$q_{ult-Nq-1B-2Ds-15}$	69	---
	$q_{ult-Nq-1A-2Ds-6}$	70	70		$q_{ult-Nq-1B-2Ds-6}$	70	---
	$q_{ult-Nq-1A-3D3x20}$	74	71[i]		$q_{ult-Nq-1B-2D3x20}$	74	---
	$q_{ult-Nq-1A-3D3x15}$	79	75[i]		$q_{ult-Nq-1B-3D3x15}$	79	---
	$q_{ult-Nq-1A-3D3x10}$	82	78[i]		$q_{ult-Nq-1B-3D3x10}$	82	---
	$q_{ult-Nq-1A-3D3x5}$	89	84[i]		$q_{ult-Nq-1B-3D3x5}$	88	---
	$q_{ult-Nq-1A-3D3x3}$	94	89[i]		$q_{ult-Nq-1B-3D3x3}$	93	---
	$q_{ult-Nq-1A-2Dc-15}$	91	91		$q_{ult-Nq-1B-2Dc-15}$	90	---
	$q_{ult-Nq-1A-2Dc-6}$	89	89		$q_{ult-Nq-1B-2Dc-6}$	89	---
Set 2A	$q_{ult-Nq-2A-2Ds-15}$	223	223	Set 2B	$q_{ult-Nq-2B-2Ds-15}$	193	193
	$q_{ult-Nq-2A-2Ds-6}$	228	228		$q_{ult-Nq-2B-2Ds-6}$	204	204
	$q_{ult-Nq-2A-3D3x20}$	241	232[i]		$q_{ult-Nq-2B-3D3x20}$	215	222[iv]
	$q_{ult-Nq-2A-3D3x15}$	279	268[i]		$q_{ult-Nq-2B-3D3x15}$	247	255[iv]
	$q_{ult-Nq-2A-3D3x10}$	310	299[i]		$q_{ult-Nq-2B-3D3x10}$	270	281[iv]
	$q_{ult-Nq-2A-3D3x5}$	364	338[i]		$q_{ult-Nq-2B-3D3x5}$	326	345[iv]
	$q_{ult-Nq-2A-3D3x3}$	409	379[i]		$q_{ult-Nq-2B-3D3x3}$	367	393[iv]
	$q_{ult-Nq-2A-2Dc-15}$	408	408		$q_{ult-Nq-2B-2Dc-15}$	376	376
	$q_{ult-Nq-2A-2Dc-6}$	394	394		$q_{ult-Nq-2B-2Dc-6}$	353	353
Set 3A	$q_{ult-Nq-3A-2Ds-15}$	491	---	Set 3B	$q_{ult-Nq-3B-2Ds-15}$	369	369
	$q_{ult-Nq-3A-2Ds-6}$	538	---		$q_{ult-Nq-3B-2Ds-6}$	424	424
	$q_{ult-Nq-3A-3D3x20}$	520	---		$q_{ult-Nq-3B-3D3x20}$	380[ii]	430[iv]
	$q_{ult-Nq-3A-3D3x15}$	635	---		$q_{ult-Nq-3B-3D3x15}$	431[ii]	530[iv]
	$q_{ult-Nq-3A-3D3x10}$	763	---		$q_{ult-Nq-3B-3D3x10}$	454[ii]	657[iv]
	$q_{ult-Nq-3A-3D3x5}$	981	---		$q_{ult-Nq-3B-3D3x5}$	699[ii]	835[iv]
	$q_{ult-Nq-3A-3D3x3}$	1132	---		$q_{ult-Nq-3B-3D3x3}$	985[ii]	1008[iv]
	$q_{ult-Nq-3A-2Dc-15}$	1251	---		$q_{ult-Nq-3B-2Dc-15}$	1050	1050
	$q_{ult-Nq-3A-2Dc-6}$	1141	---		$q_{ult-Nq-3B-2Dc-6}$	909	909
Set 4A	$q_{ult-Nq-4A-2Ds-15}$	1127	---	Set 4B	$q_{ult-Nq-4B-2Ds-15}$	767	767
	$q_{ult-Nq-4A-2Ds-6}$	1265	---		$q_{ult-Nq-4B-2Ds-6}$	948	948
	$q_{ult-Nq-4A-3D3x20}$	1215	---		$q_{ult-Nq-4B-3D3x20}$	950[iii]	930[iv]
	$q_{ult-Nq-4A-3D3x15}$	1530	---		$q_{ult-Nq-4B-3D3x15}$	1409[iii]	1261[iv]
	$q_{ult-Nq-4A-3D3x10}$	1965	---		$q_{ult-Nq-4B-3D3x10}$	1681[iii]	1500[iv]
	$q_{ult-Nq-4A-3D3x5}$	2880	---		$q_{ult-Nq-4B-3D3x5}$	1965[iii]	2290[iv]
	$q_{ult-Nq-4A-3D3x3}$	3325	---		$q_{ult-Nq-4B-3D3x3}$	2865[iii]	2517[iv]
	$q_{ult-Nq-4A-2Dc-15}$	3636	---		$q_{ult-Nq-4B-2Dc-15}$	2793	2793
	$q_{ult-Nq-4A-2Dc-6}$	3241	---		$q_{ult-Nq-4B-2Dc-6}$	2487	2487

[i]refining the mesh on the borders of the footing; [ii]modeling the complete footing;
[iii]modeling a diagonal footing; [iv]using Plaxis 3D Tunnel.

Annexe 4

Failure loads for each case of analysis in the Total and Nγ-back calculation

Case of study		Value (kPa)	Case of study		Value (kPa)
Set 1A	$q_{ult-Total-1A-2Ds-15}$	101	Set 1B	$q_{ult-Total-1B-2Ds-15}$	101
	$q_{ult-Total-1A-2Ds-6}$	103		$q_{ult-Total-1B-2Ds-6}$	103
	$q_{ult-Total-1A-3D3x20}$	111		$q_{ult-Total-1B-3D3x20}$	111
	$q_{ult-Total-1A-3D3x15}$	113		$q_{ult-Total-1B-3D3x15}$	113
	$q_{ult-Total-1A-3D3x10}$	114		$q_{ult-Total-1B-3D3x10}$	114
	$q_{ult-Total-1A-3D3x5}$	118		$q_{ult-Total-1B-3D3x5}$	118
	$q_{ult-Total-1A-3D3x3}$	119		$q_{ult-Total-1B-3D3x3}$	119
	$q_{ult-Total-1A-2Dc-15}$	113		$q_{ult-Total-1B-2Dc-15}$	113
	$q_{ult-Total-1A-2Dc-6}$	111		$q_{ult-Total-1B-2Dc-6}$	111
Set 2A	$q_{ult-Total-2A-2Ds-15}$	535	Set 2B	$q_{ult-Total-2B-2Ds-15}$	498
	$q_{ult-Total-2A-2Ds-6}$	580		$q_{ult-Total-2B-2Ds-6}$	545
	$q_{ult-Total-2A-3D3x20}$	577		$q_{ult-Total-2B-3D3x20}$	545
	$q_{ult-Total-2A-3D3x15}$	609		$q_{ult-Total-2B-3D3x15}$	549
	$q_{ult-Total-2A-3D3x10}$	637		$q_{ult-Total-2B-3D3x10}$	564
	$q_{ult-Total-2A-3D3x5}$	675		$q_{ult-Total-2B-3D3x5}$	616
	$q_{ult-Total-2A-3D3x3}$	678		$q_{ult-Total-2B-3D3x3}$	650
	$q_{ult-Total-2A-2Dc-15}$	770		$q_{ult-Total-2B-2Dc-15}$	720
	$q_{ult-Total-2A-2Dc-6}$	694		$q_{ult-Total-2B-2Dc-6}$	630
Set 4A	$q_{ult-Total-4A-2Ds-15}$	4175	Set 4B	$q_{ult-Total-4B-2Ds-15}$	2921
	$q_{ult-Total-4A-2Ds-6}$	4410		$q_{ult-Total-4B-2Ds-6}$	3733
	$q_{ult-Total-4A-3D3x20}$	5180		$q_{ult-Total-4B-3D3x20}$	4170
	$q_{ult-Total-4A-3D3x15}$	5960		$q_{ult-Total-4B-3D3x15}$	4727
	$q_{ult-Total-4A-3D3x10}$	6070		$q_{ult-Total-4B-3D3x10}$	5039
	$q_{ult-Total-4A-3D3x5}$	7430		$q_{ult-Total-4B-3D3x5}$	6370
	$q_{ult-Total-4A-3D3x3}$	7280		$q_{ult-Total-4B-3D3x3}$	7370
	$q_{ult-Total-4A-2Dc-15}$	7600		$q_{ult-Total-4B-2Dc-15}$	7240
	$q_{ult-Total-4A-2Dc-6}$	8300		$q_{ult-Total-4B-2Dc-6}$	5857

Annexe 5

Second alternative for solving "needle" failure: diagonal footing

It was mentioned in Chapter 4 that the structured mesh in a vertical plane was the main factor causing the generation of the "needle" failure when the L-symmetry (two planes of symmetry), $\varphi > 30°$ and $\psi < \varphi$ were combined in the analysis. Another solution proposed to overcome this problem is the diagonal geometrical location of the footing respect to the general geometry of the model (Figure A5.1).

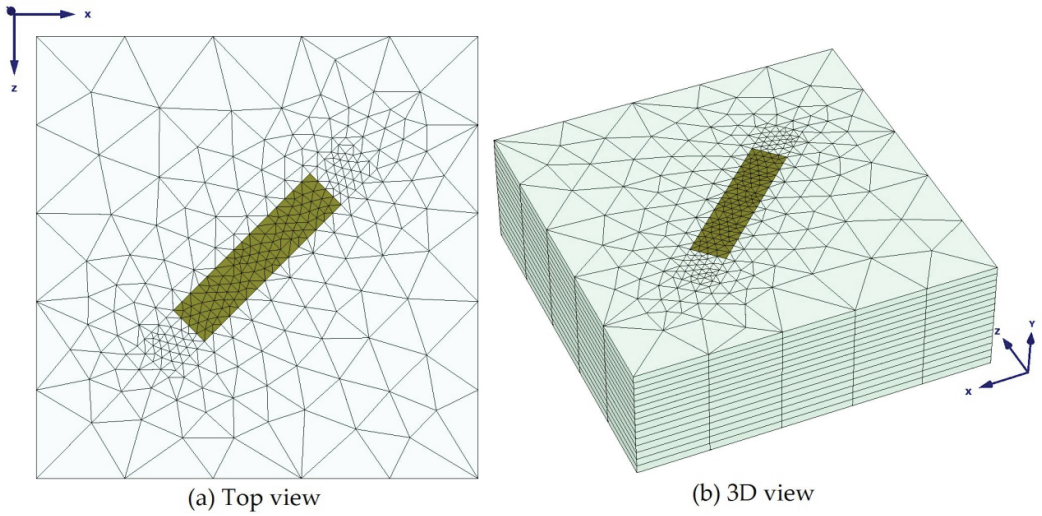

Figure A5.1: Location of the diagonal footing respect to the geometry of the model.

This arrangement allows to have the deformation flexibility for the elements along the symmetry line (commented in Chapter 4) and to create some unsymmetrical conditions in the vertical structured mesh that avoids the generation of the "needle" failure.

The diagonal footing was tested for $\varphi = 40°$ with dilatancy angle of 10° (Set 4B and $\gamma = 0$). Five different lengths L of footings were tried and the results are shown in Figure A.5.2. They are satisfactory respect to the failure pattern developed for footings of 3x20m and 3x15m; for the rest of the footings, some

traces of the "needle" failure pattern tried to be shown. Furthermore, a sensitivity problem of the failure load values was observed.

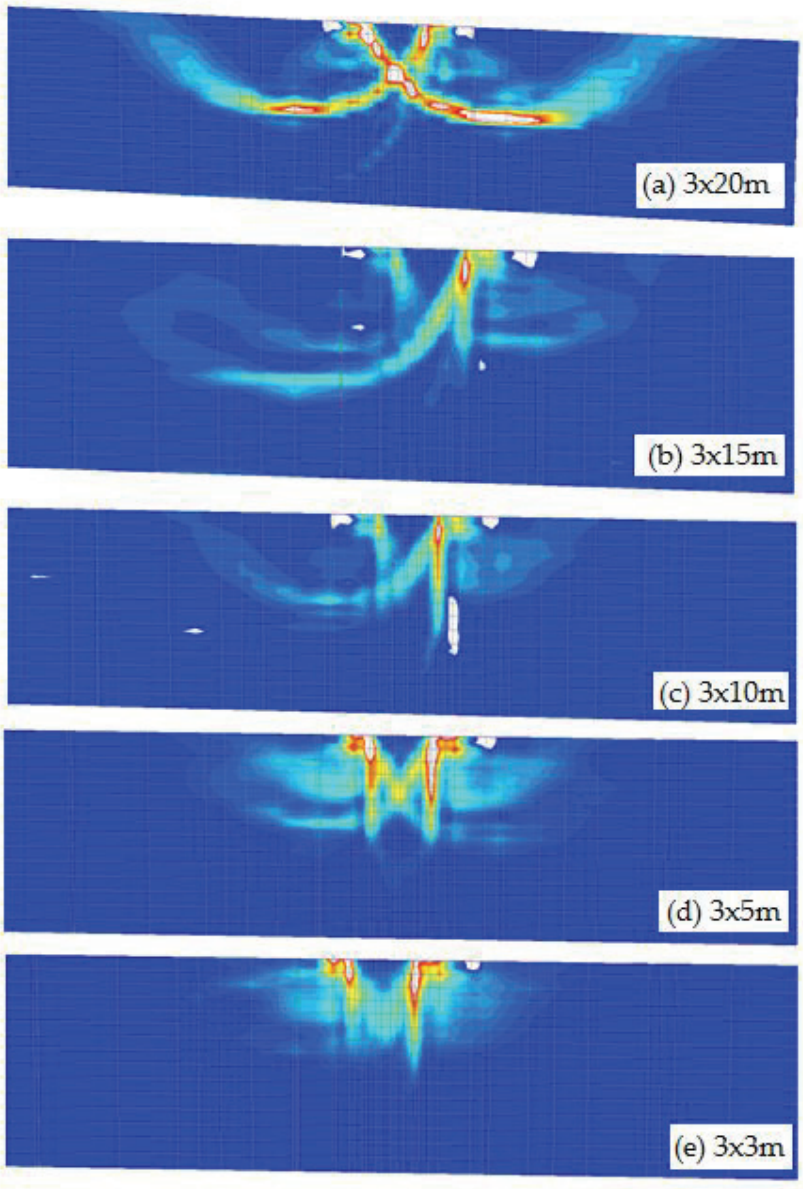

Figure A5.2: Failure pattern as incremental shear strains for $\varphi = 40°$ and $\psi = 10°$ (Set 4B and $\gamma = 0$) for the diagonal footing to the geometry of the model.

The 3x10m was chosen to study the problem about the sensitivity of the failure load related to the initial load given for reaching the failure. The general procedure was detailed in Chapter 3. Summarizing, an initial high load (L1) was given initially to the model, and then the reached load value (L2) were the calculation stopped was written. The next step was to load (L3) the model again with a smaller value of the load reached (L3 < L2) and finally, perform a c-phi reduction calculation to get a factor (FS) that multiplies L3. The failure load (FL) will be FS*L3. The Table A5.1 details the values of the analysis done for this problem.

Table A5.1: Calculation details for load sensitivity analysis in diagonal footings.

Parameter	Case 1	Case 2
Initial load L1 (kPa)	2500	1800
Stops at L2 (kPa)	1170	1681.2
Second load L3 (kPa)	1150	1650
Factor FS	1.13	1.025
Failure Load FL (kPa)	1299.5	1691.25

The Failure Load is a mean value taken from the load-displacement curve which oscillates due to the non-associated behaviour of the material. Therefore, the failure load is not unique. It can vary from the value chosen in ±0.3 - 0.6%.

As a result that the 3x10m footing was chosen to perform the sensitivity analysis, there was no possibility of calculating the exact value of the failure load. However, the failure load value for the strip footing under the same set of parameters (in associated flow rule) reaches 1083 kPa. For similar calculations using PLAXIS-3D Tunnel the value reached was 1500 kPa.

The Case 2 in Table A5.1 has a failure load value closer to the one obtained with PLAXIS 3D-Tunnel. Consequently, the final result (FL) shows some dependency of the initial load given to the model (L1). However, more investigation in this field should be done to identify the nature of this behaviour.

Annexe 6

First version of paper to publish

Special features for three dimensional bearing capacity calculations

P. Paniagua & S. Nordal
Norwegian University of Science and Technology, Trondheim, Norway

ABSTRACT: Three-dimensional finite element analysis has become a useful tool for computing the bearing capacity of rectangular footings and the corresponding shape factors. Some cares have to be taken when symmetry in the geometry of the model, non-associated flow rule and high friction angles ($\varphi > 30°$) in the soil material are combined in the analysis. When using symmetry for calculation of bearing capacity, at least, one vertical plane of unstructured mesh should be used. Otherwise, it is not recommendable to use symmetry in the model.

1. INTRODUCTION

Bearing capacity calculations are an important part of the design of shallow foundations. This bearing capacity is often based on the superposition method of Terzaghi' (1943) which adds individual contributions from cohesion, friction, overburden and self weight in the form of non-dimensional bearing capacity factors Nc, Nq and $N\gamma$.

The basis for the bearing capacity factors are partly theoretical limit load solutions and partly approximate engineering formula combined with empiricism. The bearing capacity factors are extended from strip loads to rectangular square or circular footings by shape factors. Some shape factors are based on theoretical solutions but most of them are based on interpolations, model tests and other empirical results. Nowadays, numerical computations like Finite Elements (FE) can be performed in two and three dimensions for obtaining accurate shape factors for rectangular and square/circular footings.

For the present study, FE simulations have been performed to obtain shape factors. However, approaching the solution has not been straight forward. Some difficulties have been affronted and solutions to overcome them have been tested.

The following paragraphs summarize some special features (SF) that must be taken into account when collapse loads are being calculated. These resulted from the difficulties that appeared during the numerical modeling of the bearing capacity problem when symmetry in the geometry of the model, non-associated flow rule and high friction angles ($\varphi > 30°$) in the soil material were combined.

2. SETTING THE PROBLEM

FE numerical calculations were performed in two and three dimensions of strip (plane strain conditions), circular (axi-symmetrical conditions) and five rectangular footings (3x20m, 3x15m, 3x10m, 3x5m and 3x3m) for different soil friction angles in order to obtain the shape factors corresponding to the relative footing size B/L.

The general three dimensional (3D) analysis was divided in three fundamental calculations according to which part of the bearing capacity equation (Equation 1) was being investigated:

(a) Weightless soil with cohesion and friction: for the Nq part in Equation 1.

(b) Soil with self-weight, cohesion and friction: for the complete Equation 1.

(c) Back-calculation of the soil-weight factor $N\gamma$: due to the conservative results of adding the factors of the bearing capacity equation (superposition principle) (Griffiths, 1982; Erickson and Drescher, 2002).

$$q_{ult} = s_q\,(p' + a)\,N_q + s_\gamma\,0.5\gamma B\,N_\gamma - a \qquad (1)$$

During the 3D study of the bearing capacity factor Nq, a particular failure pattern was obtained when the symmetry of the footing (along its length L), the non-associative flow rule and $\varphi > 30°$ were combined in the analyses for all the footings lengths: 20m, 15m, 10m, 5m and 3m.

This problem was identified when simulations were performed using symmetry (modeling just a quarter of the footings) and not using it. Any problem or difference in the results of the ultimate load and failure pattern was observed for friction angles lower than 30° in associated and non-associated flow rule cases. However, when friction angles higher than 30° (specifically, 33° and 40°) and non-associated flow rule were used, the failure loads were not closer to the expected theoretical values and the

collapse pattern started to be localized in a type of punching failure. Specifically, the failure mechanism observed in this case had a "needle" shape going deeper around the FE elements border, especially when refinement on the footing borders was done (Figure 1).

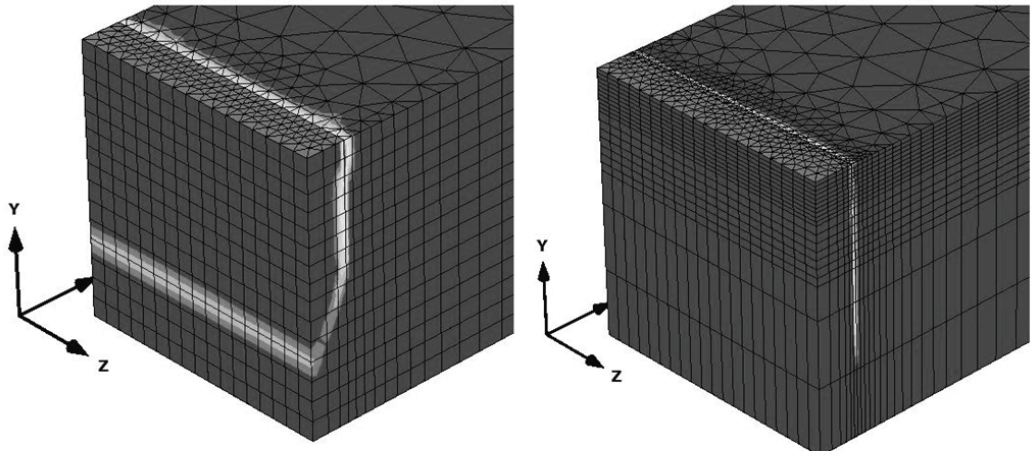

(a) (b)

Figure 1. "Needle" failure when $\varphi = 33°$ and $\psi = 3°$ modeling a quarter of a 3x20m footing (1.5x10m, two planes of symmetry) as a plot of incremental shear strains: (a) Mesh without being refined on border and (b) Mesh with refinement on the borders of the footing. It should be mentioned that the same behaviour was observed for $\varphi = 40°$ and $\psi = 10°$.

3. FINDING EXPLANATIONS TO THE PROBLEM

Two other simulations were performed using just one plane of symmetry for the footing. One plane along its short side B (B-symmetry, 3x10m footing) and the other one along its long side L (L-symmetry, 1.5x20m), which means that half of a 3x20m footing was modelled for both cases. Figure 2 shows the results obtained. Surprisingly, the footing of 3x10m (Figure 2a) showed the failure pattern expected for the bearing capacity problem. On the other hand, the footing of 1.5mx20m (Figure 2b) shows a similar "needle" failure mechanism like the ones presented in Figure 1.

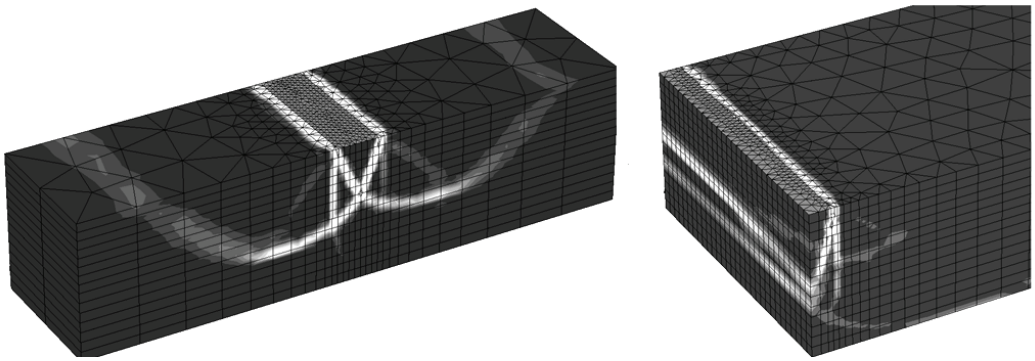

(a) (b)

Figure 2. Failure pattern when $\varphi = 33°$ and $\psi = 3°$ modeling using one plane of symmetry: (a) along the short side B (B-symmetry, footing of 3x10m) and (b) along the long side L (L-symmetry, footing of 1.5x10m). The same behaviour was observed for $\varphi = 40°$ and $\psi = 10°$.

These results seem to confirm that the use of symmetry along the footing length is affecting the final failure mechanism. In this case ($\varphi = 33°$ and $\psi = 3°$), the symmetry along the central length axis of the footing is restricting the deformation of the soil material in addition to the restriction of volume expansion caused by the low dilatancy angle in the non-associated flow rule. Therefore, to take the symmetry line along the length of the footing is not the best option because it suppresses the deformation flexibility of the elements in the vertical plane.

Figure 3 shows an example of this deformation flexibility at failure when the elements along the central line (symmetry line) have a non-symmetric deformation when the full width of the footing is modelled.

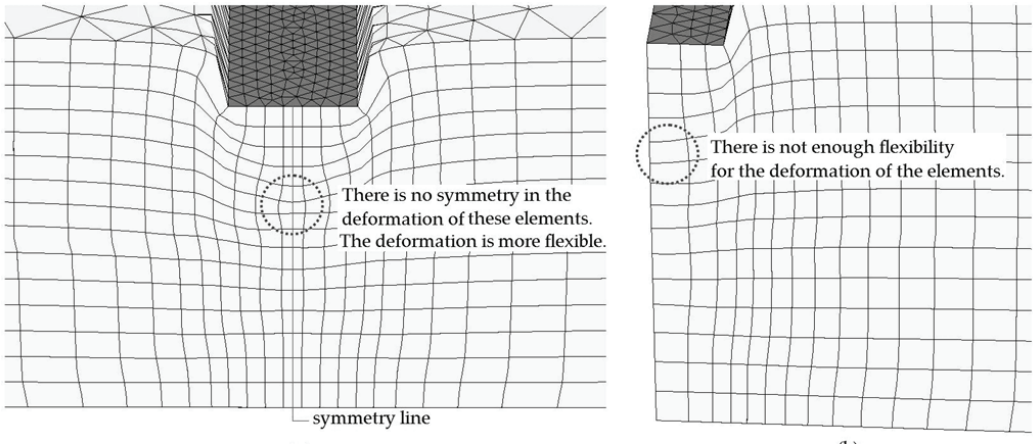

(a) (b)

Figure 3. Deformed mesh at failure when φ = 33° and ψ = 3° for: (a) Symmetry along the width B of the footing (B-symmetry) and (b) Symmetry along the length L of the footing (L-symmetry). The same behaviour was observed for φ = 40° and ψ = 10°.

It was demonstrated that the use or not of L-symmetry plays an important role in the numerical determination of the bearing capacity for non-associated cases with friction angles higher than 30°. However, another important point was to find an explanation to which factors were causing such atypical failure mechanism (punching) when symmetry along the length of the footing was used.

As a result of the observation that the failure pattern was following the alignment of the mesh arrangement in the vertical plane and that in the FE code PLAXIS 3D Foundation the two vertical planes have a structured mesh; simulations in PLAXIS 2D were performed with a structured mesh. To achieve that, vertical lines were defined in a plane strain model for a coarse and very fine mesh as is shown in Figure 4a and 4b. As was expected, the results show that the "needle" failure pattern appeared also following the borders of the mesh elements (Figure 4c and 4d), even though, some small tendencies of following the log-spiral failure surface tried to be developed. However, these tendencies only respond to some unstructured mesh pattern that tries to be form on the right side of the model as a result of the mesh refinement.

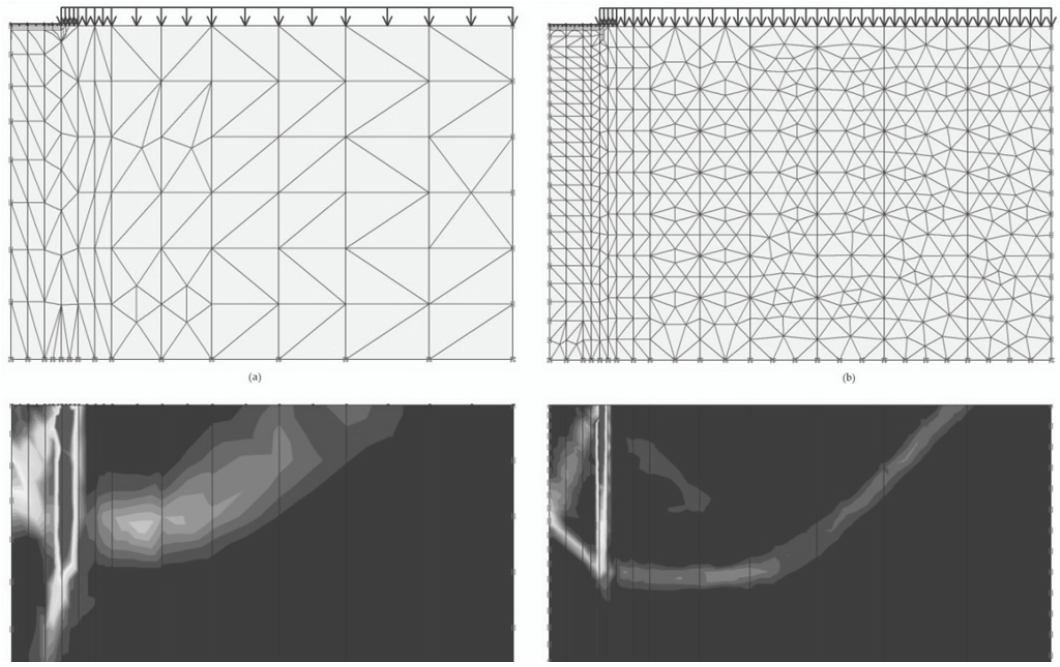

Figure 4. 2D simulations results with symmetry along the length of the footing and structured mesh when $\varphi = 33°$ and $\psi = 3°$: (a) Coarse structured mesh, (b) Very fine structured mesh, (c) Failure pattern as incremental shear strains for a coarse structured mesh, (d) Failure pattern as incremental shear strains for a very fine structured mesh. The same behaviour was observed for $\varphi = 40°$ and $\psi = 10°$.

4. SOLUTIONS TO THE PROBLEM

Having identified that the structured mesh in a vertical plane was the main factor causing the generation of the "needle" failure when the L-symmetry, a $\varphi > 30°$ and $\psi < \varphi$ were combined in the analysis; the alternative of using another FE code that allowed the generation of an unstructured mesh in the vertical plane for approaching to the FE solution was analyzed.

For that proposal, the FE code PLAXIS 3D Tunnel was chosen. Simulations were performed for the non-associated flow rule cases with the friction angles of 33° and 40°. All the footings sizes were tried (3x20m, 3x15m, 3x10m, 3x5m and 3x3m) and good results were obtained when refers to shapes of the failure mechanisms and ultimate load values (and corresponding shape factors for rectangular footings). The collapse mechanism are shown in Figure 5a for $\varphi = 33°$ and in Figure 5b for $\varphi = 40°$.

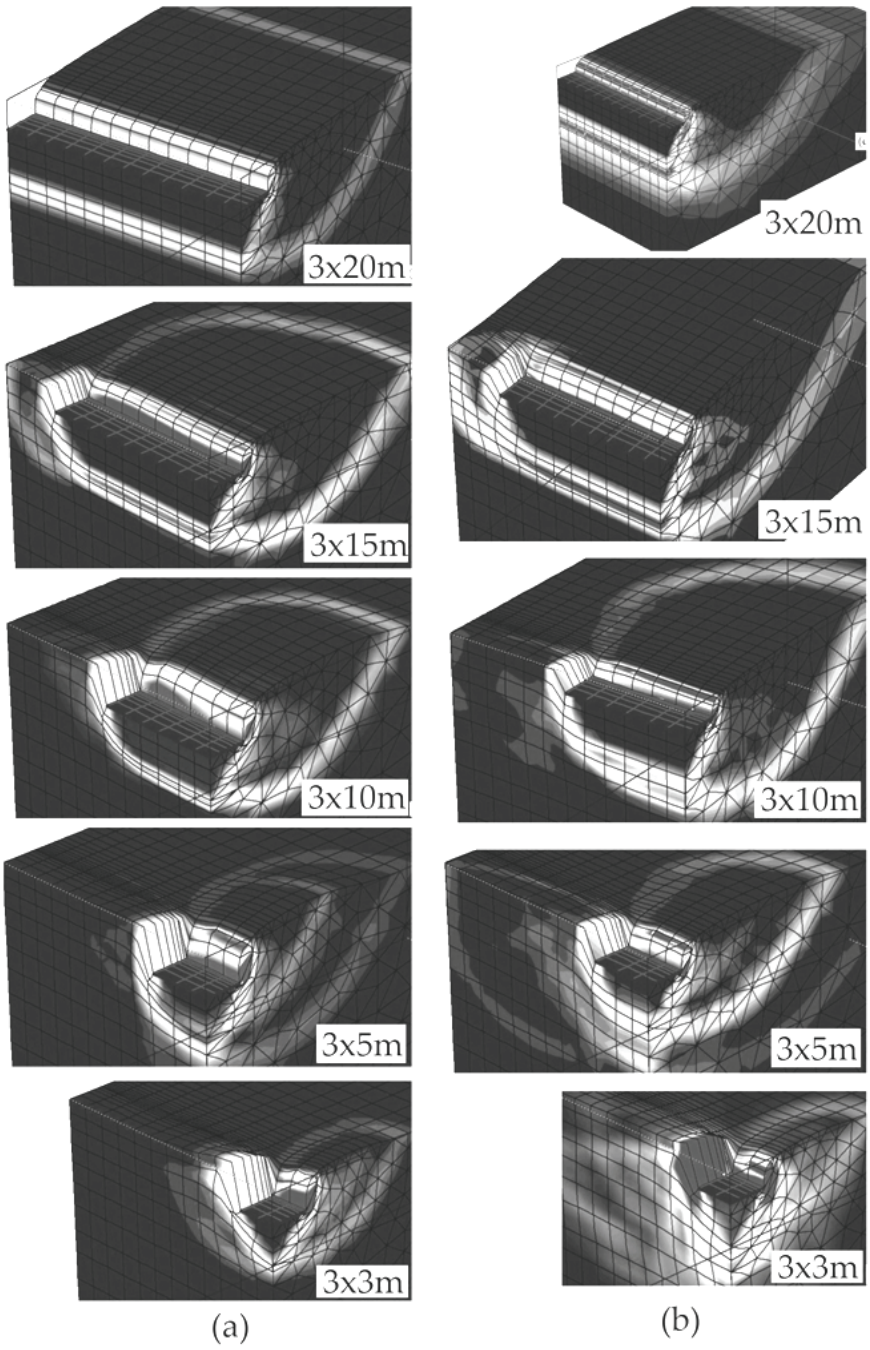

Figure 5. Collapse mechanisms using unstructured mesh in one vertical plane for: (a) $\varphi = 33°$ and $\psi < \varphi$ and (b) $\varphi = 40°$ and $\psi < \varphi$.

A positive point about the use of the FE code PLAXIS 3D Tunnel is that the result for the failure load tends to be more stable due to incremental multipliers algorithm for the loading input. However, when PLAXIS 3D Tunnel is used, the number of FE under the footing in the plane where the structured mesh is being used should be controlled, because too few elements can overpredict failure loads values especially when small footings are being studied (for instance, Figure 5b for 3x3m footing).

5. CONCLUSIONS

In general, when 3D-FE analysis is tried it is highly recommended to model the full geometry of the footing, without any symmetrical simplification. However, if symmetry is required in the model in order to refine areas that can lead to problems without increasing the calculation time, an unstructured mesh should be present in one of the vertical planes of the model. This is a healthy practice when non-associated materials are studied. Actually, the use of non-associated flow rule is a must in the bearing capacity calculations. It will give more realistic values for the ultimate failure load and the bearing capacity factors that can be derived from them.

6. REFERENCES

Brinch-Hansen, J. 1961. A general formula for bearing capacity. *Danish Geotechnical Institute Bulletin*. Vol. 11, pp. 38-46.

Brinch-Hansen, J. 1970. A revised and extended formula for bearing capacity. *Danish Geotechnical Institute Bulletin*. Vol. 28, pp. 5-11.

De Beer, E.E. 1970. Experimental determination of the shape factors and the bearing capacity factors of sand. *Géotechnique.* Vol. 20, No. 4, pp. 387-411.

Erickson, H.L. and Drescher, A. 2002. Bearing capacity of circular footings. *Journal of Geotechnical and Environmental Engineering*. Vol. 128, No. 1, pp. 38-43.

Griffiths, D.V. 1982. Computation of bearing capacity factors using FE. *Géotechnique.* Vol. 32, No. 3, pp. 195-202.

Loukidis, D. and Salgado, R. 2009. Bearing capacity of strip and circular footings in sand using FE. *Computers and Geotechnics*. No. 36, pp. 871-879.

Lyamin, A.V., Salgado, R., Sloan, S.W. and Prezzi, M. 2007. Two- and three-dimensional bearing capacity of footings in sand. *Géotechnique*. Vol. 57, No. 8, pp. 647-662.

Meyerhof, G.G. 1951. The ultimate bearing capacity of foundations. *Géotechnique*. Vol. 2, pp. 301-331.

Meyerhof, G.G. 1963. Some recent research on the bearing capacity of foundations. *Canadian Geotechnical Journal.* Vol. 1, No. 1, pp. 16-26.

Michalowski, R. 2001. Upper-bound load estimates on square and rectangular footings. *Géotechnique*. Vol. 51, No. 9, pp. 787-798.

Nordal, S. 2007. *TBA 4115 Finite Element in geotechnical engineering: lecture notes*. Geotechnical Division. Norwegian University of Science and Technology.

Prandtl, L. 1921. Uber die eindringungsfestigkeit plastisher baustoffe und die festigkeit von schneide. *Zeitschrift für angewandte mathematik und mechanik*, Basel, Switzerland. Vol. 1, No. 1, pp. 15-20.

Potts, D.M. and Zdravkovic, L. 1999. *Finite Element analysis in geotechnical engineering: applications*. London: Thomas Telford Ltd.

Reissner, H. 1924. Zum erddruckproblem. *First International Conference on Applied Mechanics Proceedings,* Delft, Netherlands. pp. 295-311.

Salgado, R., Lyamin, A.V., Sloan, S.W. and Yu, S. 2004. Two- and three dimensional bearing capacity of foundations in clay. *Géotechnique*. Vol. 54, No. 5, pp. 297-306.

Terzaghi, K. 1943. *Theoretical soil mechanics.* New York: John Wiley.

Vesić, A.S. 1963. Bearing capacity of deep foundations in sand. National Academy of Sciences, National Research Council. *Highway Research Record*. No. 39, pp. 112-153.

Vesić, A.S. 1973. Analysis of ultimate loads of shallow foundations. *Journal of the soil mechanics and foundations division*. ASCE. Vol. 99, No. 1, pp. 45-73.

Zhu, M. and Michalowski, R.L. 2005. Shape factors for limit loads on square and rectangular footings. *Journal of Geotechnical and Geoenvironmental Engineering.* ASCE. Vol. 131, No. 2, pp. 223-231.